Interaction and force measurements

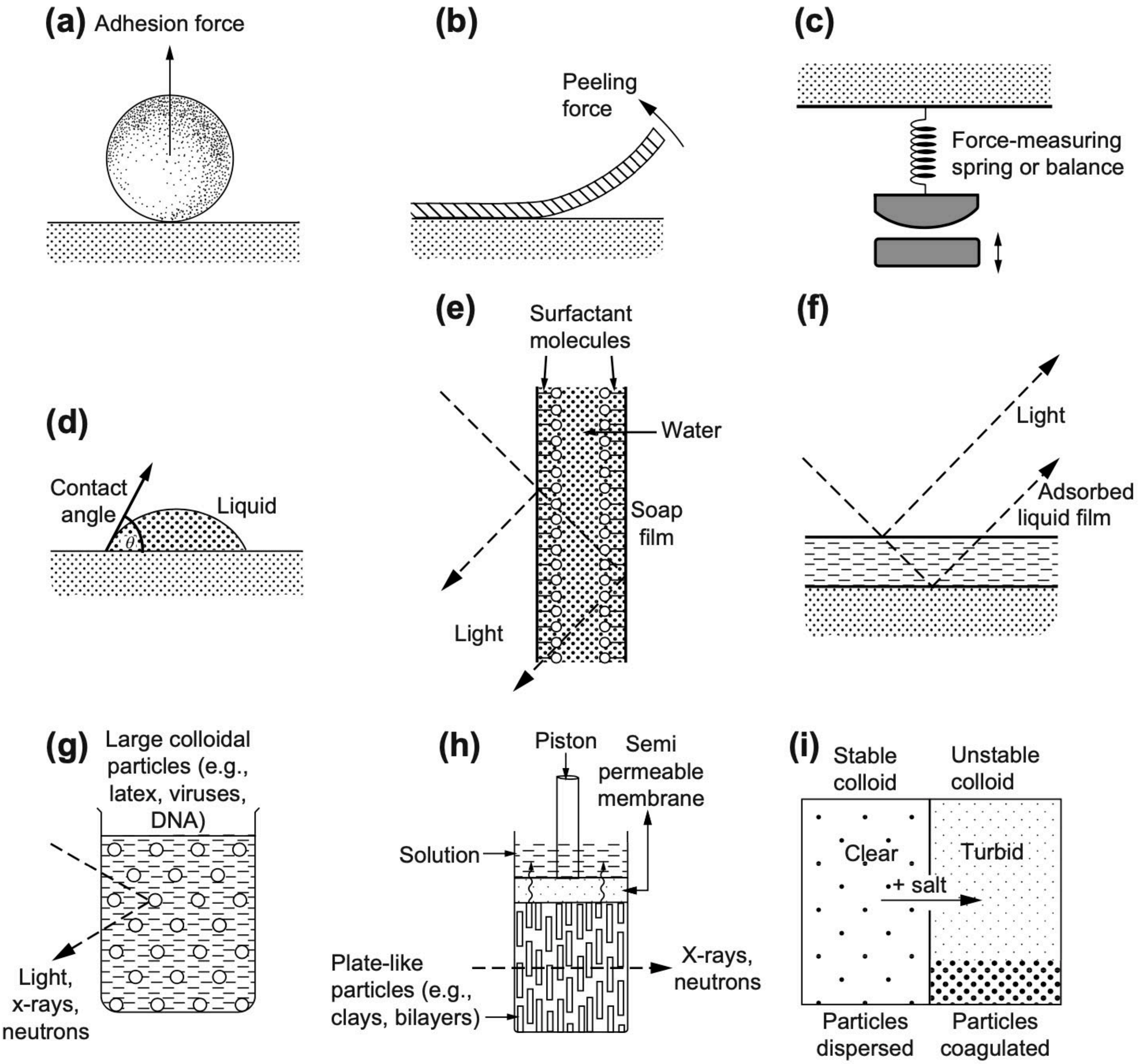
(a) Adhesion force
(b)
Peeling force
(c)
Force-measuring spring or balance
(d)
Contact angle
θ
Liquid
(e)
Surfactant molecules
Water
Soap film
Light
(f)
Light
Adsorbed liquid film
(g)
Large colloidal particles (e.g., latex, viruses, DNA)
Light, x-rays, neutrons
(h)
Piston
Semi permeable membrane
Solution
Plate-like particles (e.g., clays, bilayers)
X-rays, neutrons
(i)
Stable colloid
Unstable colloid
Clear
Turbid
+ salt
Particles dispersed
Particles coagulated

Direct force measurements

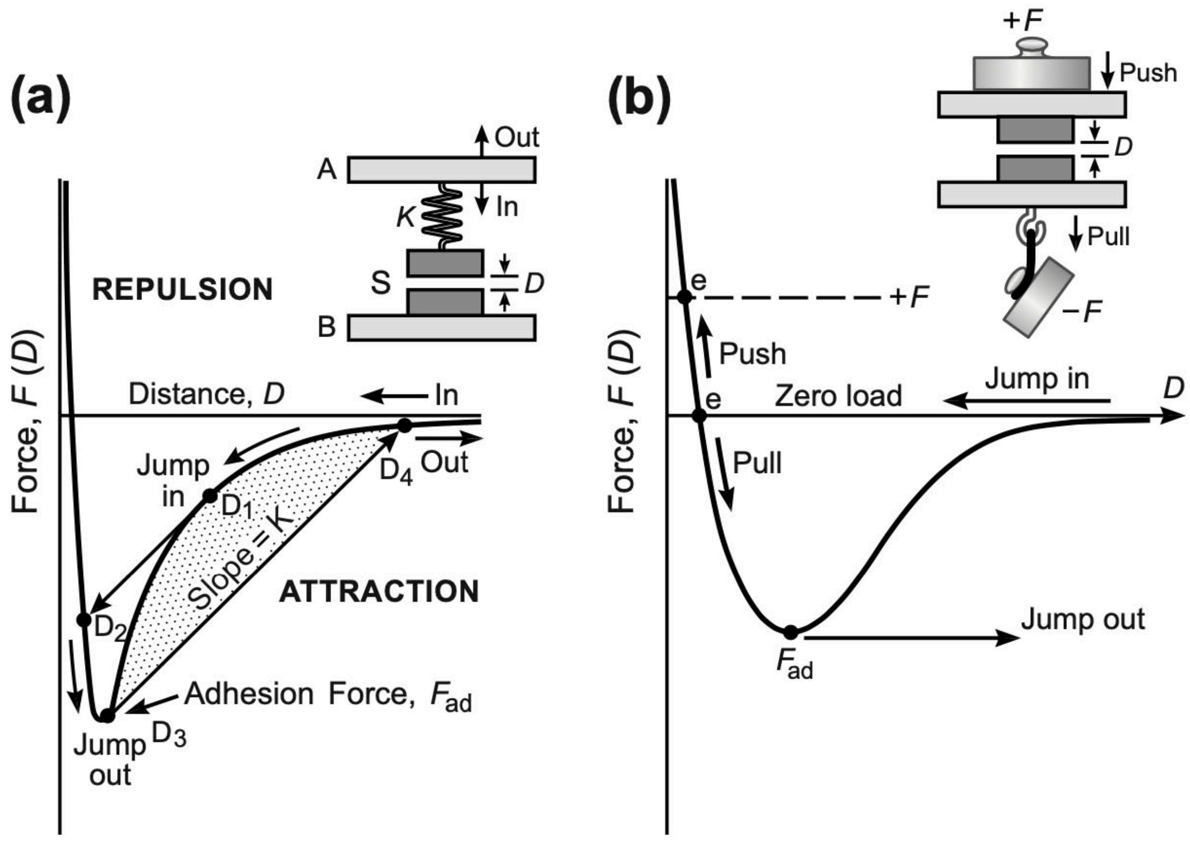

FIGURE 12.3 Measuring forces via **(a)** a spring (externally applied force ∝ spring displacement: ($F_{ext} = K\Delta D$), and **(b)** a constant force (F_{ext} = constant). For the typical force-law or force-distance curves $F(D)$ shown, instabilities occur at the positions shown, manifested by an inward jump on the way in (on approach) and an outward jump on the way out (on separation). **(a)** These jump instabilities will occur only if the effective spring constant K is lower than the maximum slope of the $F(D)$ curve. Thus, if the system is infinitely stiff ($K = \infty$) there will be no instabilities on approach or separation. In contrast, if a constant external force $+F$ is applied to one of the surfaces **(b)**, K is effectively zero, and jumps will occur to the upper equilibrium points at **e** on approach, and out from F_{ad} on separation. No equilibrium is possible at surface separations between the **Jump in** and **Jump out** points.

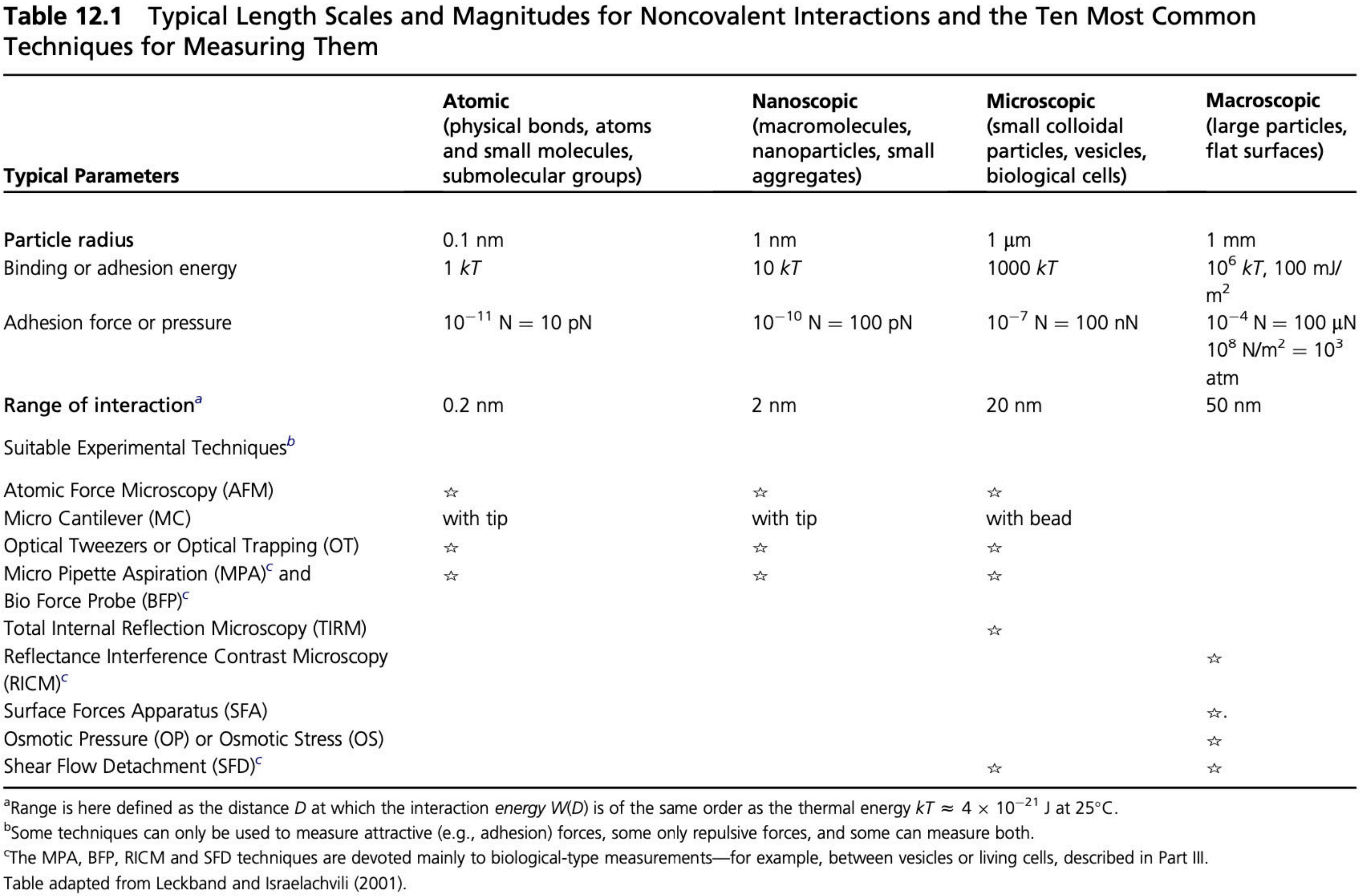

Table 12.1 Typical Length Scales and Magnitudes for Noncovalent Interactions and the Ten Most Common Techniques for Measuring Them

Typical Parameters	**Atomic** (physical bonds, atoms and small molecules, submolecular groups)	**Nanoscopic** (macromolecules, nanoparticles, small aggregates)	**Microscopic** (small colloidal particles, vesicles, biological cells)	**Macroscopic** (large particles, flat surfaces)
Particle radius	0.1 nm	1 nm	1 μm	1 mm
Binding or adhesion energy	1 kT	10 kT	1000 kT	10^6 kT, 100 mJ/m^2
Adhesion force or pressure	10^{-11} N = 10 pN	10^{-10} N = 100 pN	10^{-7} N = 100 nN	10^{-4} N = 100 μN 10^8 N/m^2 = 10^3 atm
Range of interaction[a]	0.2 nm	2 nm	20 nm	50 nm
Suitable Experimental Techniques[b]				
Atomic Force Microscopy (AFM)	☆	☆	☆	
Micro Cantilever (MC)	with tip	with tip	with bead	
Optical Tweezers or Optical Trapping (OT)	☆	☆	☆	
Micro Pipette Aspiration (MPA)[c] and Bio Force Probe (BFP)[c]	☆	☆	☆	
Total Internal Reflection Microscopy (TIRM)			☆	
Reflectance Interference Contrast Microscopy (RICM)[c]				☆
Surface Forces Apparatus (SFA)				☆.
Osmotic Pressure (OP) or Osmotic Stress (OS)				☆
Shear Flow Detachment (SFD)[c]			☆	☆

[a] Range is here defined as the distance D at which the interaction *energy* $W(D)$ is of the same order as the thermal energy $kT \approx 4 \times 10^{-21}$ J at 25°C.

[b] Some techniques can only be used to measure attractive (e.g., adhesion) forces, some only repulsive forces, and some can measure both.

[c] The MPA, BFP, RICM and SFD techniques are devoted mainly to biological-type measurements—for example, between vesicles or living cells, described in Part III.

Table adapted from Leckband and Israelachvili (2001).

Surface forces apparatus (SFA)

Tabor and Winterton (1969)
Israelachvili and Tabor (1972, 1973)
Israelachvili and Adams, 1978
Israelachvili, 1987b

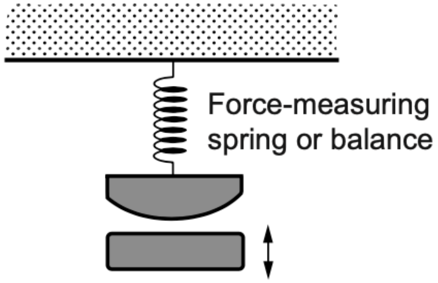

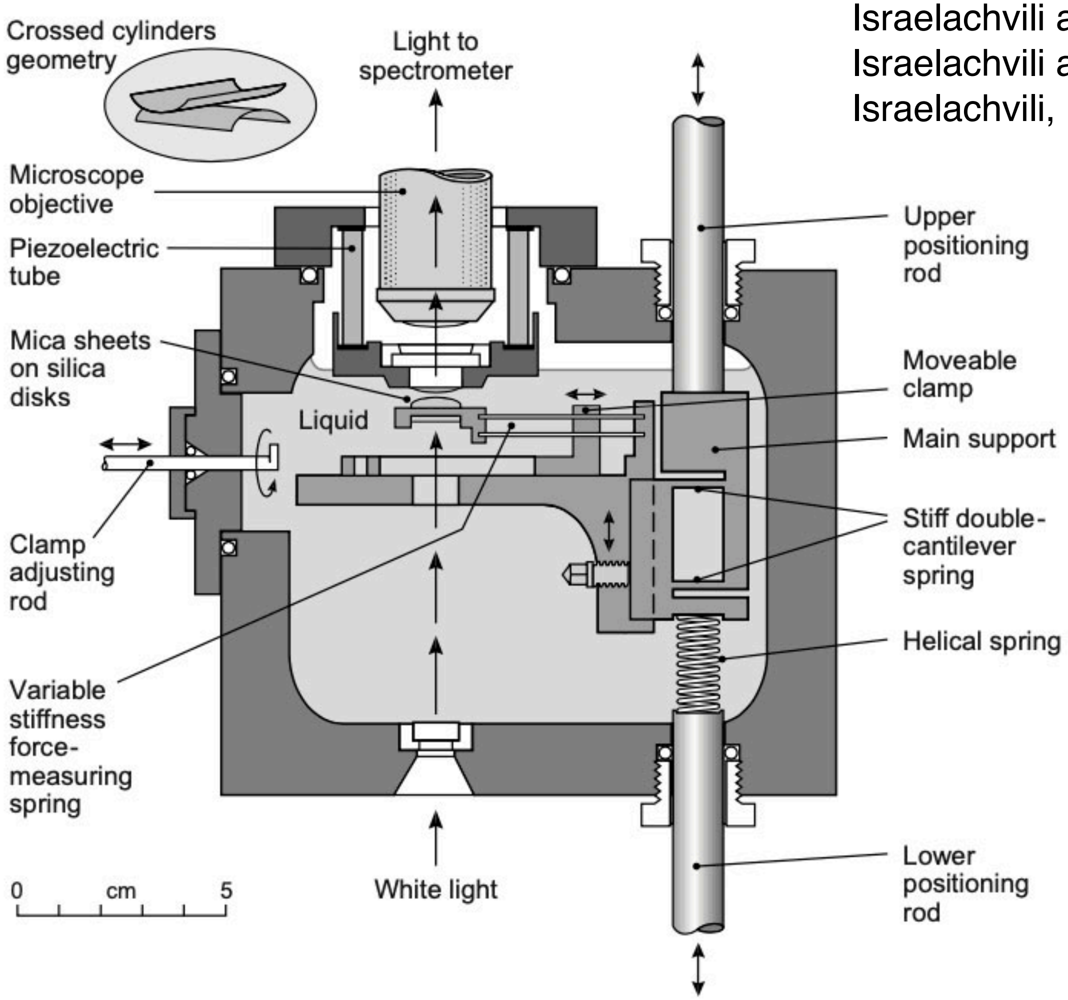

Two crossed-cylinders
Mica surfaces in air, vacuum, or liquid
Multiple Beam Interferometry (MBI) using “fringes of equal chromatic order” (FECO)

SFA measurement

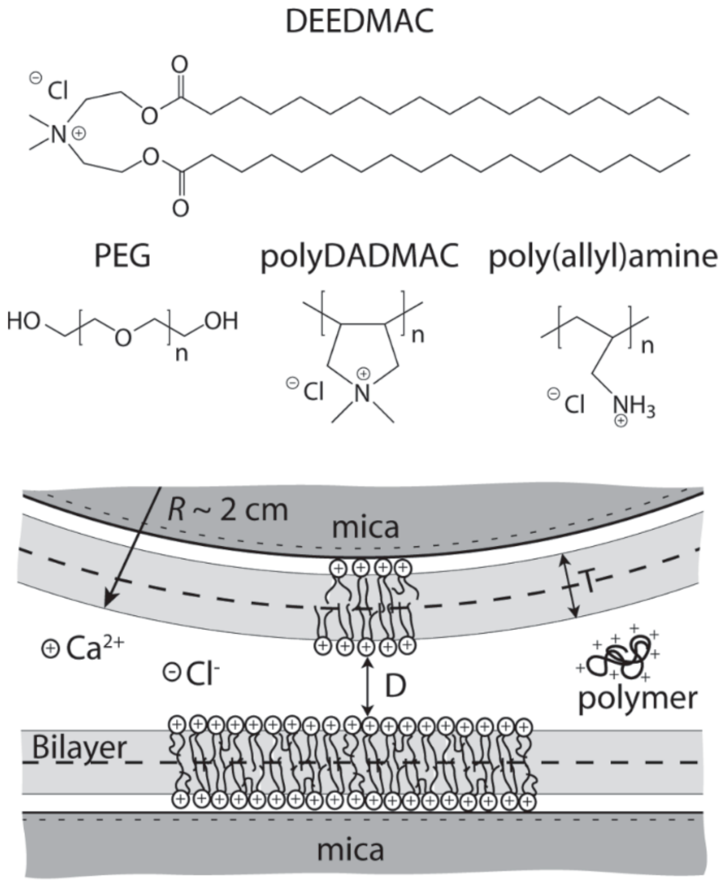

Figure 1. Top: The cationic surfactant DEEDMAC used to make the supported bilayers in the SFA studies. Middle: The polymers PEG, polyDADMAC, and poly(allyl)amine used to study the repulsive electrostatic and attractive depletion forces between DEEDMAC bilayers. Bottom: Schematic of the supported bilayers and surface geometry in the SFA experiments.

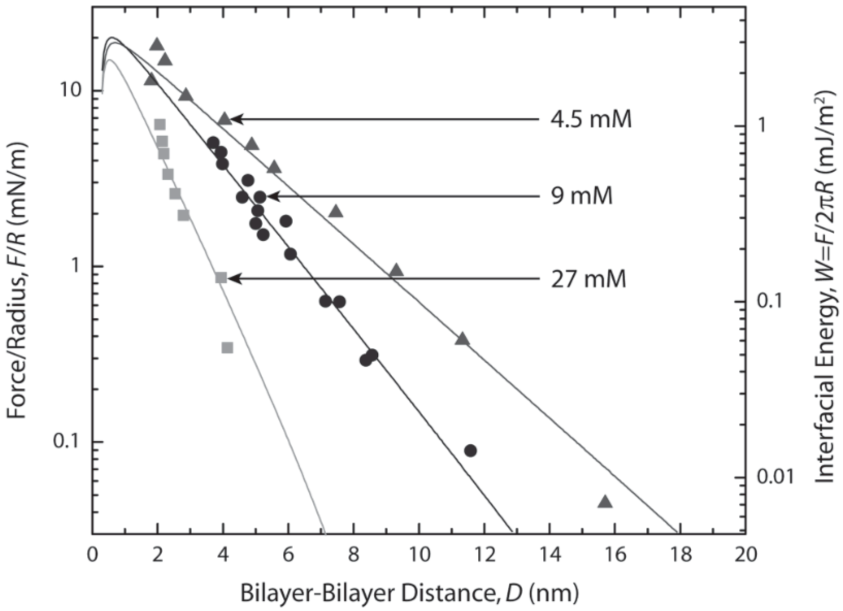

Figure 2. Measured forces between DEEDMAC bilayers in various $CaCl_2$ solutions at pH 4. Solid lines are DLVO fits using the parameters given in Table 1.

Atomic force microscopy (AFM)

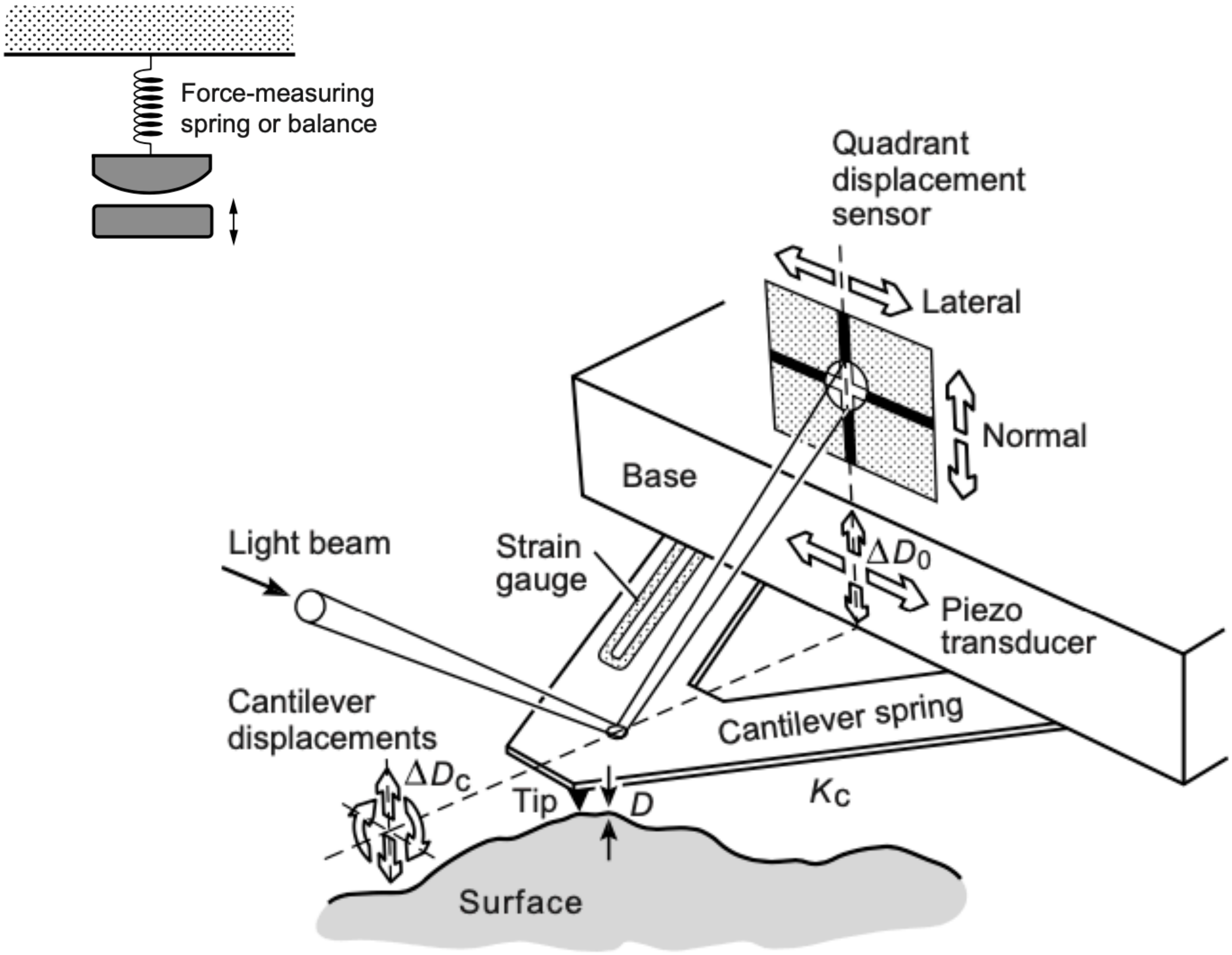

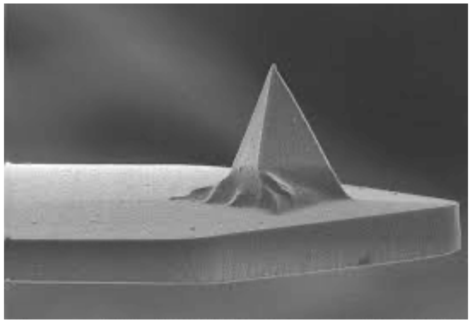

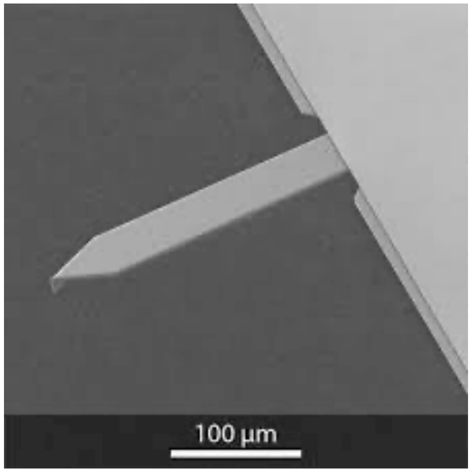

Related to profilimetry
Scanning mode or tapping mode

AFM scans of surface topology

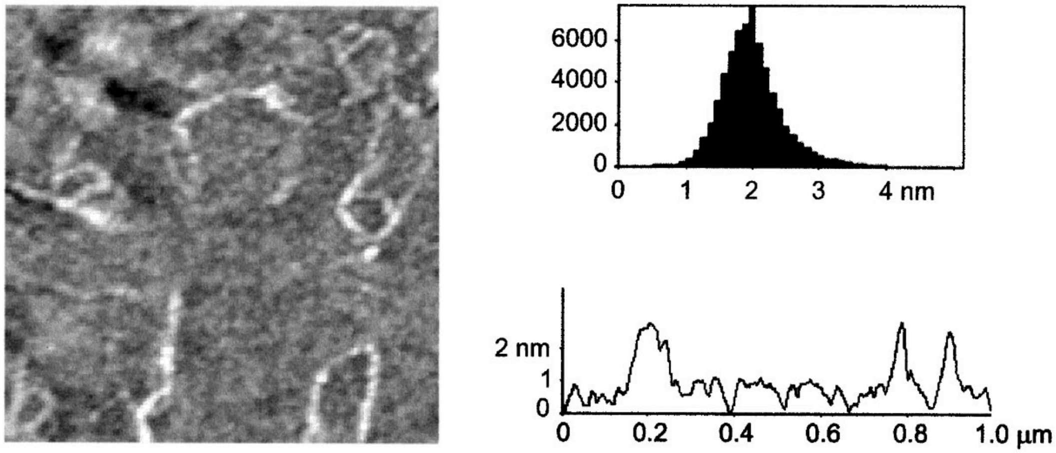

Figure 5. AFM scan of roughness on the surface of a glass slide within a typical 1 μm square. The histogram shows the distribution of elevations on the 2D image, and the line graph shows the profile of elevations along a horizontal line bisecting the 2D scan.

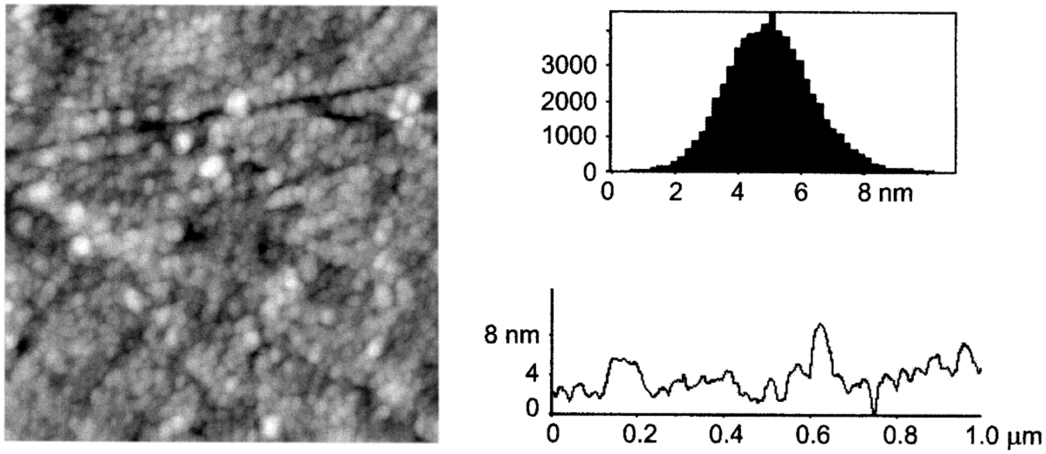

Figure 6. AFM scan of roughness on the surface of a glass slide, spin-coated with a 1 μm thick PS film, within a typical 1 μm square. The histogram shows the distribution of elevations on the 2D image, and the line graph shows the profile of elevations along a horizontal line bisecting the 2D scan.

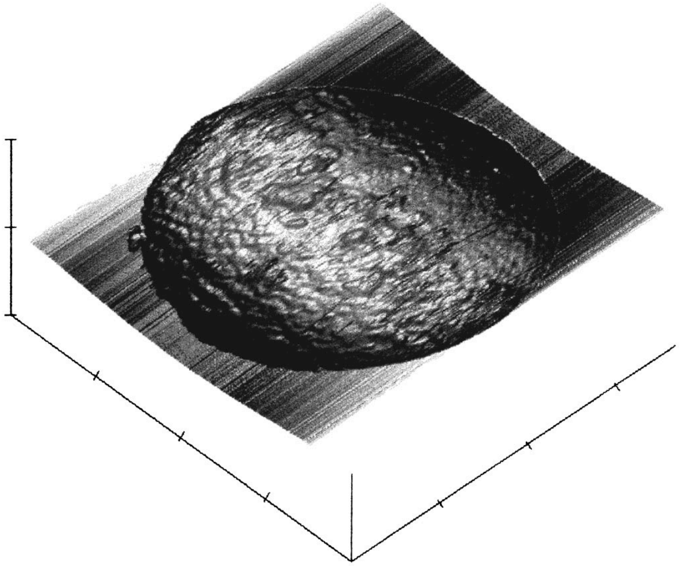

Figure 7. AFM scan of the top surface of a PS sphere (courtesy of Robert Considine). The lateral scale is 1 μm/division, and the vertical scale is 1.5 μm/division. The larger asperities have a height of 40 nm.

M. A. Bevan, D. C. Prieve, Direct Measurement of retarded van der Waals Attraction. Langmuir. 15, 7925–7936 (1999).

Colloidal probe AFM

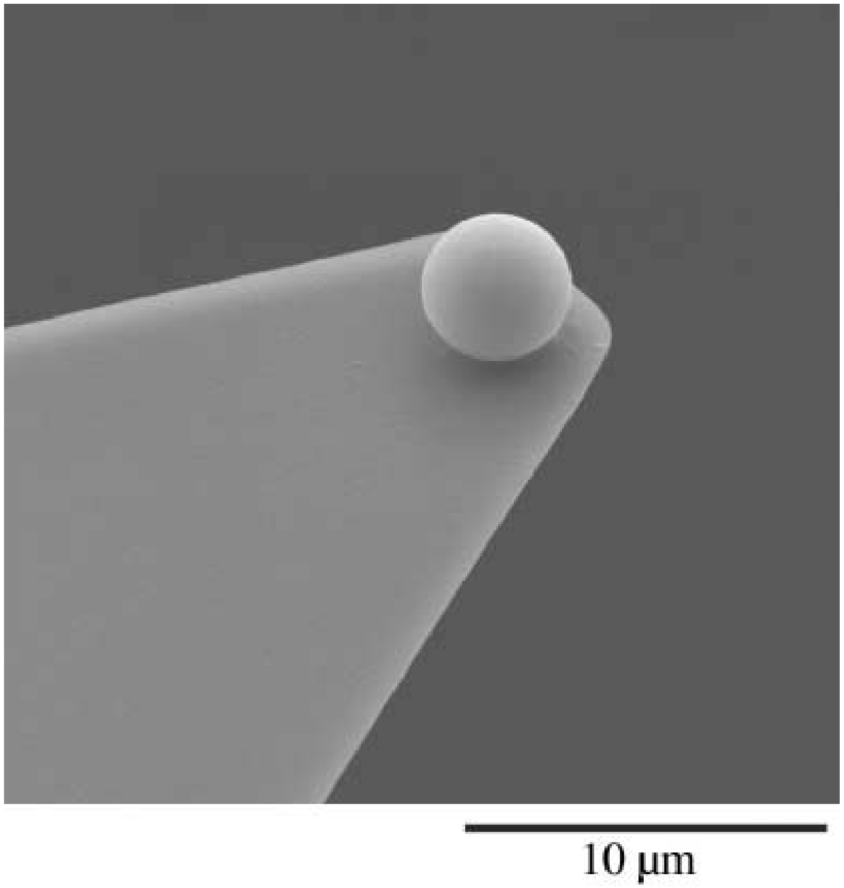

Fig. 1: Scanning electron micrograph of silanized silica microsphere glued to the end of a tipless atomic force microscope cantilever.

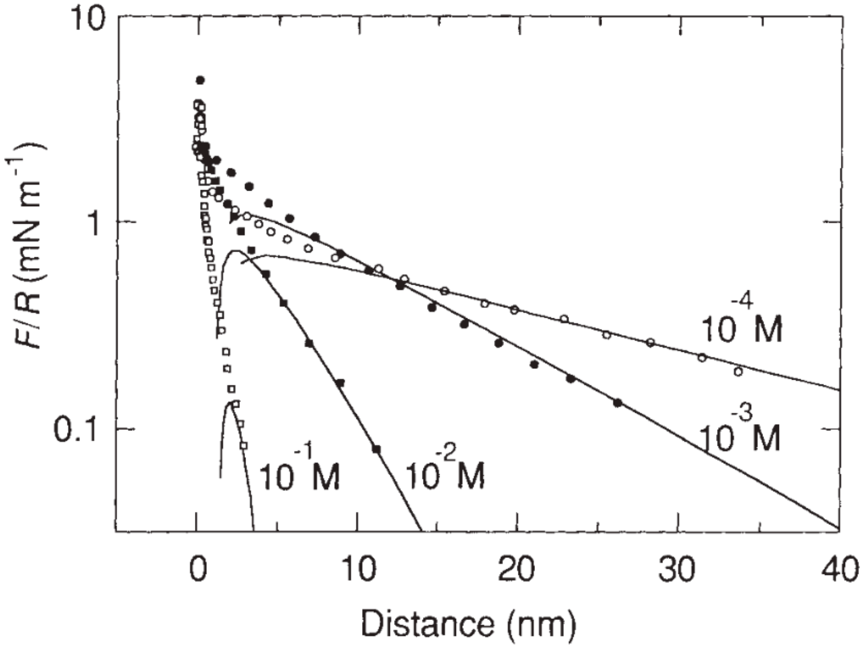

W. A. Ducker, T. J. Senden, R. M. Pashley, Nature. 353, 239–241 (1991).
M. Kappl, H.-J. Butt, Part. Part. Syst. Charact. 19, 129–143 (2002).

Total internal reflection microscopy (TIRM)

Prieve, 1999
Prieve and Frej, 1990
Prieve et al., 1990

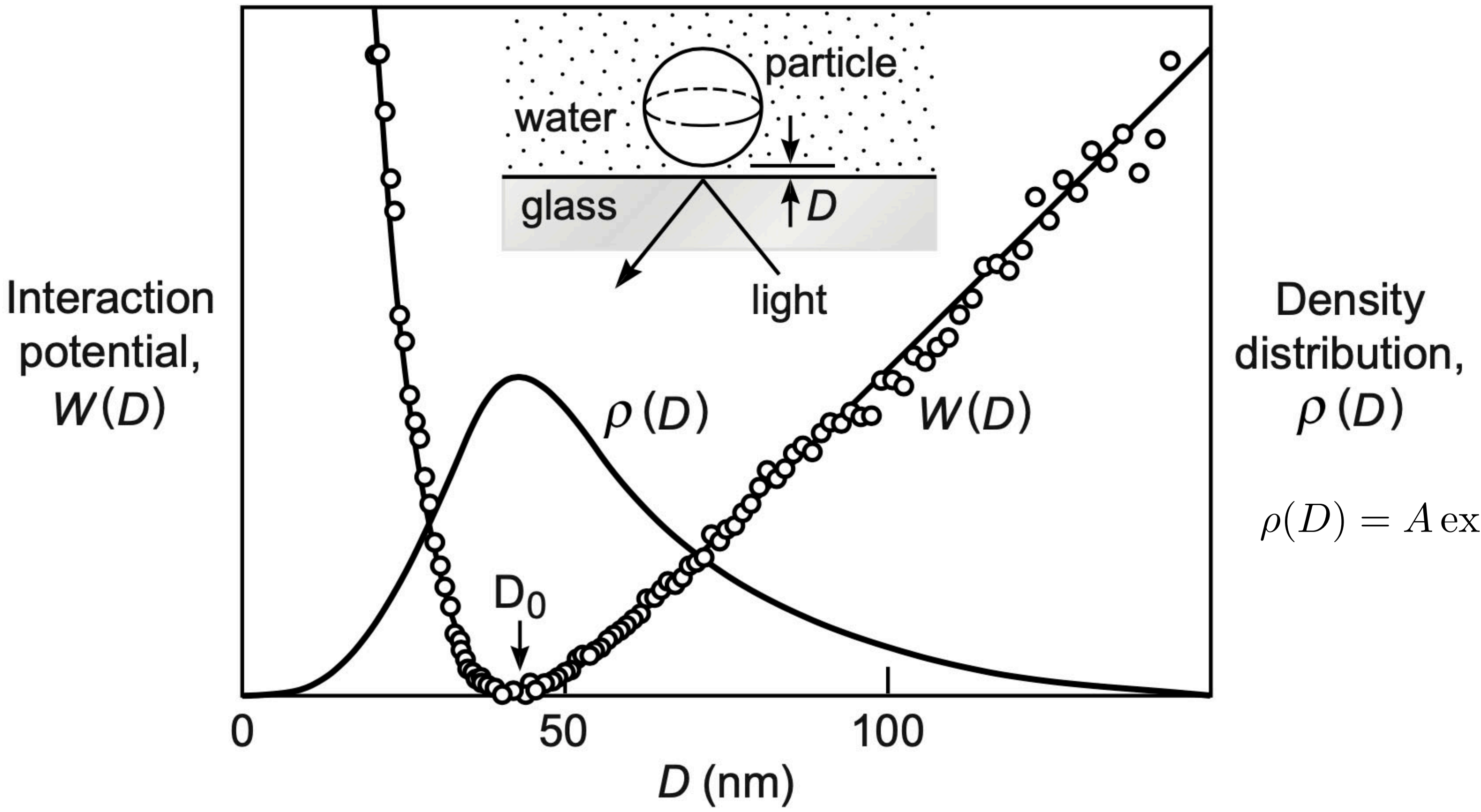

$$\rho(D) = A \exp\left[-\frac{\phi(D)}{kT}\right]$$

TIRM measurement

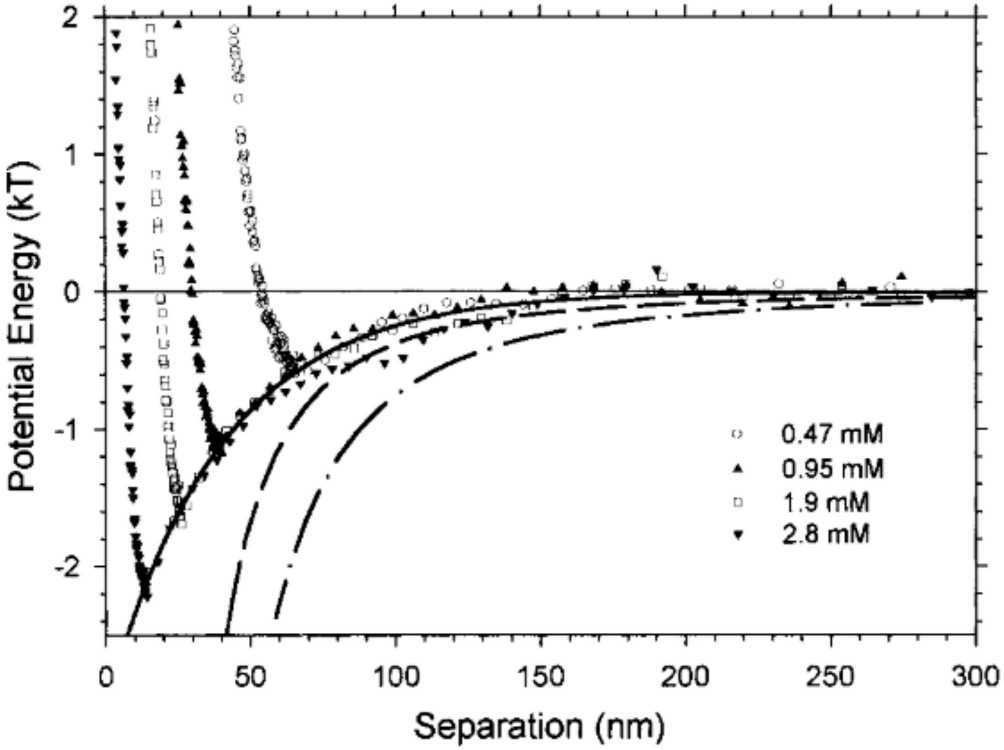

Figure 1. Profiles of the colloid interactions between the same 6 μm PS sphere and a glass slide in solutions having different ionic strengths. The solid line is an empirical fit given by eq 5, the dashed line shows the van der Waals interaction predicted from the Lifshitz–Derjaguin equation (eq 3), and the dot–dash line shows the van der Waals interaction predicted from the Lifshitz–Hamaker equation (eq 4).

$$E(l) = -\frac{A_{132}(l)}{12\pi l^2} \qquad (1)$$

$$A_{132}(l) = -\frac{3}{2}kT\sum_{n=0}^{\infty}{}'\int_{r_n}^{\infty} x\{\ln[1-\Delta_{13}\Delta_{23}e^{-x}] + \ln[1-\bar{\Delta}_{13}\bar{\Delta}_{23}e^{-x}]\}\,dx$$

$$\Delta_{jk} = \frac{\epsilon_j s_k - \epsilon_k s_j}{\epsilon_j s_k + \epsilon_k s_j} \qquad \bar{\Delta}_{jk} = \frac{s_k - s_j}{s_k + s_j}$$

$$s_k^{\;2} = x^2 + \left(\frac{2\xi_n l}{c}\right)^2(\epsilon_k - \epsilon_2)$$

$$r_n = \frac{2l\xi_n\sqrt{\epsilon_2}}{c} \qquad \epsilon_k = \epsilon_k(i\xi_n) \qquad \xi_n = \frac{nkT}{\hbar}$$

$$\phi(h) = 2\pi a\int_h^{\infty} E(l)\,dl \qquad (3)$$

$$\phi(h) = -\frac{A(h)}{6}\left\{\frac{2a}{h}\frac{h+a}{h+2a} - \ln\left(\frac{h+2a}{h}\right)\right\} \qquad (4)$$

M. A. Bevan, D. C. Prieve, Direct Measurement of retarded van der Waals Attraction. Langmuir. 15, 7925–7936 (1999).

Interaction measurements

TIRM, surfactant micelles

Sober, D. L.; Walz, J. Y. *Langmuir* 1995, 11, 2352–2356.

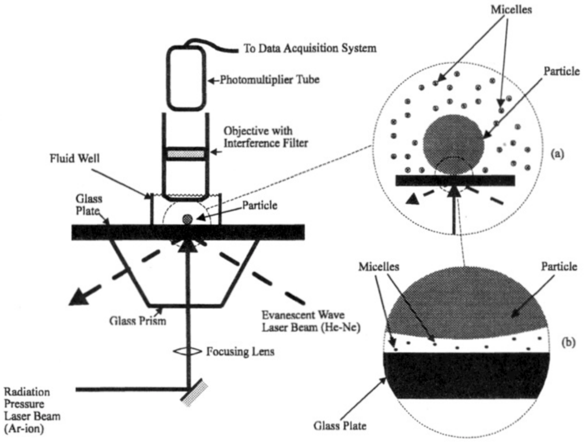

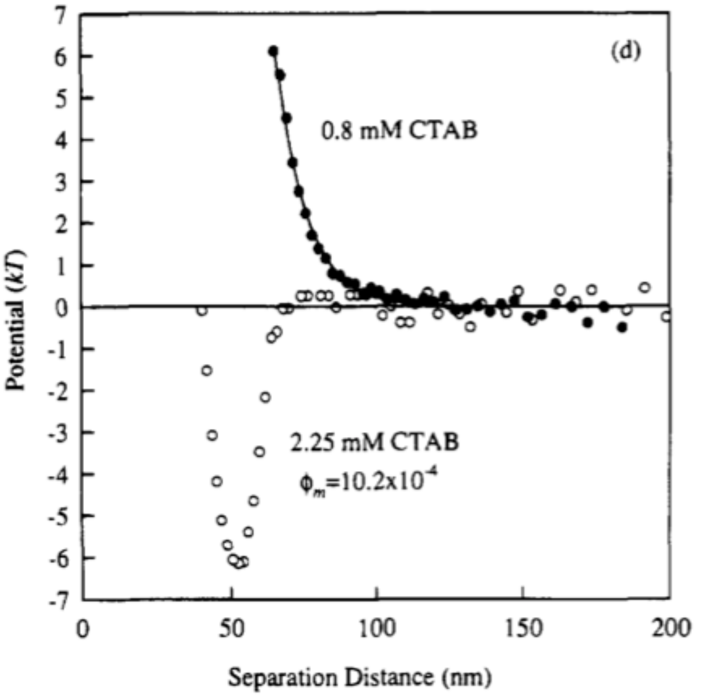

TIRM, rigid rods

Helden, L.; Roth, R.; Koenderink, G. H.; Leiderer, P.; Bechinger, C. *Phys. Rev. Lett.* 2003, 90, 48301.

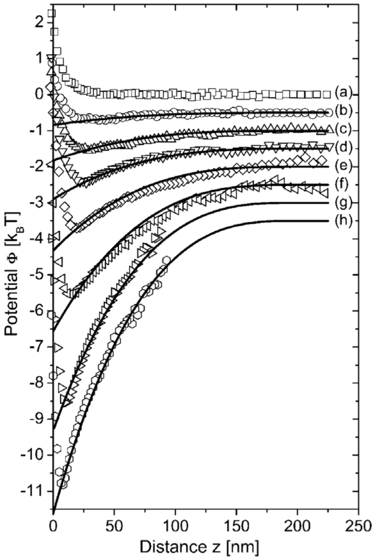

TIRM, polyelectrolytes

Biggs, S.; Dagastine, R. R.; Prieve, D. C. *J. Phys. Chem.* B 2002, 106, 11557–11564.

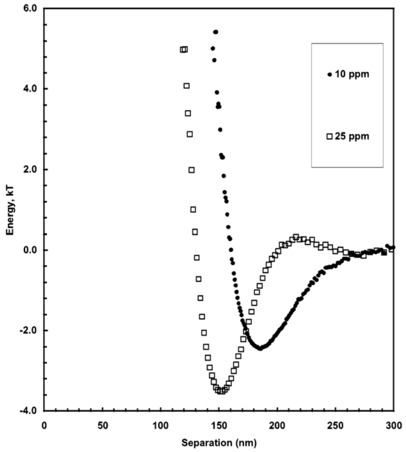

Optical tweezers

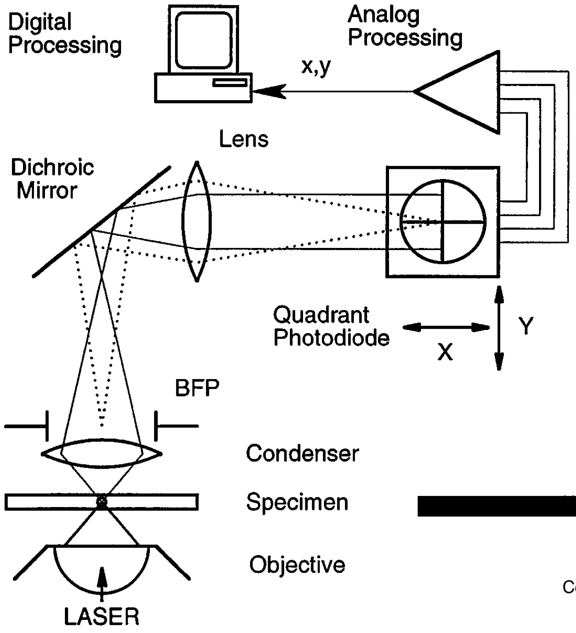

Back focal plane detection

Laser tweezer apparatus

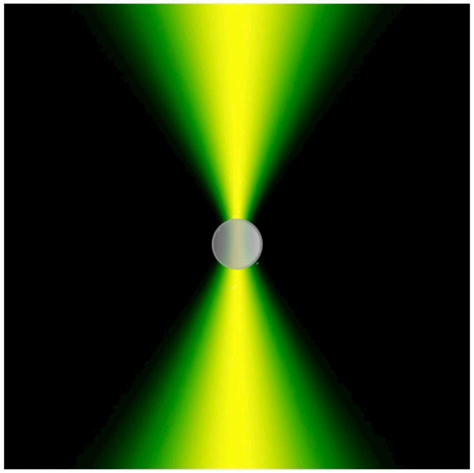

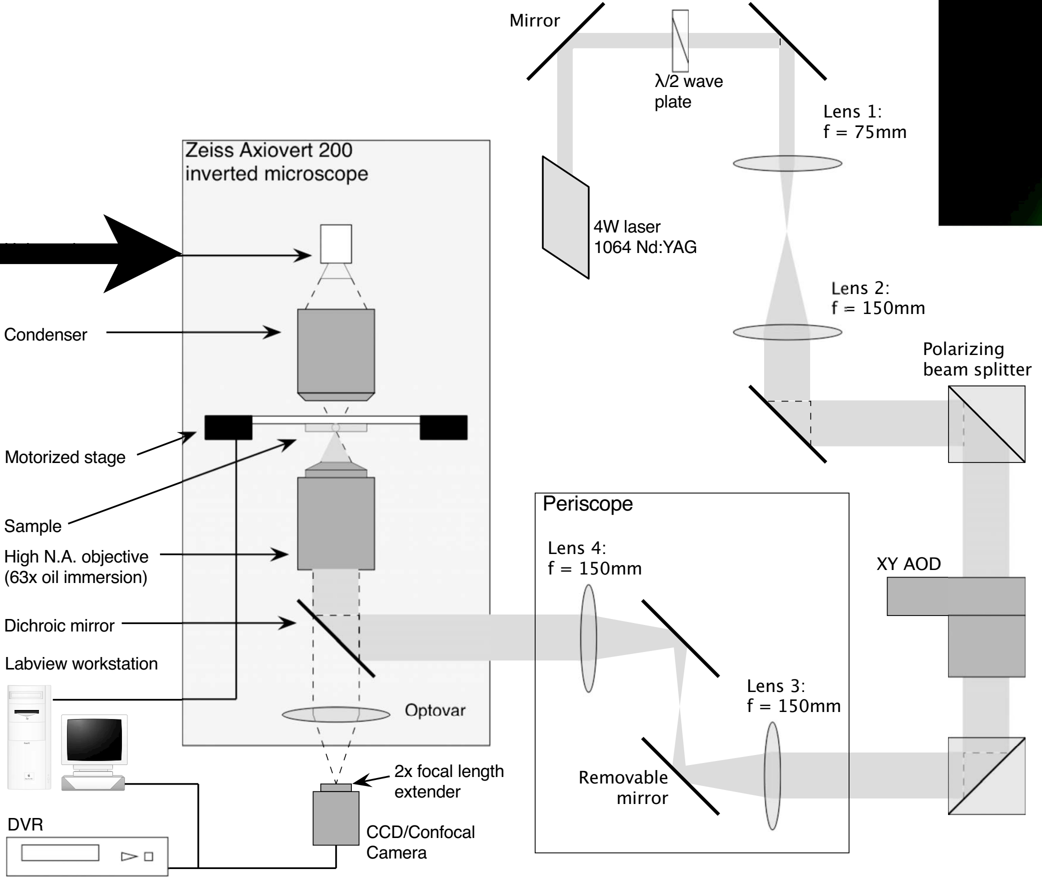

Measuring colloidal “stickiness”

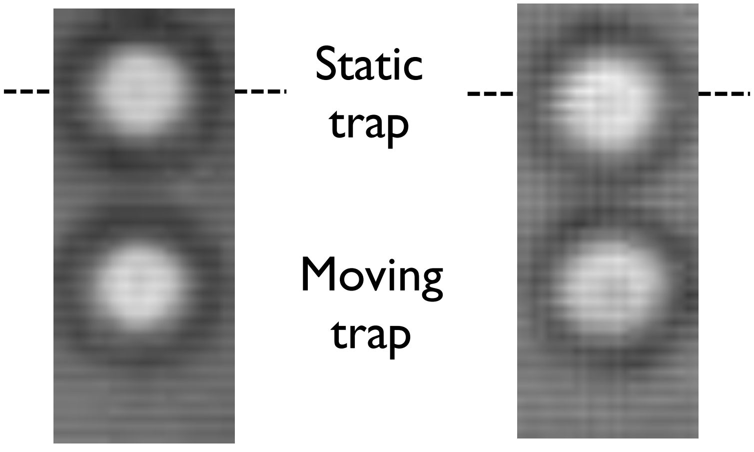

Repulsive

Attractive

A single bond rupture

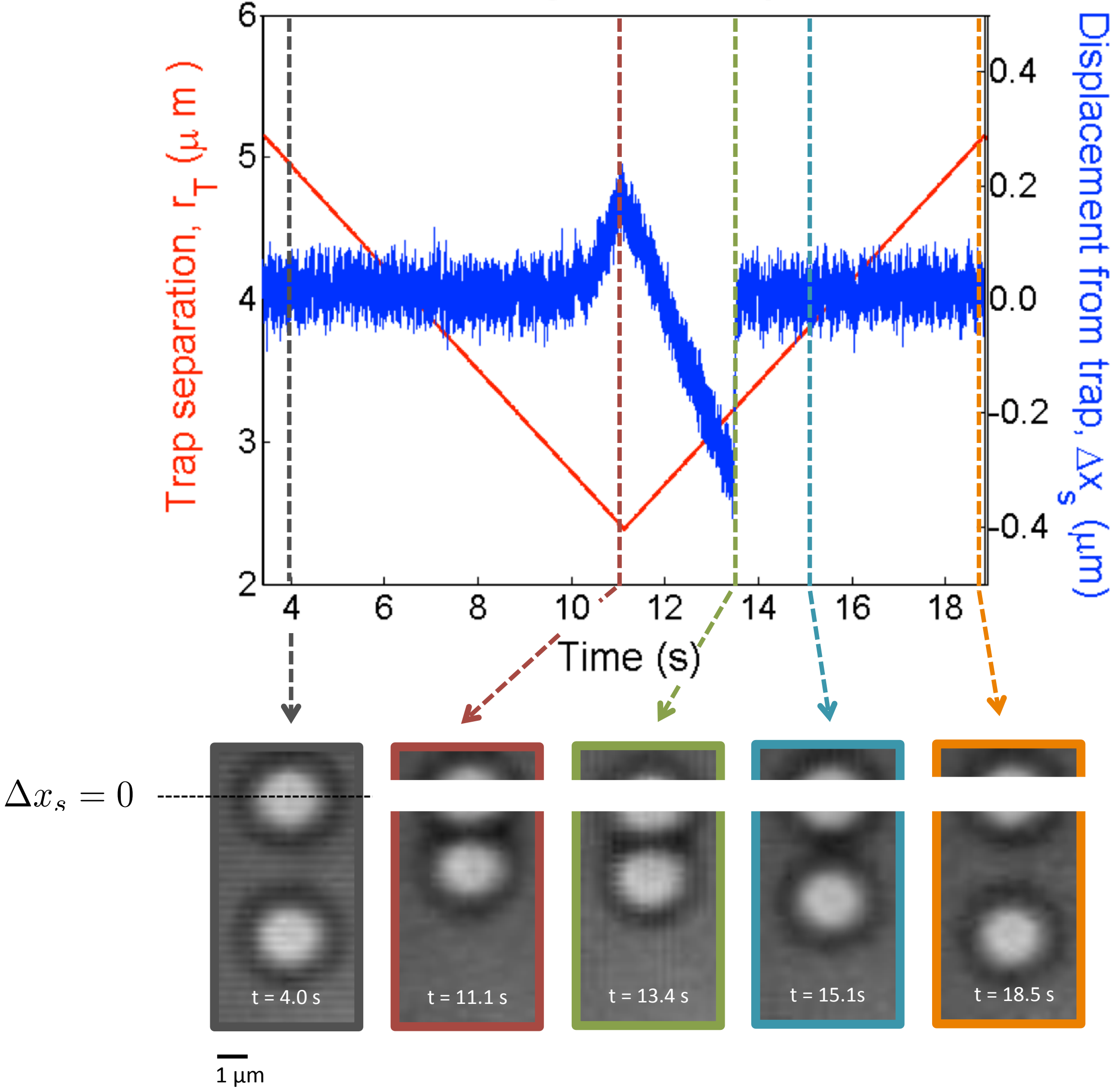

“Line tweezer” interaction measurements

Depletion attraction between flexible rods

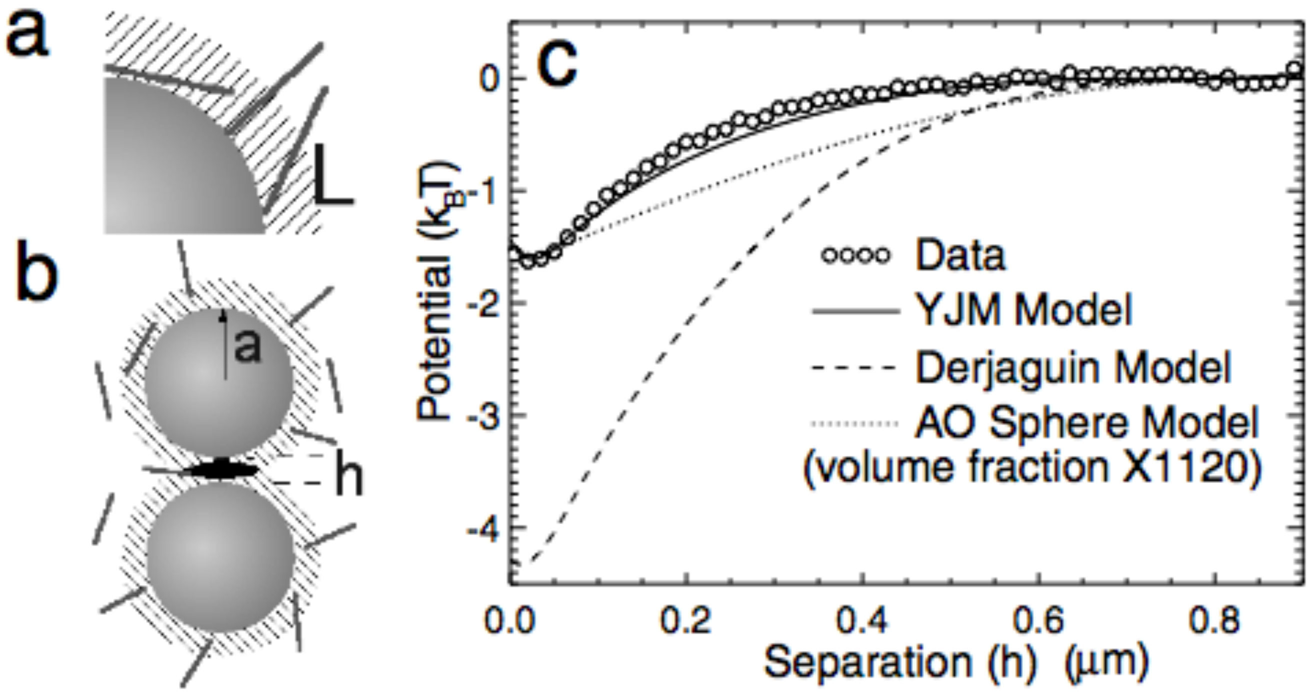

Lin, K.; Crocker, J. C.; Zeri, A. C.; Yodh, A. G. *Phys. Rev. Lett.* 2001, 87, 88301.

Direct force measurements and interpretation

Measurements use curved interfaces
(sphere-flat, two spheres, crossed cylinders)

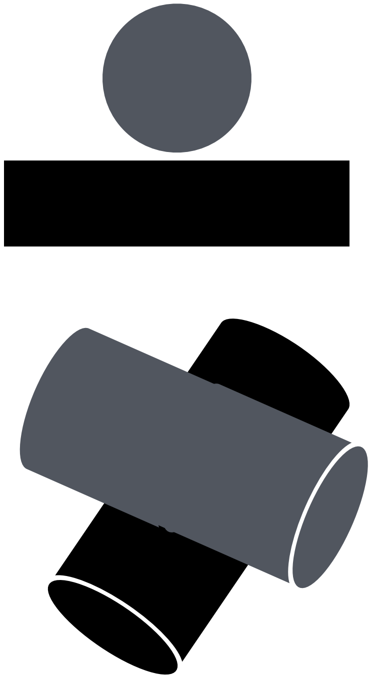

$$W(D)_{\mathrm{curved}} = -\int_{\infty}^{D} F(D)_{\mathrm{curved}} dD$$

$$W(D)_{\mathrm{flat}} = \frac{F(D)_{\mathrm{curved}}}{2\pi R}$$

Derjaugin approximation

$$P(D)_{\mathrm{flat}} = \frac{dW_{\mathrm{flat}}}{dD} = \frac{dF(D)_{\mathrm{curved}}/dD}{2\pi R}$$

Direct force measurements and interpretation

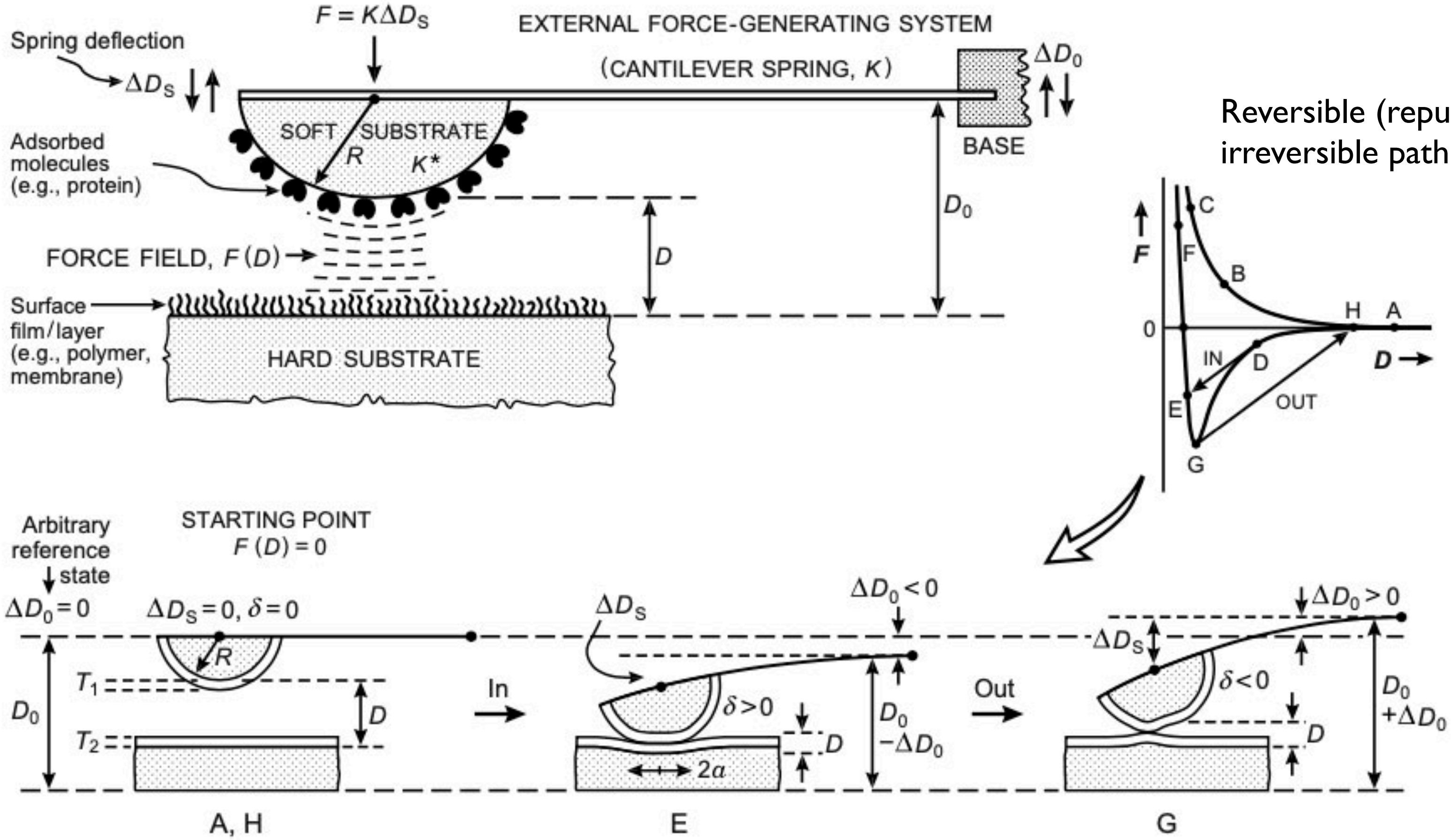

Reversible (repulsion) and irreversible paths (attraction)

FIGURE 12.4 Generic geometry for force-measuring techniques that employ springs, showing the relevant parameters that must be controlled and/or measured, preferably as a function of time t, during a force measurement: the force F, the undeformed surface radius R, the surface separation D, the spring deflection ΔD_s, the force-measuring (cantilever) spring constant K such that $F(D) = K\Delta D_s$, the effective stiffness of the material K^* and its elastic deformation δ (see JKR theory in Chapter 17 and Figure 12.5), the flattened area $A = \pi a^2$ of the surfaces when in contact, and the film thicknesses T_1 and T_2. One can define a laboratory reference distance D_0 such as that when the base is moved the change in the surface separation ΔD is given by Eq. (12.6): $\Delta D = \Delta D_0 \pm \Delta D_s \pm \delta$.

Two oil droplets interacting

R. R. Dagastine et al., Dynamic Forces Between Two Deformable Oil Droplets in Water. Science. 313, 210–213 (2006).

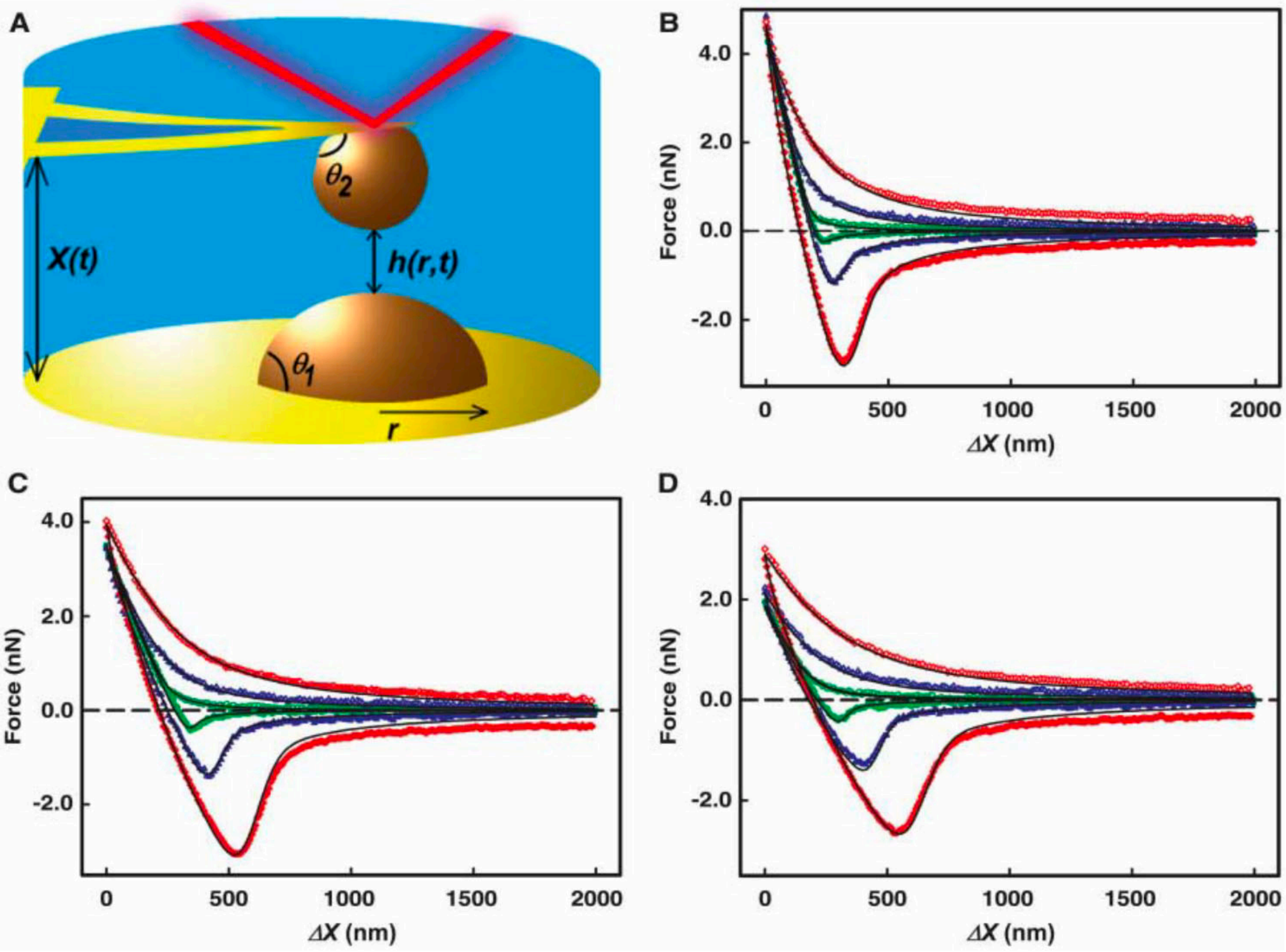

Fig. 1. (**A**) A schematic of the experiment between two oil droplets, one immobilized on the cantilever and the other immobilized on the substrate of an atomic force microscope. (**B** to **D**) The dynamic interaction force *F* versus piezo drive motion Δ*X* between two decane droplets in aqueous solution in the presence of SDS at a series of approach (open symbols) and retract (filled symbols) velocities (green circles, 2 μm/s; blue triangles, 9.3 μm/s; red diamonds, 28 μm/s) over a range of SDS concentrations: (B) 0.1 mM, (C) 3 mM, and (D) 10 mM. The points refer to the experimental data, and the solid lines are the calculated force curves from a comprehensive model of the dynamic droplet interactions.

JKR apparatus

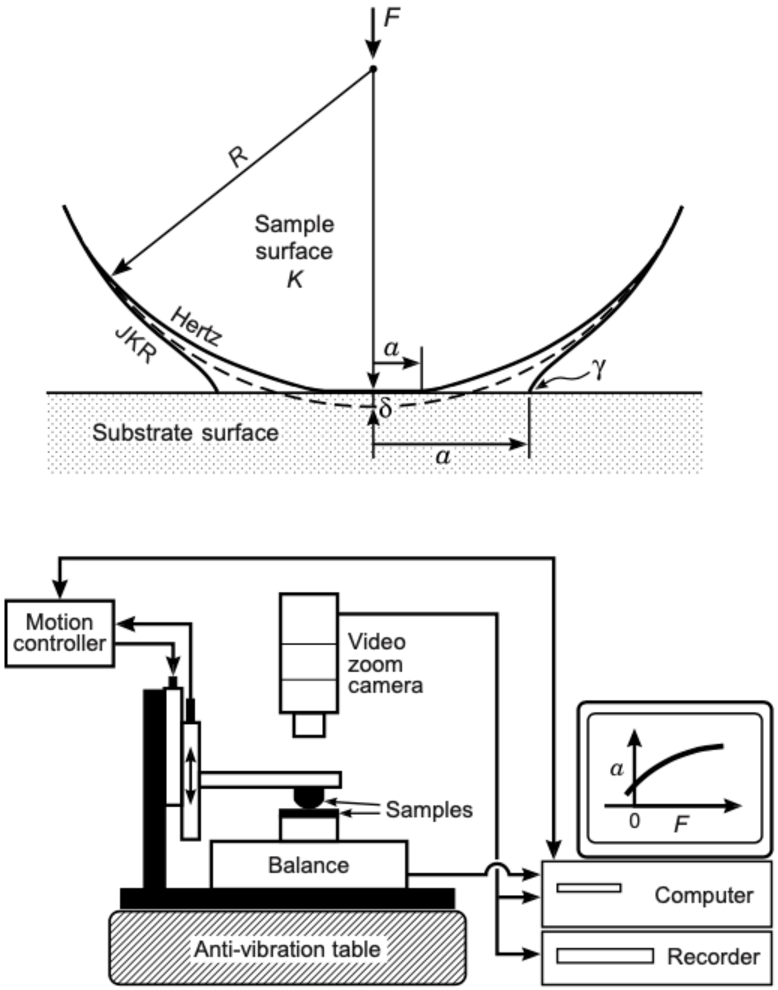

FIGURE 12.5 A JKR apparatus named after the Johnston-Kendall-Roberts theory of adhesion mechanics (Johnson et al., 1971), developed by Tirrell and coworkers (Mangipudi et al., 1995; Tirrell, 1996) to study the adhesion forces and deformations of macroscopic solids. The device allows for the measurement of the molecular contact radius *a* as a function of the applied load *F*, including negative loads. The results can then be used to test theories of adhesion and contact mechanics such as the JKR and Hertz theories (Chapter 17). This technique also enables the measurement of surface energies γ via Eq. (11.17) or Eq. (12.10).

Adhesion between elastic particles
JKR Theory

Johnson, Kendall and Roberts, Proc. R. Soc. London, Ser. A 324, 301 (1971).

$$P_0 = 0 \qquad a_c = \left[\frac{3\pi a^2 W_{SL}}{2K}\right]^{1/3}$$

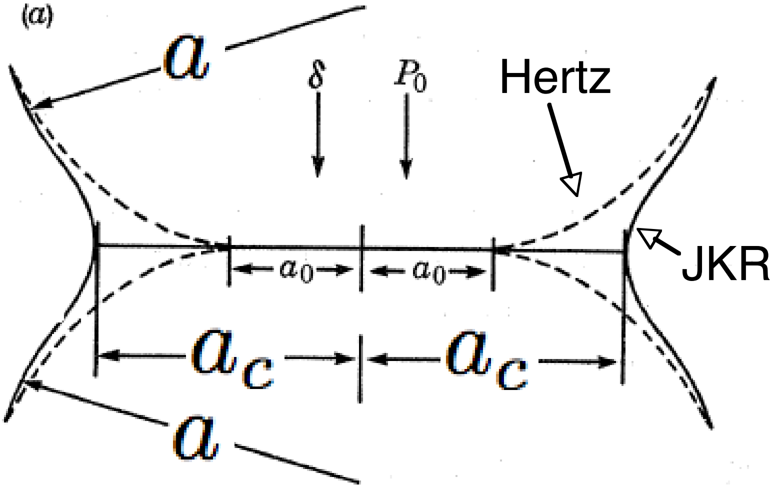

Surface adhesion energy:

$$W_{SL} = \gamma_S + \gamma_L - \gamma_{SL}$$

$$W_{SL} = \gamma_L(1 + \cos\theta_0) \approx 93\mathrm{mJ/m^2}$$

where[1] $\theta_0 = 73.7 \pm 0.3^\circ$

$\gamma_L \approx 72 - 73\mathrm{mN/m}$

Elastic modulus: $K = \dfrac{2E}{3(1-\nu^2)}$

$K \approx 2.5\mathrm{GPa}$ [2]

[1] Kwok et al. J. Colloid Interface Sci. 206, 44 (1998).
[2] Jarvis and Scheiman, J. Phys. Chem. 72, 74 (1968).

Instabilities

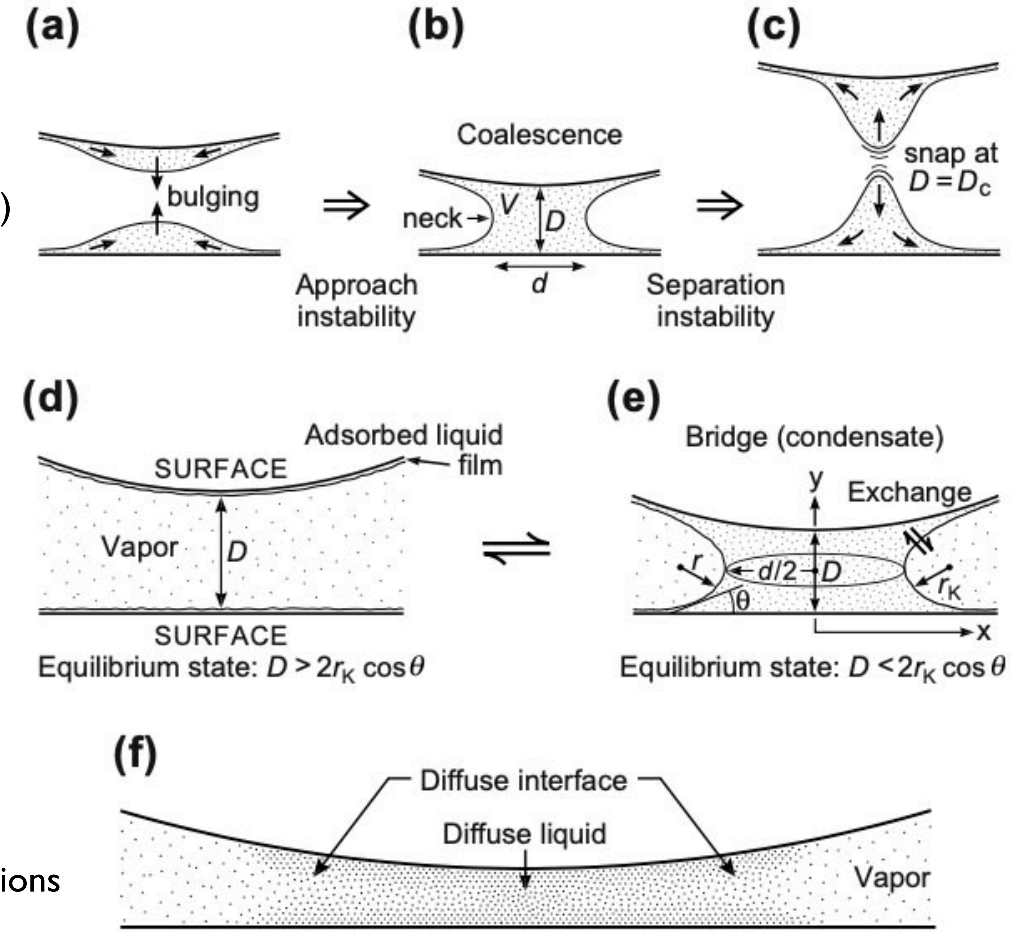

Constant volume
(e.g. low vapor pressure)

$$D_c \approx \pi d \approx (4\pi V)^{1/3}$$

VL equilibrium

Continuous transitions

FIGURE 12.6 The different geometries of liquid bridges can give rise to instabilities in the "capillary forces" measured on approach or separation of two surfaces. Shown here are the rapid *mechanical* instabilities and slower *thermodynamic transitions* that can occur on approach **(a → b)** and separation **(b → c)** of two surfaces with a liquid film on each. At **(c)** a mechanical instability (rapid snapping) occurs at a critical distance $D_c \propto V^{1/3}$, where V is the (constant) volume of the liquid. At thermodynamic equilibrium (d and e), V is no longer constant; instead, the mean curvature of the liquid-vapor interface is now constant and equal the Kelvin radius r_K (Ch. 17). Some transitions in confined geometries and thin films can be slow and/or continuous rather than abrupt (Stroud et al., 2001).

Interaction measurements

TIRM, surfactant micelles

Sober, D. L.; Walz, J.Y. *Langmuir* 1995, 11, 2352–2356.

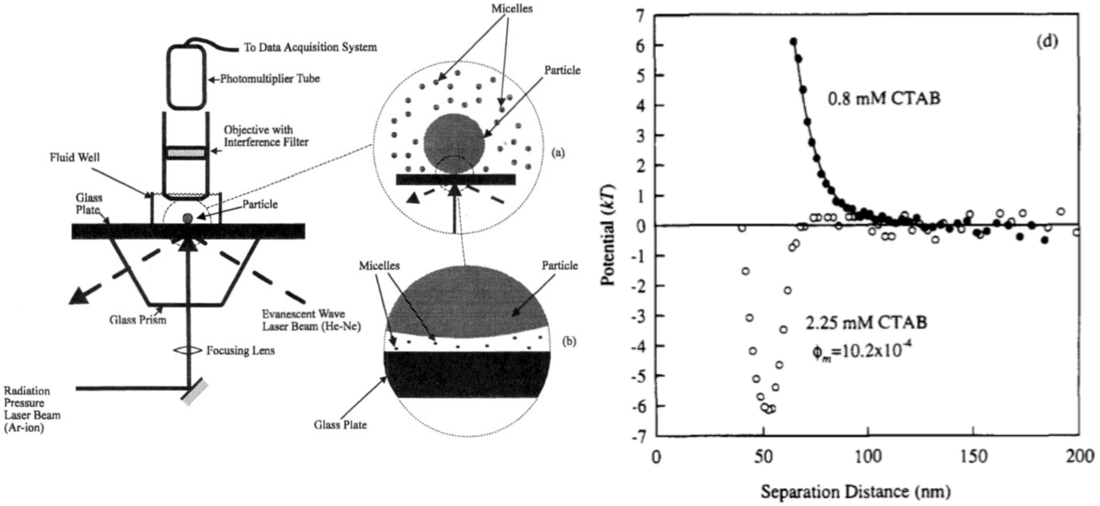

TIRM, polyelectrolytes

Biggs, S.; Dagastine, R. R.; Prieve, D. C. *J. Phys. Chem.* B 2002, 106, 11557–11564.

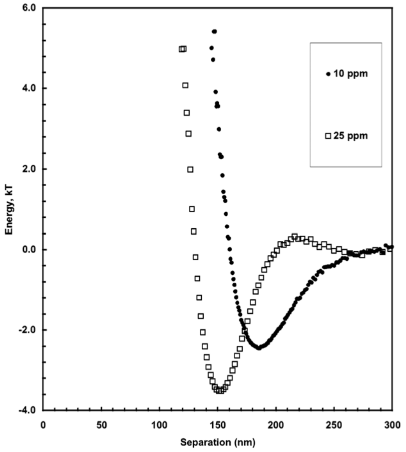

Line tweezers, flexible rods

Lin, K.; Crocker, J. C.; Zeri, A. C.; Yodh, A. G. *Phys. Rev. Lett.* 2001, 87, 88301.

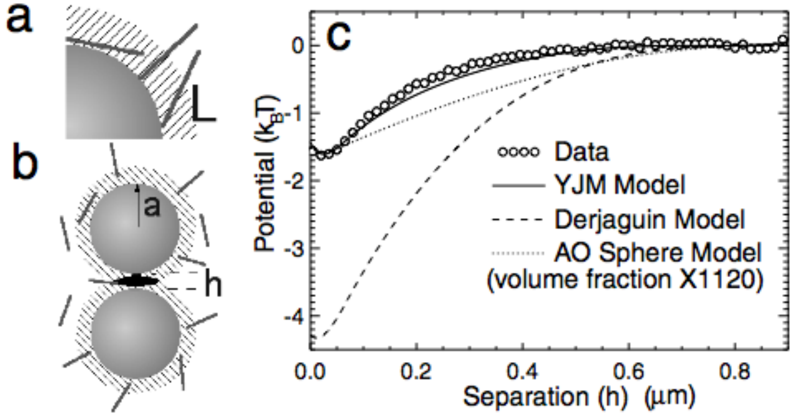

TIRM, rigid rods

Helden, L.; Roth, R.; Koenderink, G. H.; Leiderer, P.; Bechinger, C. *Phys. Rev. Lett.* 2003, 90, 48301.

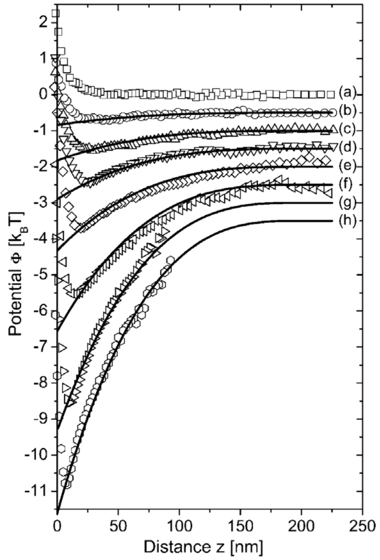

Optical micromanipulation

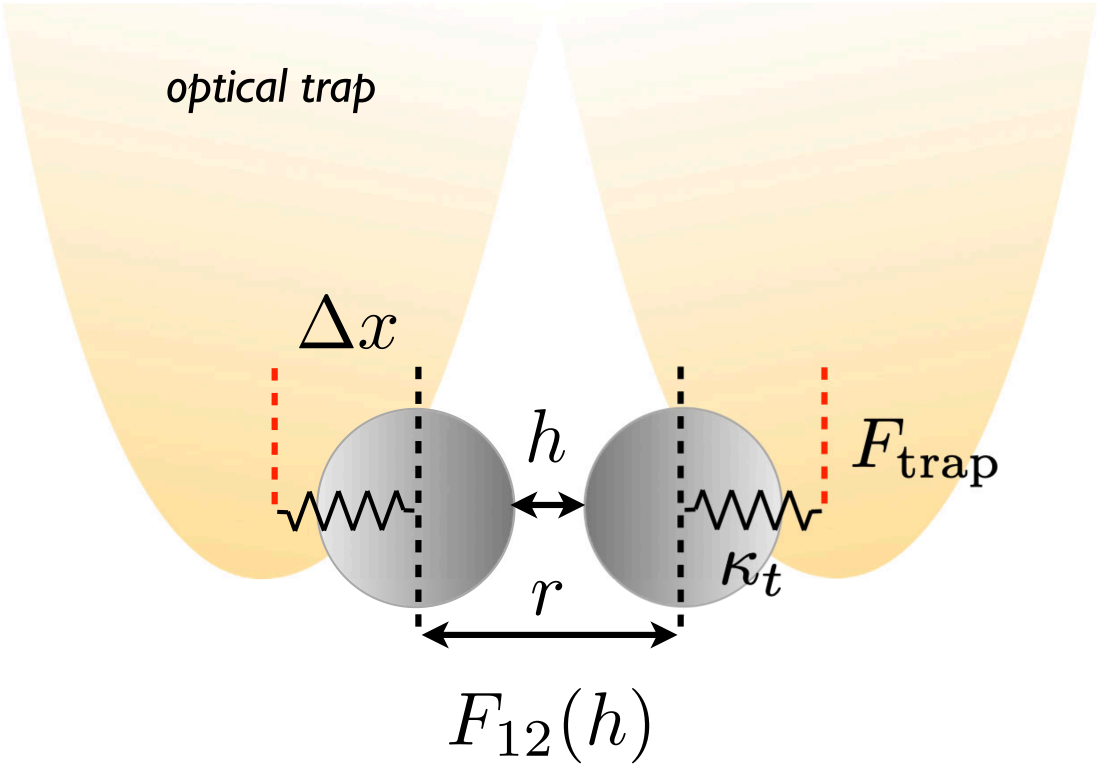

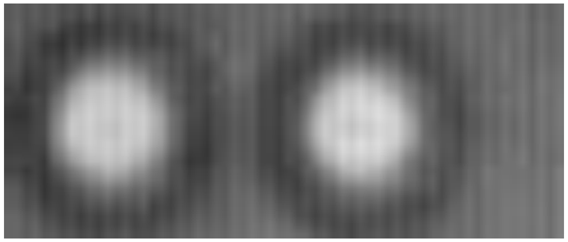

Radiation forces

Photon momentum

$$\mathbf{p} = \hbar \mathbf{k}$$

$$|\mathbf{k}| = 2\pi/\lambda$$

Radiation pressure acting on macroscopic surface

$$P_{rad} \sim 2qI_0/c$$

$$I_0 = 1000 \mathrm{W/m^2}$$

$$q = 0.1$$

$$\underline{\approx 10^{-8} \mathrm{N/m^2}}$$

Radiation force exerted on micrometer diameter particle

Particle diameter $2a = 1 \mu m$

Laser power $10 \mathrm{mW}$

$$F_{rad} \approx 10^{-11} \mathrm{N}$$

$$kT/a \approx 10^{-14} \mathrm{N}$$

$$\underline{F_{rad} \sim 10^3 kT/a}$$

Radiation forces in a Gaussian beam

A. Ashkin. Phys. Rev. Lett., 24:156–159, 1970.
A. Ashkin. Proc. Natl. Acad. Sci. USA, 94:4853–4860, 1997.

Collimated TEM_{00}

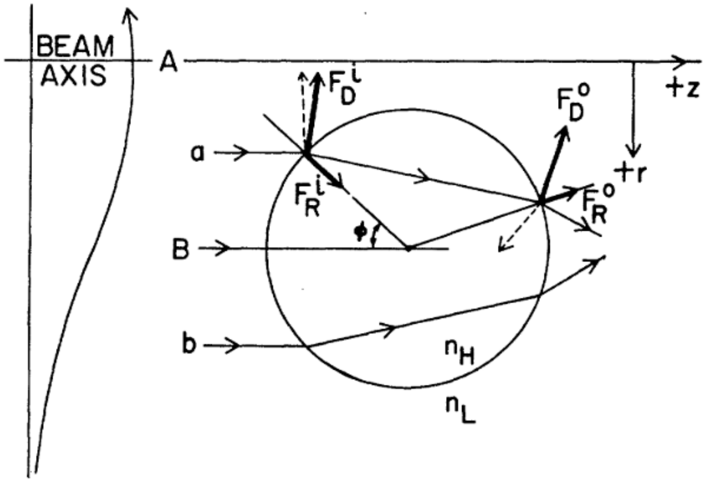

Ray a

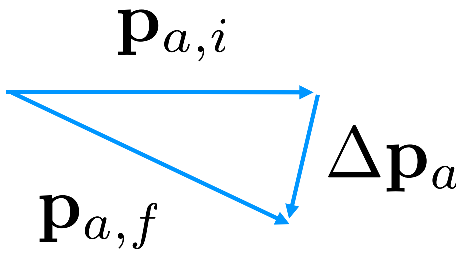

Ray b

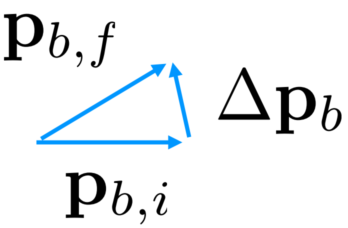

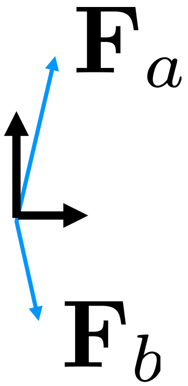

Resultant force imparted on particle

Focused Gaussian beam

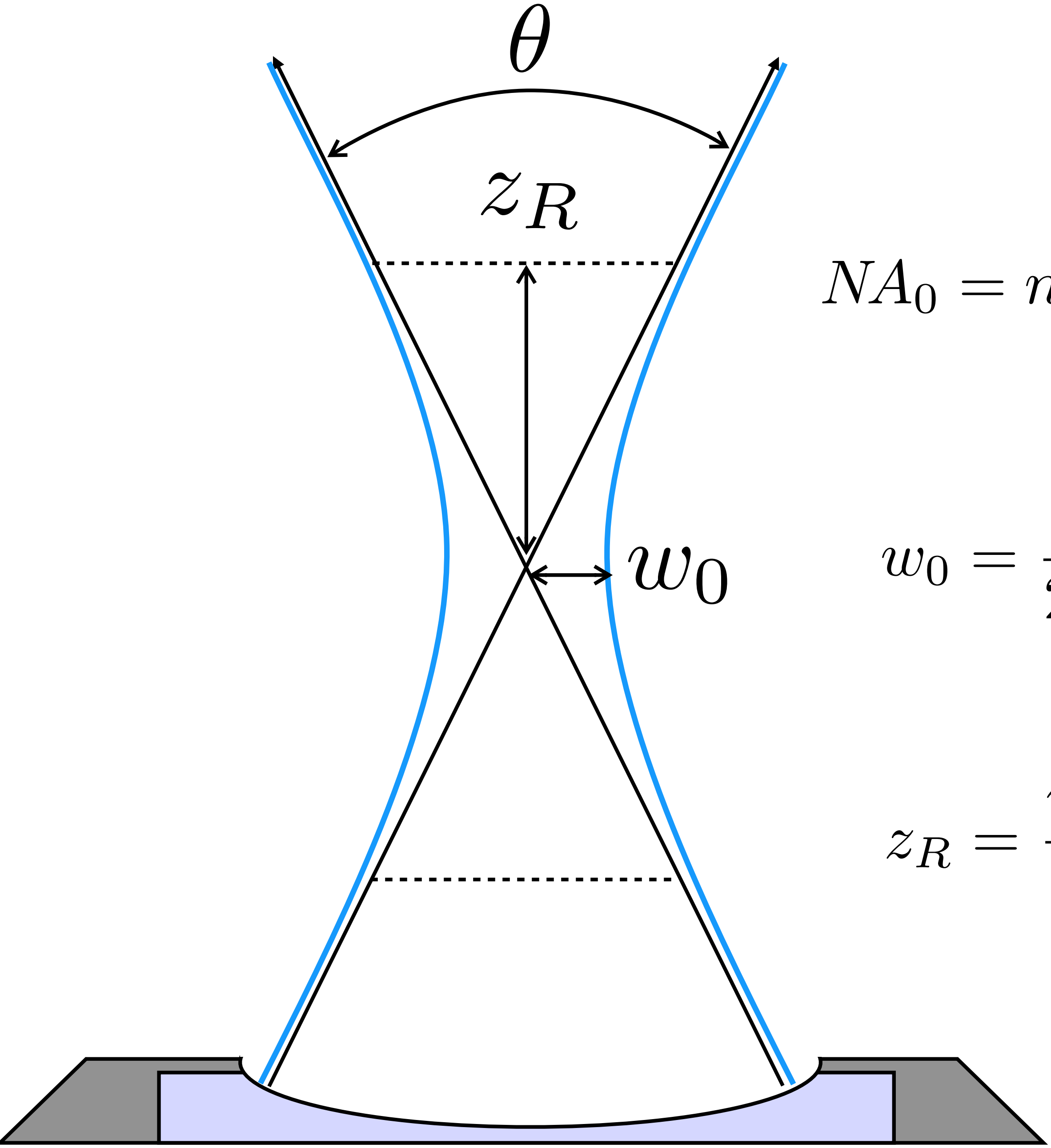

$$NA_0 = n \sin\theta$$ Numerical aperture

$$w_0 = \frac{\lambda}{2NA_0}$$ Diffraction limited beam width

$$z_R = \frac{\pi n w_0^2}{\lambda}$$ Rayleigh length

J. Mertz. *Introduction to Optical Microscopy*.
Roberts, Greenwood Village, Colorado, 2010.

Radiant field

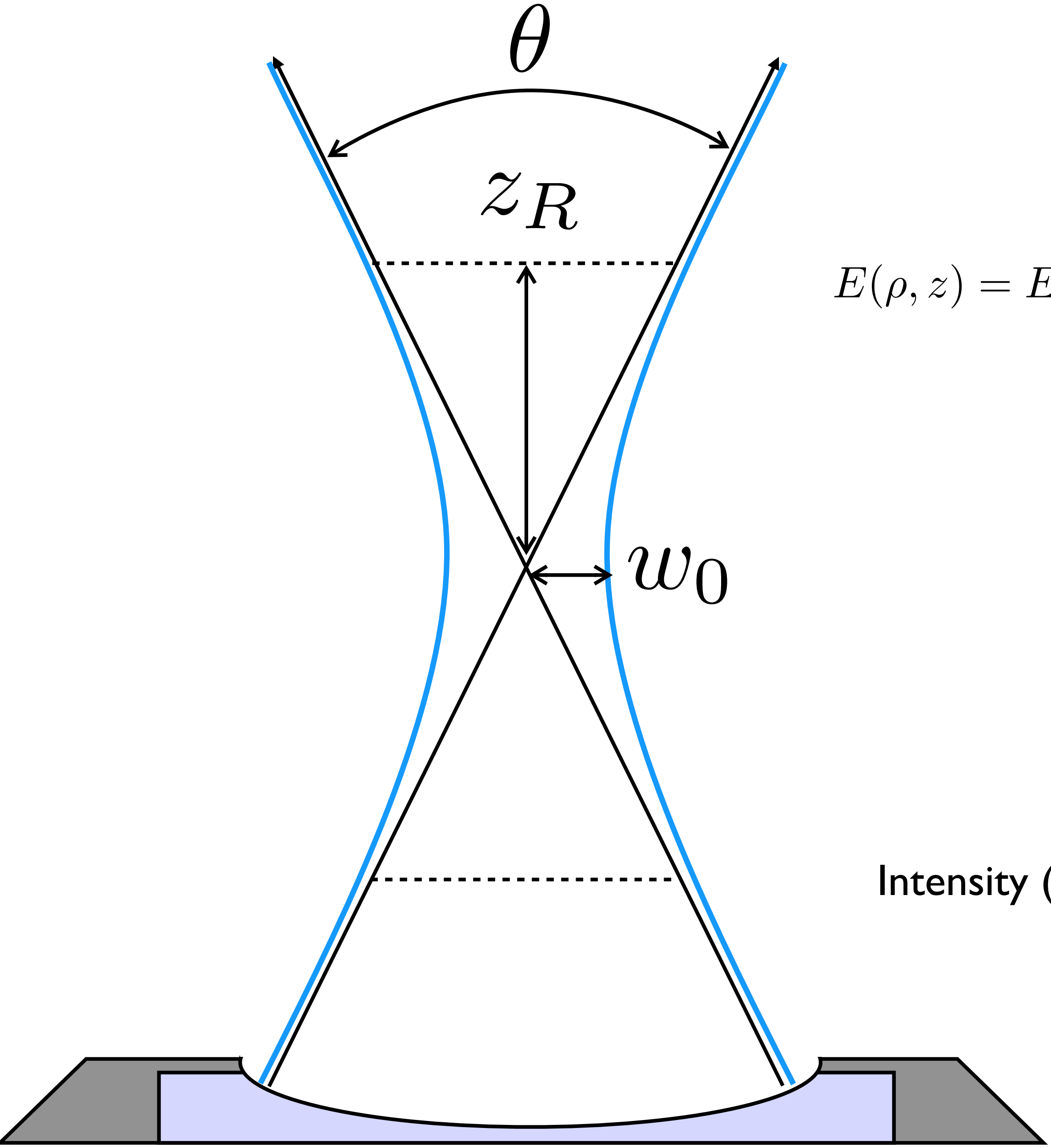

Radiant field

$$E(\rho, z) = E_0 \frac{w_0}{w(z)} e^{i2\pi\kappa z} e^{-\rho^2/w(z)^2} e^{i\pi\kappa\rho^2/R(z)} e^{-i\eta(z)}$$

$$w(z) = w_0\sqrt{1 + z^2/z_R^2}$$

$$R(z) = z\left(1 + z_R^2/z^2\right)$$

$$\eta(z) = \tan^{-1}(z/z_R)$$

$$\kappa = n/\lambda$$

Intensity (irradiance) $I(\rho, z) = \langle E(\rho, z)E^*(\rho, z)\rangle$

$$[=] W/m^2$$

J. Mertz. *Introduction to Optical Microscopy*.
Roberts, Greenwood Village, Colorado, 2010.

Density plot of beam intensity

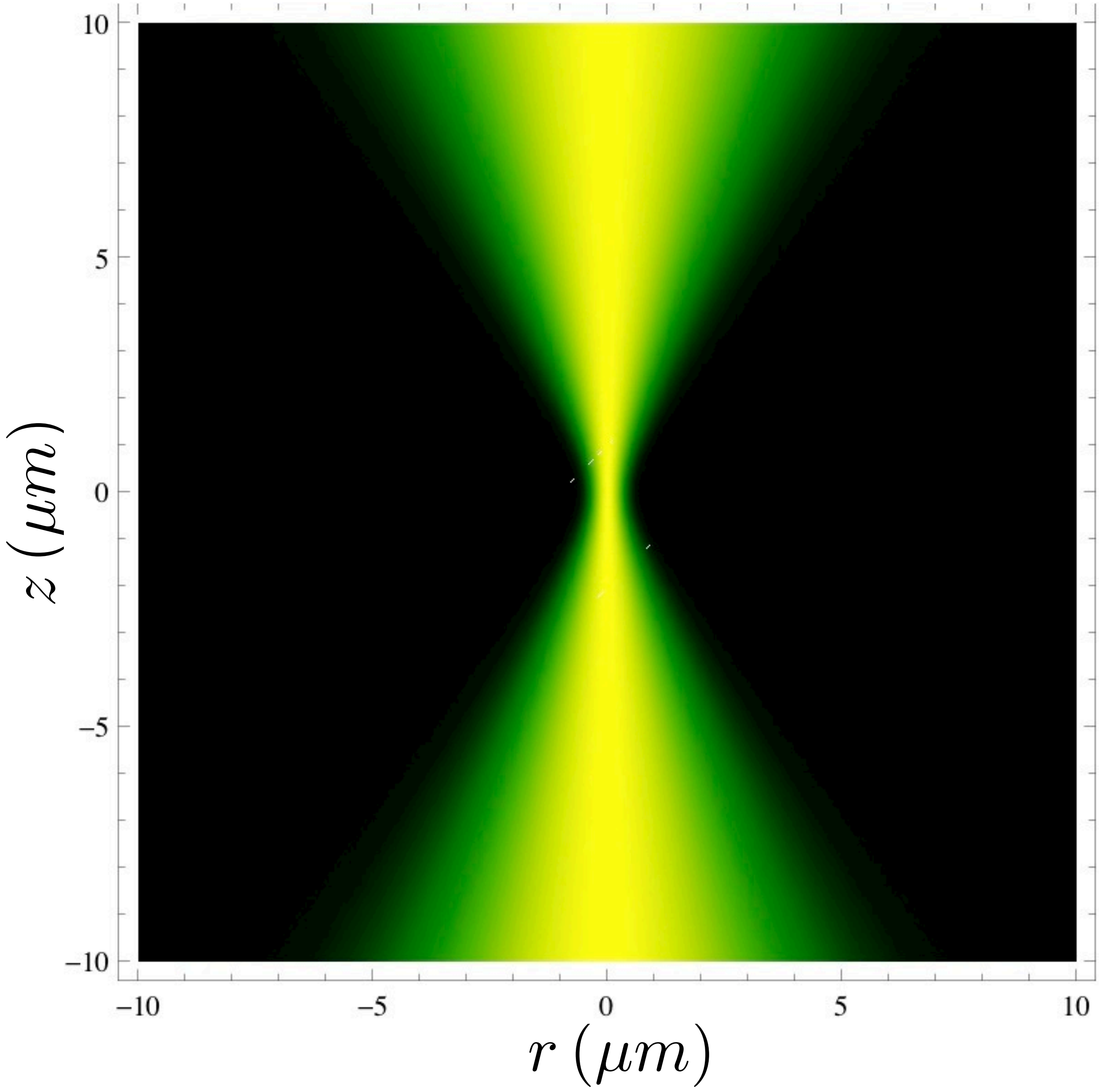

Typical values

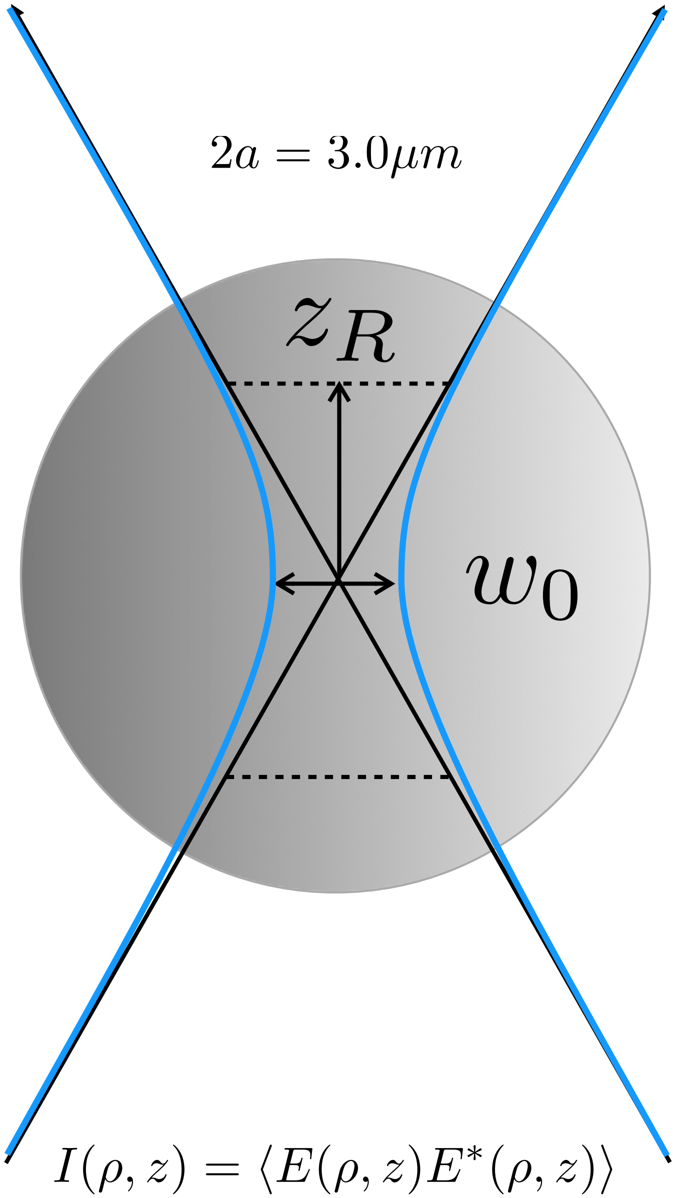

$$I(\rho, z) = \langle E(\rho, z) E^*(\rho, z) \rangle$$

$$\lambda_{vacuum} = 1064\text{nm}$$

$$NA_0 = 1.1$$

$$\theta = 58^\circ$$

$$w_0 = 0.48\mu m$$

$$z_R = 0.92\mu m$$

$$a > z_R$$

Beam diverges with full angle

Analyze in ray-optic regime

Gradient force trap

A. Ashkin, et al. Opt. Lett., 11:288–290, 1986.

Ray optic regime

$d \gg \lambda$

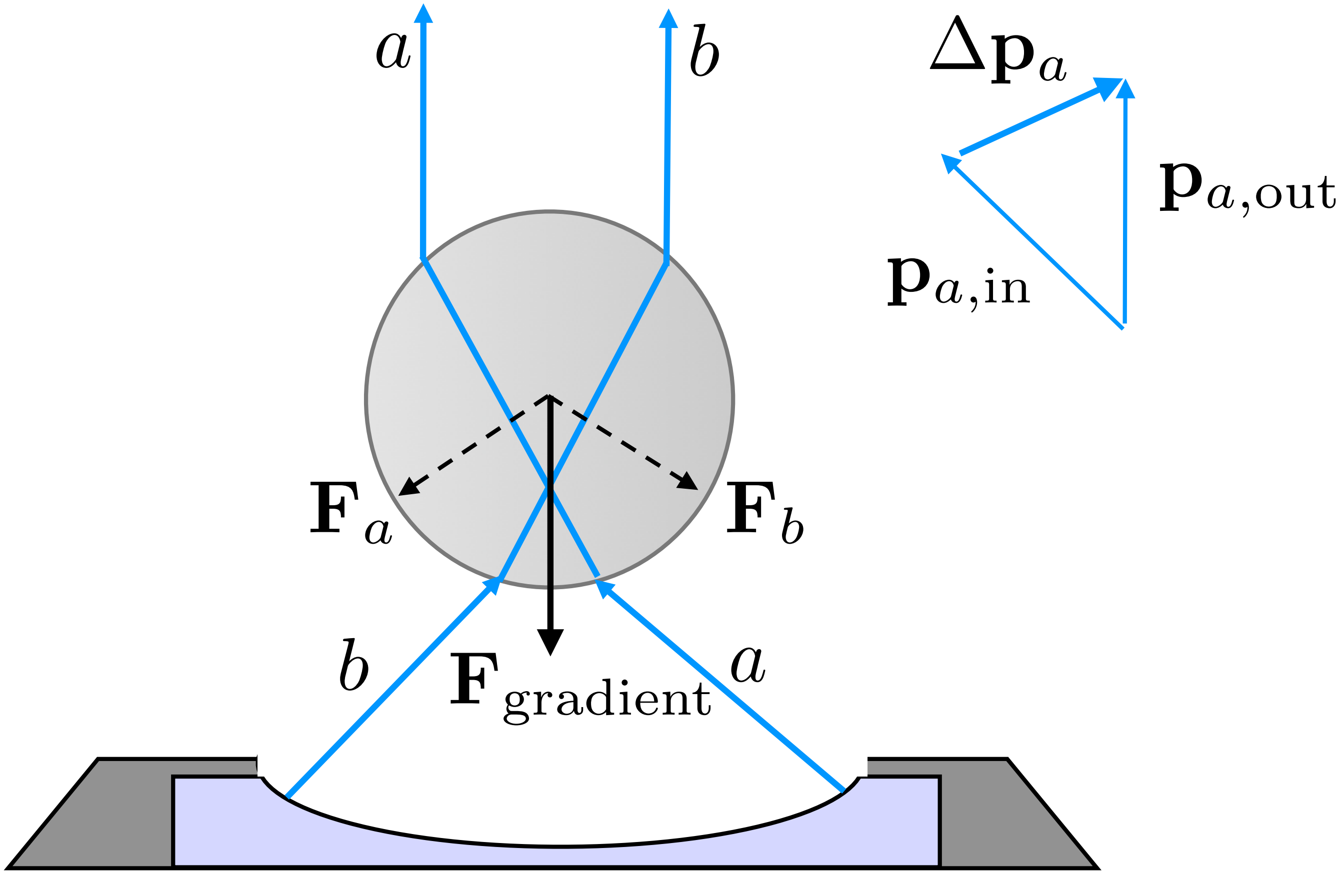

High NA objective

Gradient force trap

Ray optic regime

$d \gg \lambda$

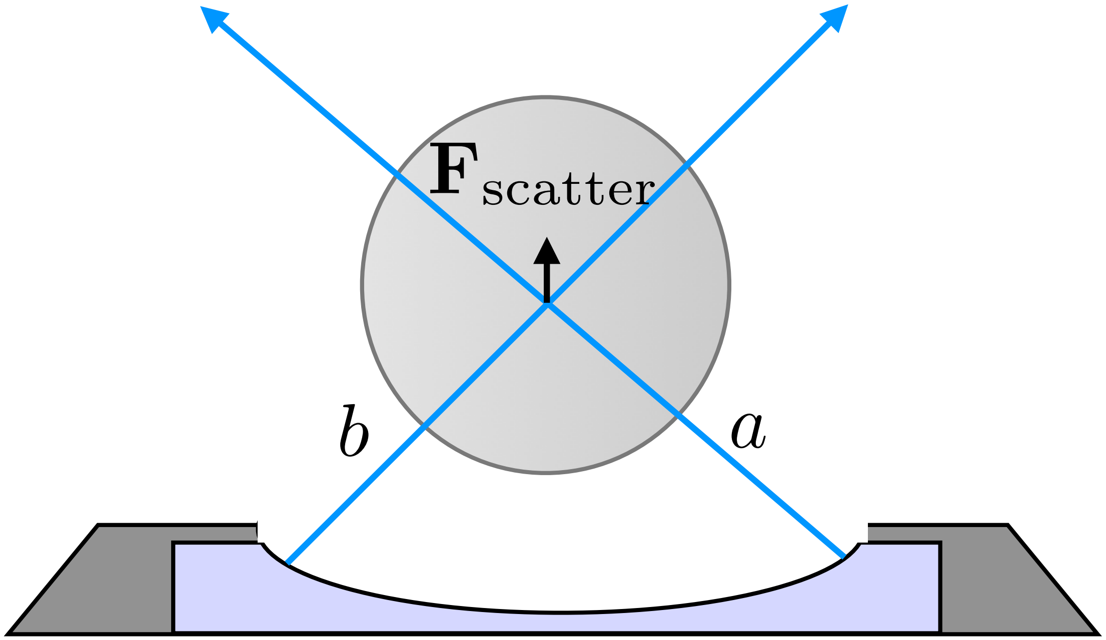

High NA objective

Lateral displacement

Ray optic regime

$$d \gg \lambda$$

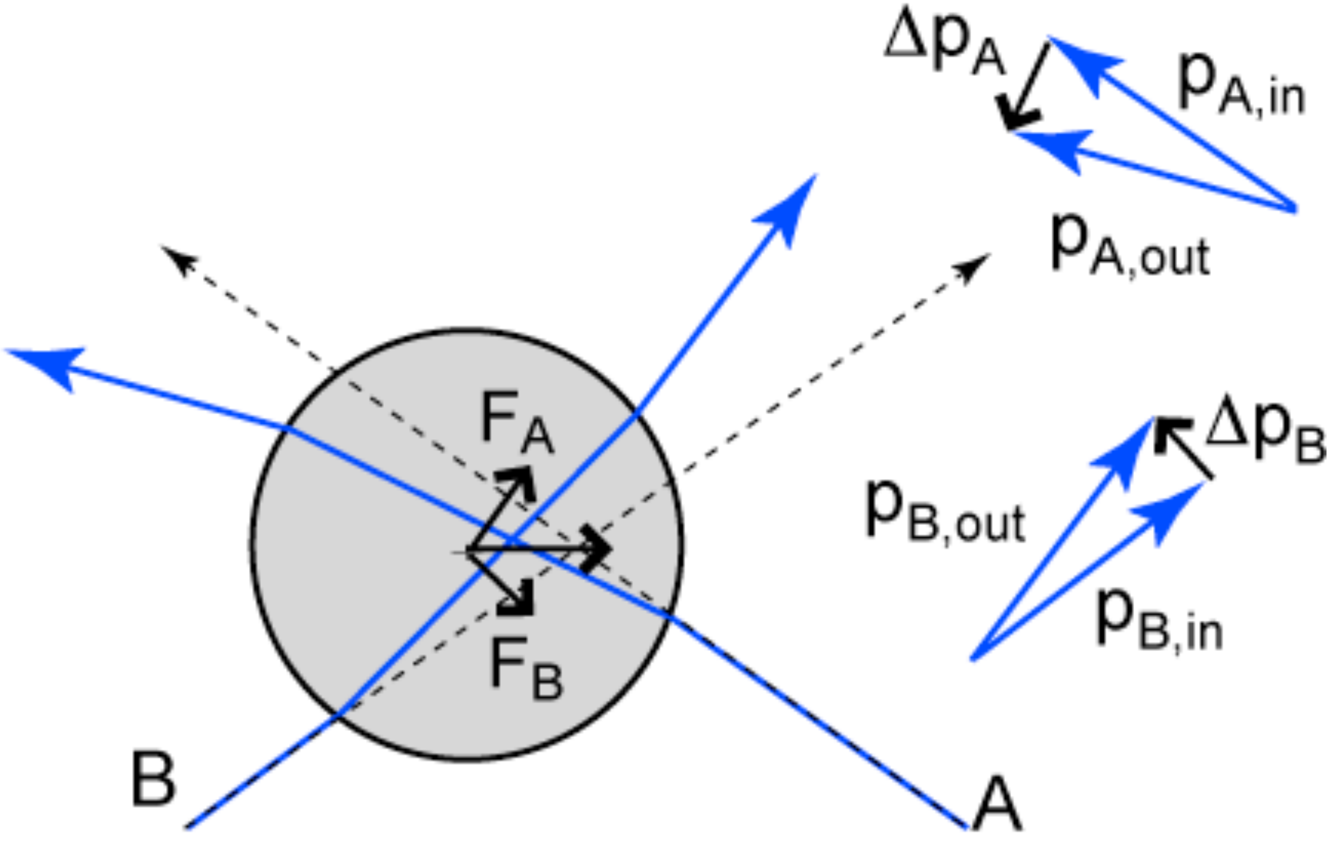

Rayleigh regime

$$d \ll \lambda$$

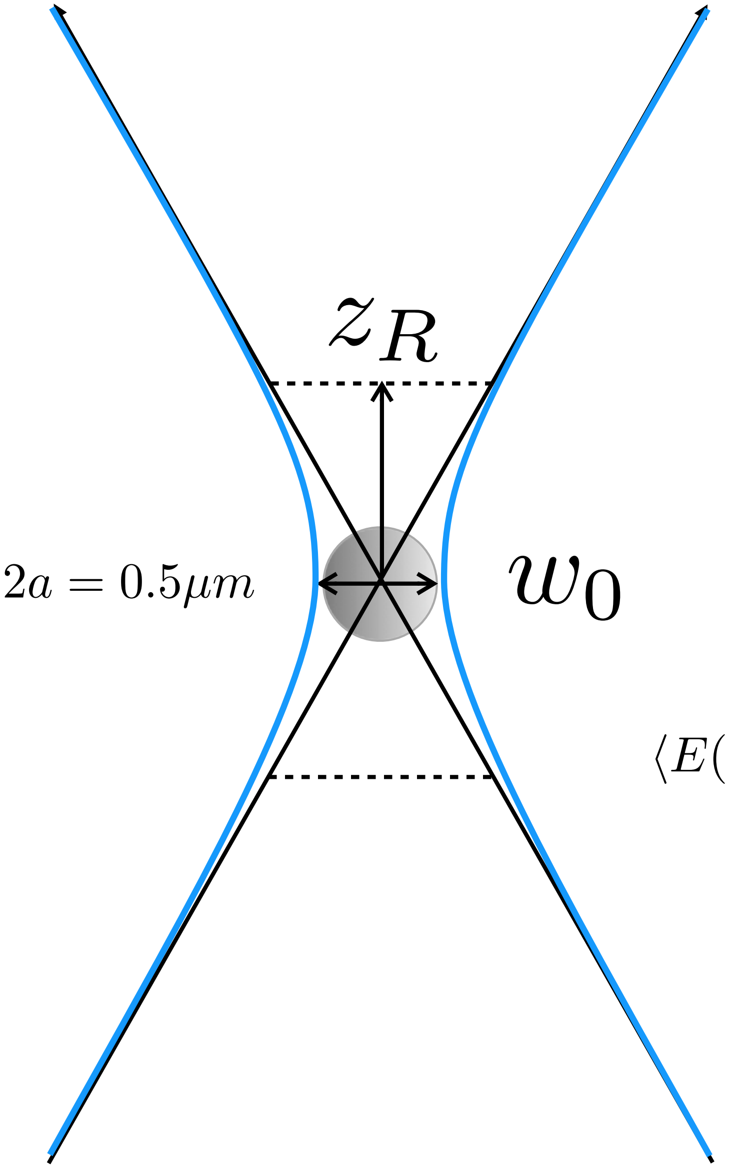

Induced dipole $\mathbf{p} = \alpha \mathbf{E}$

Energy and force $U = -\mathbf{p} \cdot \mathbf{E}$ $\mathbf{F} = \nabla(\mathbf{p} \cdot \mathbf{E})$

$$\mathbf{F}_{gradient} = 2\pi\epsilon\epsilon_0 \Re\{\alpha(\omega)\} a^3 \nabla \langle E(\rho, z) E^*(\rho, z) \rangle$$

$$\mathbf{F}_{gradient} = \frac{4\pi\epsilon_0 a^3}{c} \left[\frac{n_p^2 - n_s^2}{n_s(n_p^2 + 2n_s^2)} \right] \nabla I$$

$$\langle E(\rho, z) E^*(\rho, z) \rangle = \frac{2I(\rho, z)}{cn_s\epsilon_0} = \left(\frac{2}{cn_s\epsilon_0} \right) \left(\frac{I_0 e^{-2\rho^2/w(z)^2}}{1 + z^2/z_R^2} \right)$$

$$w(z) = w_0 \sqrt{1 + z^2/z_R^2}$$

Important parameters for optical trapping

The ability to optically trap a particle depends on:

The particle size and shape

The refractive index contrast between the particle and medium

The amount of light absorbed by the particle and sample

The laser wavelength

The laser power

The quality of the beam and focus

The laser mode (Gaussian, Laguerre-Gaussian, etc.)

“Steady drag” measurements

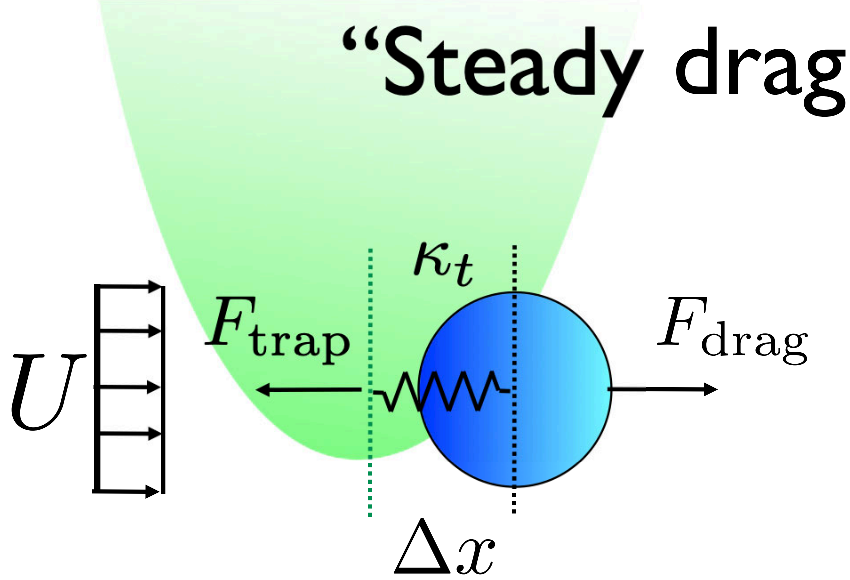

$$F_{\mathrm{drag}} = 6\pi a \eta U = \kappa_t \Delta x$$

$$F_{\mathrm{drag}} > F_{t,\mathrm{max}}$$

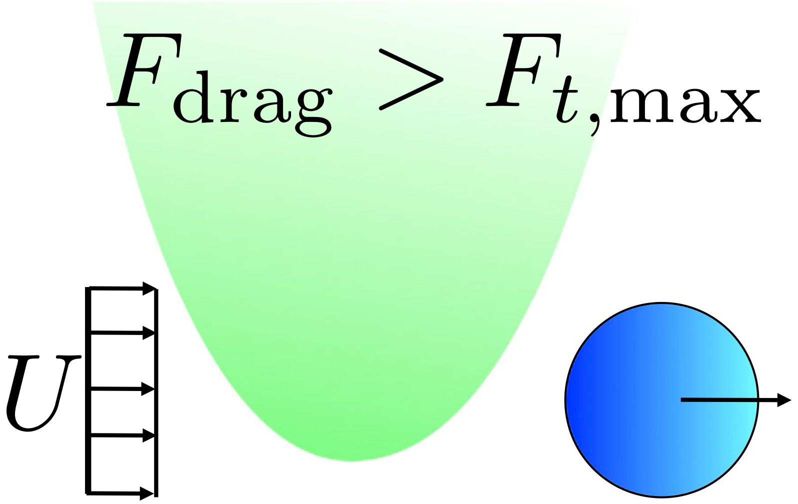

Calibration, 3.2μm PS in water

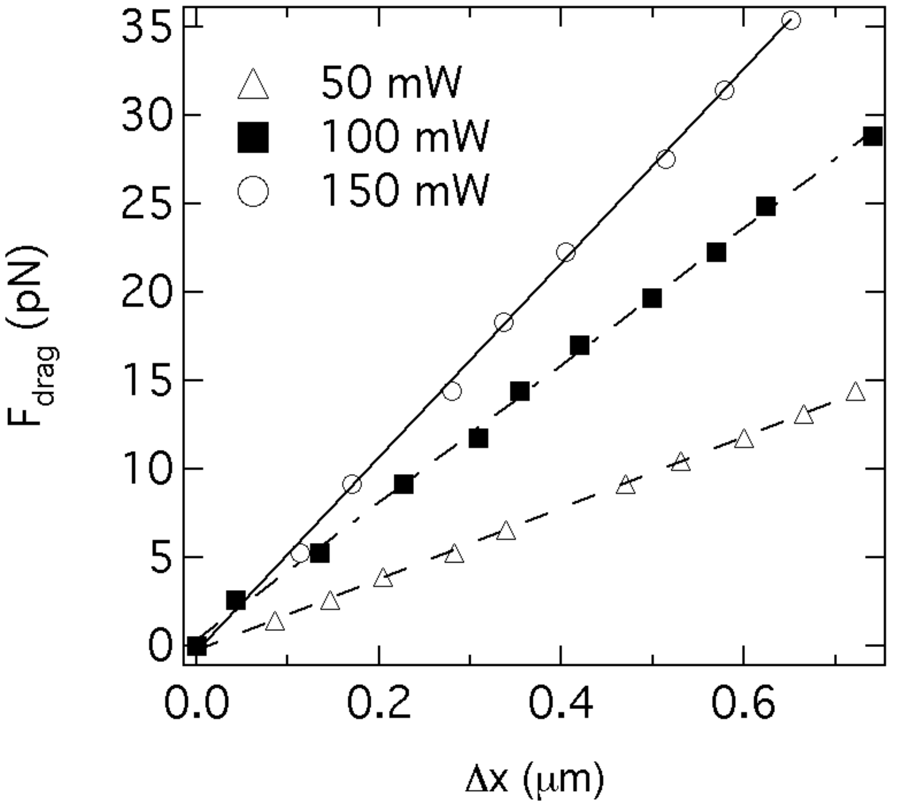

$$\kappa_t = 10 - 60 \text{ pN}/\mu m$$

Optical tweezer calibration

1 µm polystyrene, Nd:YAG (λ=1064nm)

R. M. Simmons, J. T. Finer, S. Chu, and J. A. Spudich. Biophys. J., 70:1813–1822, 1996.

Trap stiffness

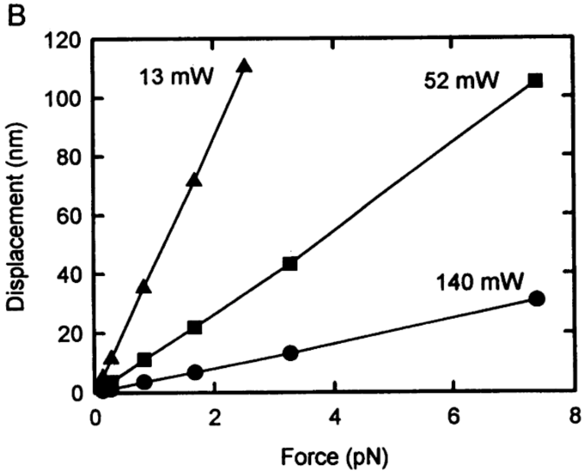

Escape force

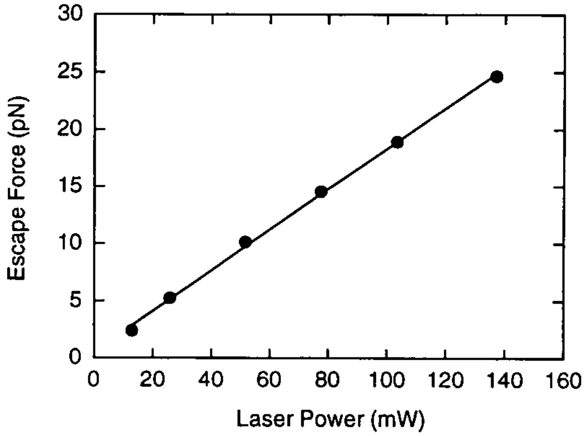

Particle size dependence

$$\kappa_T \sim a^3$$ Rayleigh regime

Plateaus in ray-optic

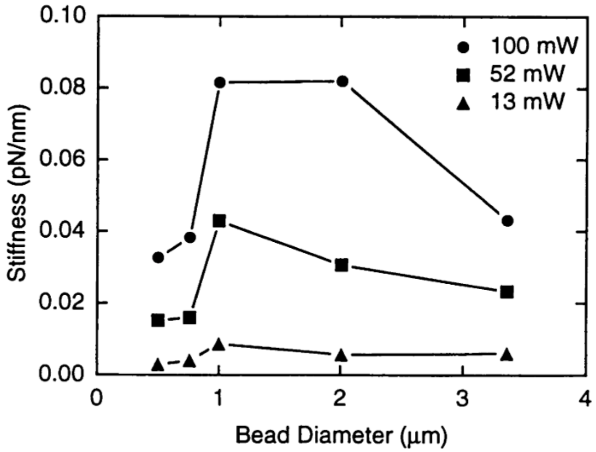

Trap calibration–power spectral method

- Use power spectral density (PSD) from photodiode detector
- Fit corner frequency to find trap stiffness, α
- Langevin equation

$$\beta\dot{y} + \alpha y = F(t)$$

- PSD & corner frequency

$$S_{yy} = \frac{kT}{2\pi\beta(f_0^2+f^2)}$$

$$f_0 = \alpha(2\pi\beta)^{-1}$$

Force calibration, 0.6μm silica particle

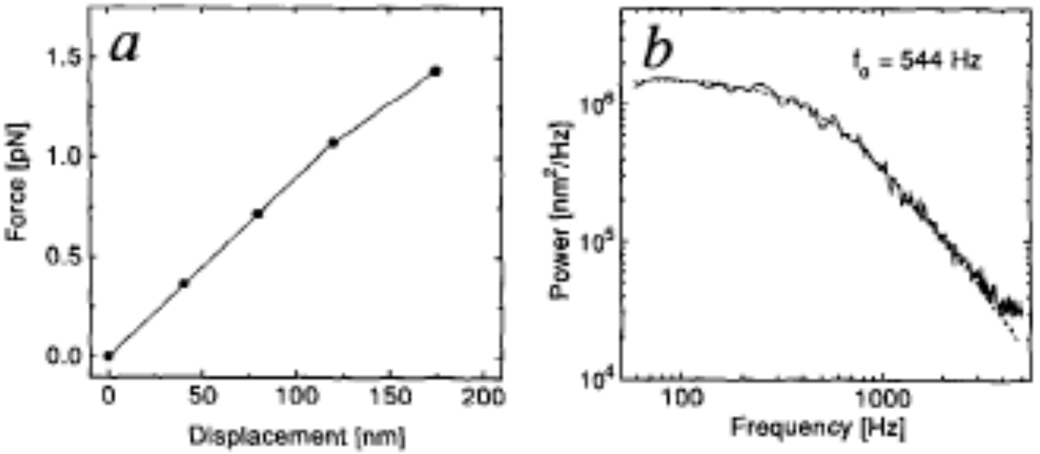

Figure 10 Force calibration of an optical trap. (*a*) Force versus displacement for a trapped silica bead (diameter ~0.6 μm; power ~14 mW), calibrated according to Equations 14 and 15 ($x_o = 2$ μm; $\beta = 5.7 \times 10^{-6}$ pN s/nm). Stiffness is constant out to 150 nm ($\alpha = 9.0 \times 10^{-3}$ pN/nm), beyond which it decreases. (*b; Solid line*) The thermal noise spectrum of a trapped silica bead measured with the optical trapping interferometer (diameter ~0.6 μm; power ~28 mW). (*Dotted line*) The fit by a Lorentzian. The corner frequency of the Lorentzian (544 Hz) implies $\alpha = 1.9 \times 10^{-2}$ pN/nm.

Adapted from K. Svoboda and S.M. Block, 1994.

Optical tweezer experiment

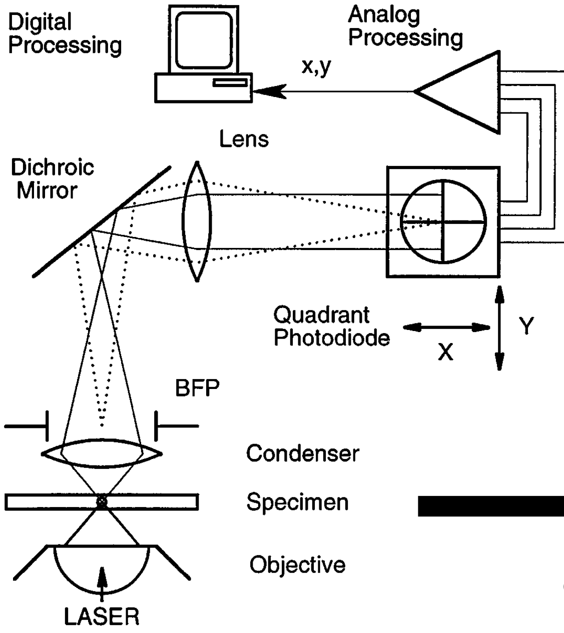

Back focal plane detection

Laser tweezer apparatus

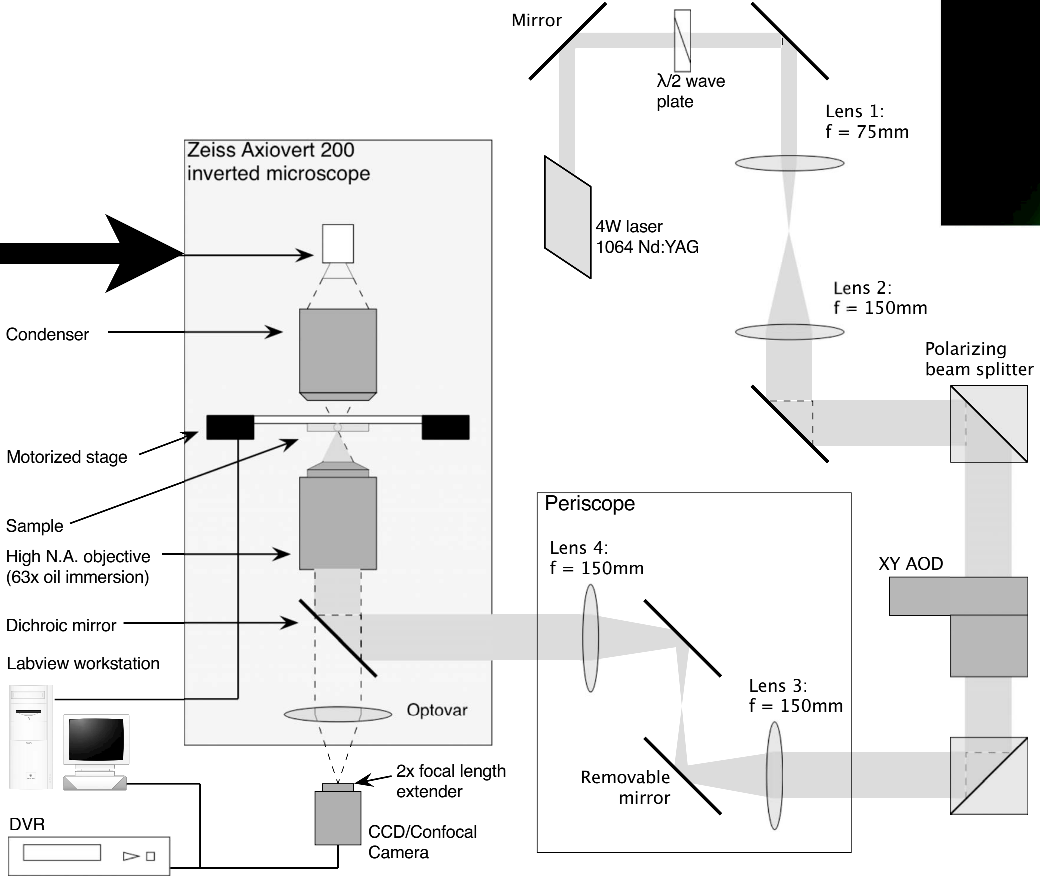

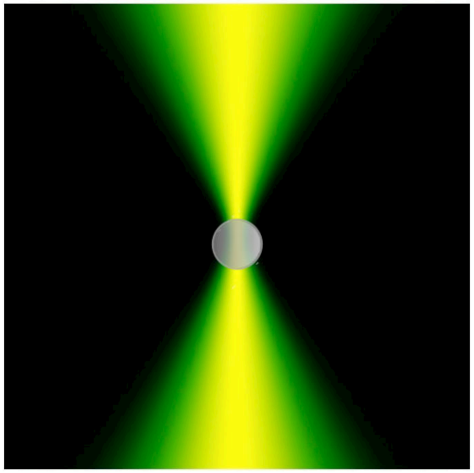

Measurement of particle position: Back focal plane detection

Scattered light collected by condenser is imaged onto a quadrant photodiode

Spatial resolution ~ nm,

Frequency response ~ 10kHz

Source can be trap laser or co-aligned laser

Fixed vs. moving reference frame

Can be extended to two independent beams by splitting polarization

Bandwidth improved using non-Si detectors

Gittes and Schmidt, Optics Lett. 23:7, 1998.
Peterman et al., Rev. Sci. Instrum. 74:3246, 2003.

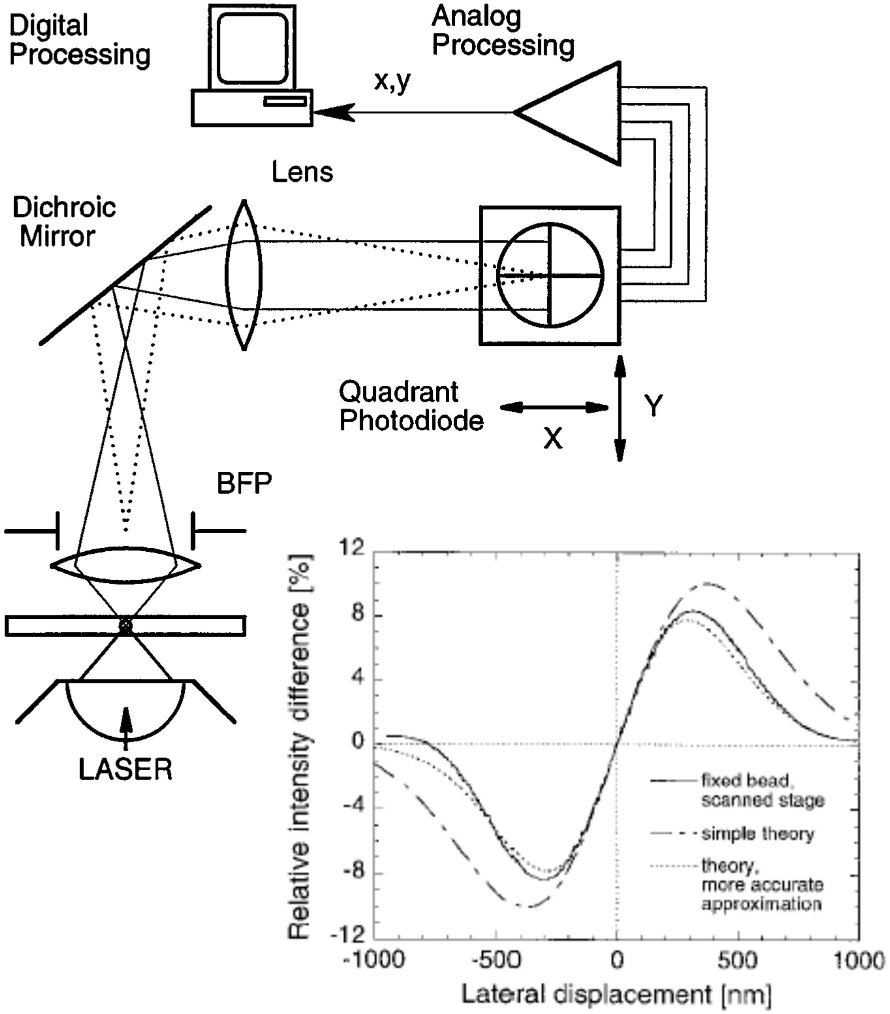

Rupturing “bonds” between colloids

Swan, J. W., Shindel, M. & Furst, E. M. *Phys. Rev. Lett.* 109, 198302 (2012).

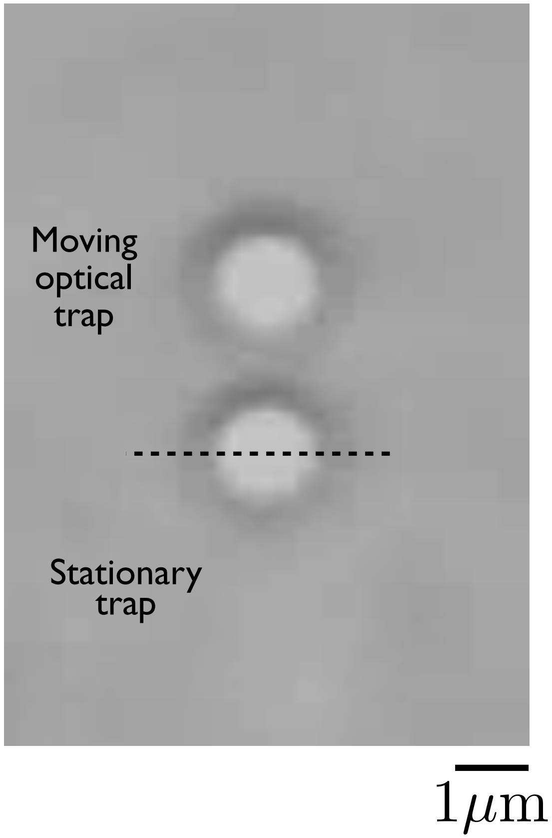

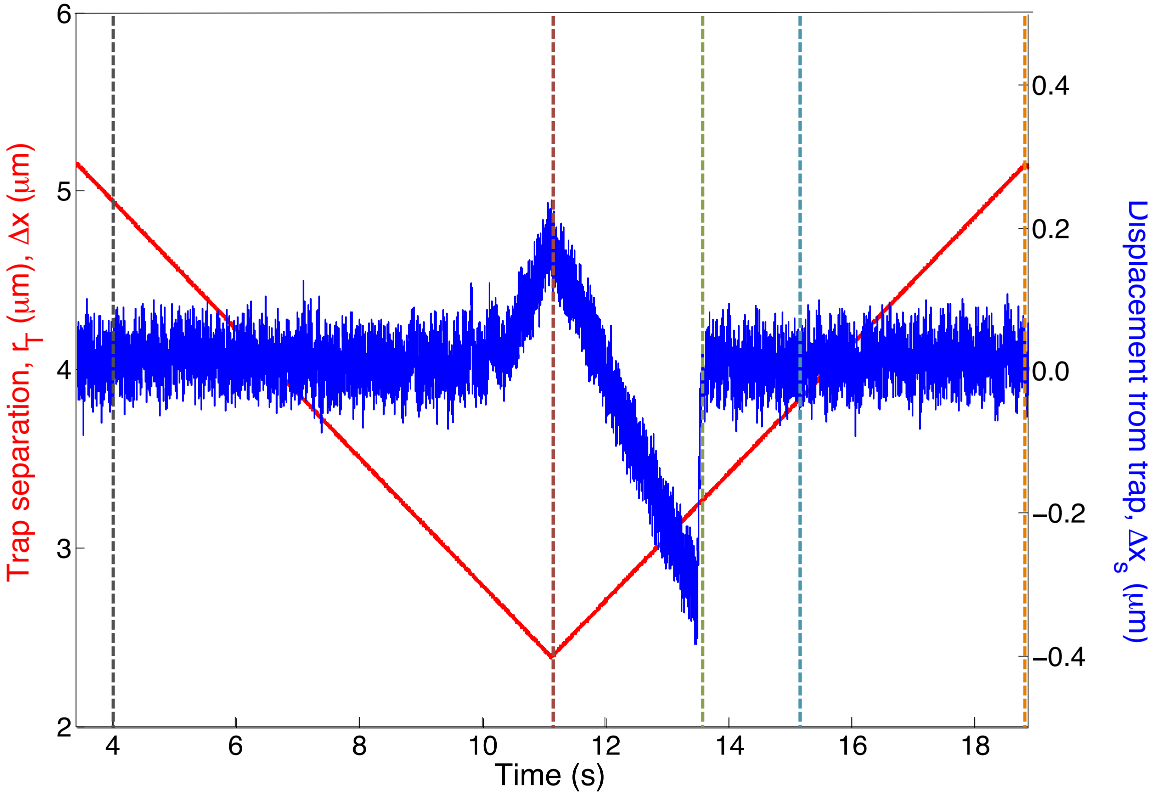

Measuring thermal rupture forces

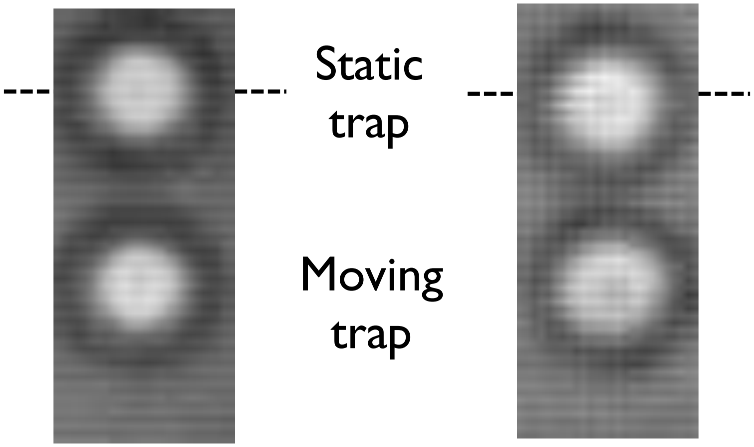

$c/c^* = 0$ $c/c^* = 0.83$

A single bond rupture

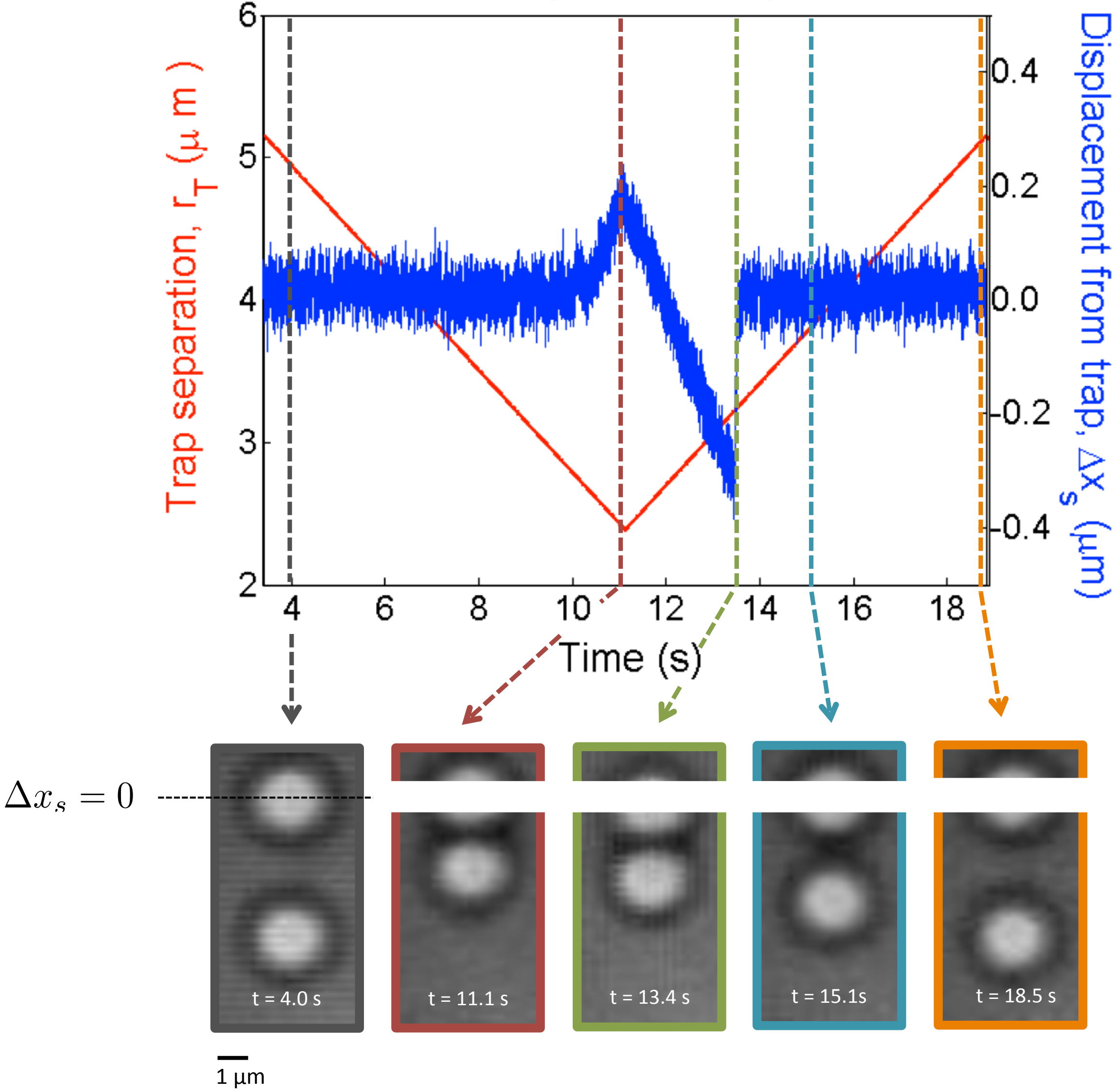

Repeated cycles

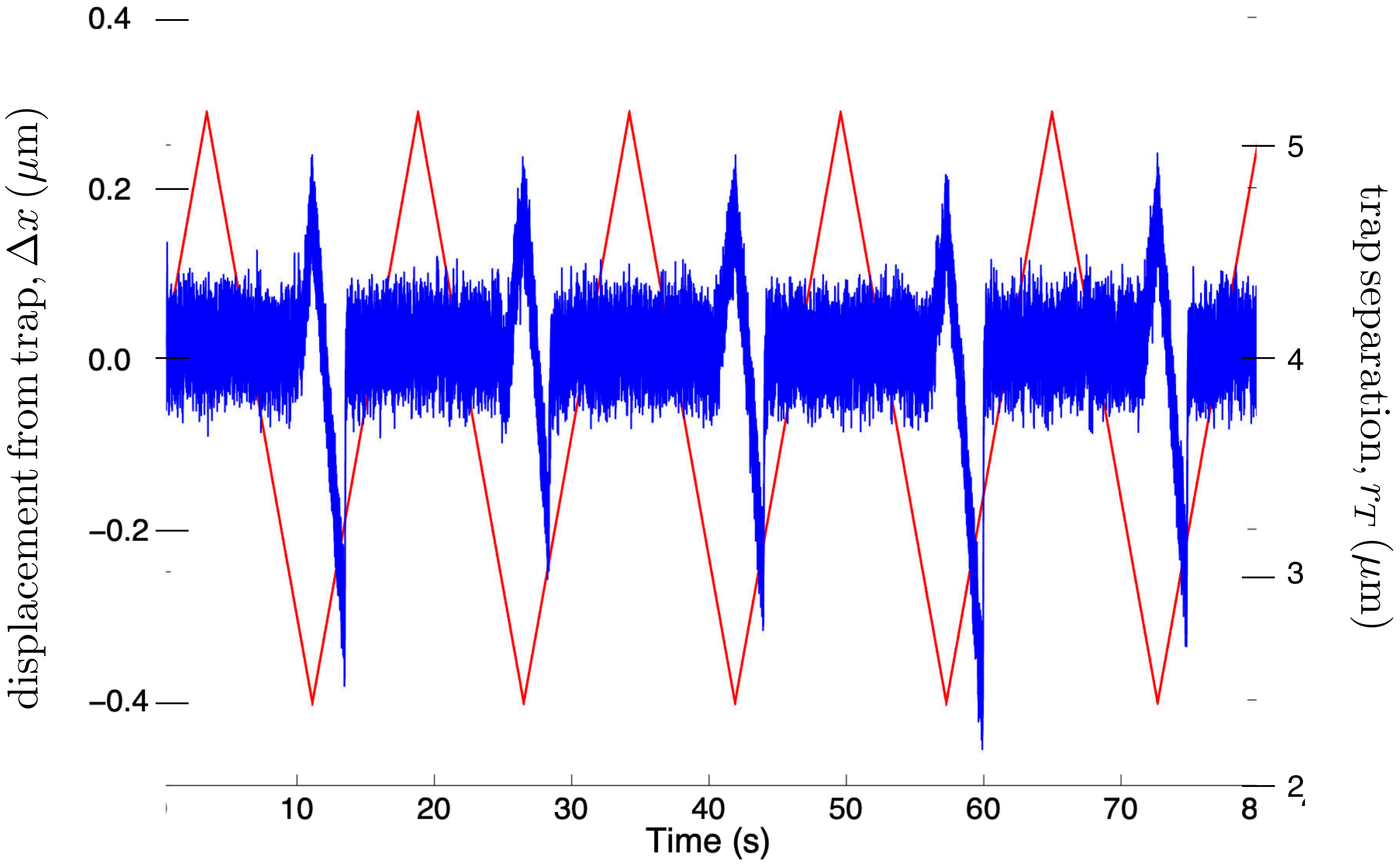

Multiple trajectories

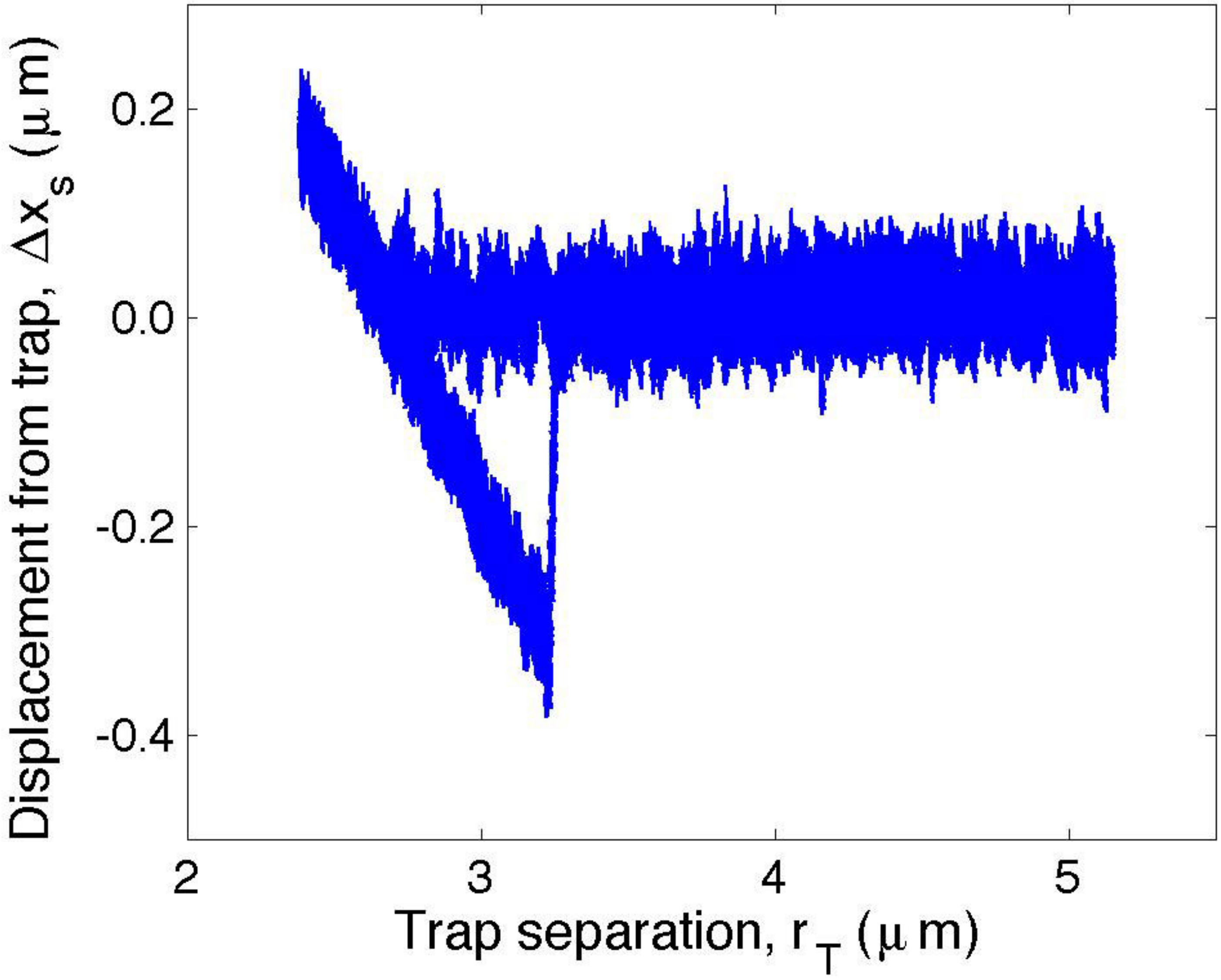

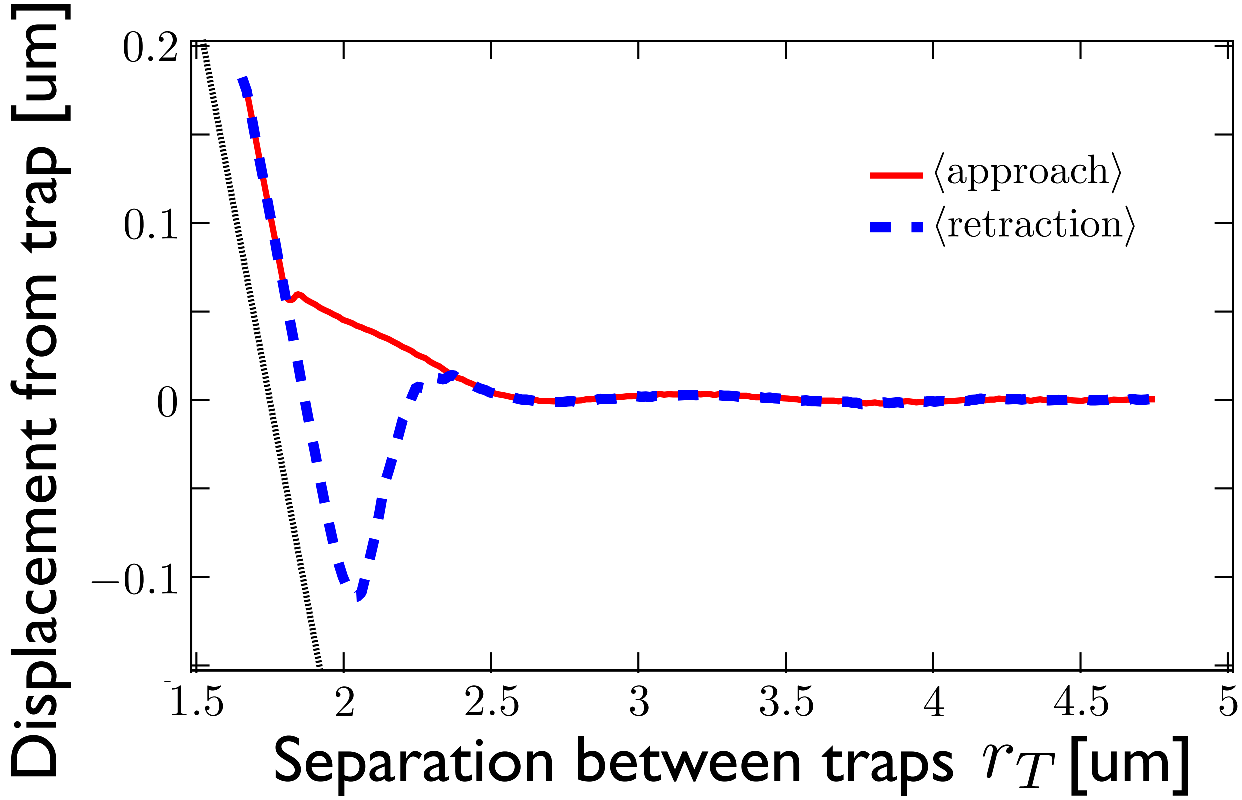

Swan, J. W., Shindel, M. & Furst, E. M. *Phys. Rev. Lett.* 109, 198302 (2012).

Two state trajectory model

$$\text{retraction} = \begin{cases} -r_T & \text{with } P(r_T) \\ \langle\text{approach}\rangle & \text{with } 1 - P(r_T) \end{cases}$$

bonded

ruptured

Probability of being bonded

$$P(r_T) = \frac{\langle\text{retraction}\rangle - \langle\text{approach}\rangle}{(-r_T) - \langle\text{approach}\rangle}$$

Thermal rupture force distribution

Swan, J.W., Shindel, M. & Furst, E. M. *Phys. Rev. Lett.* 109, 198302 (2012).

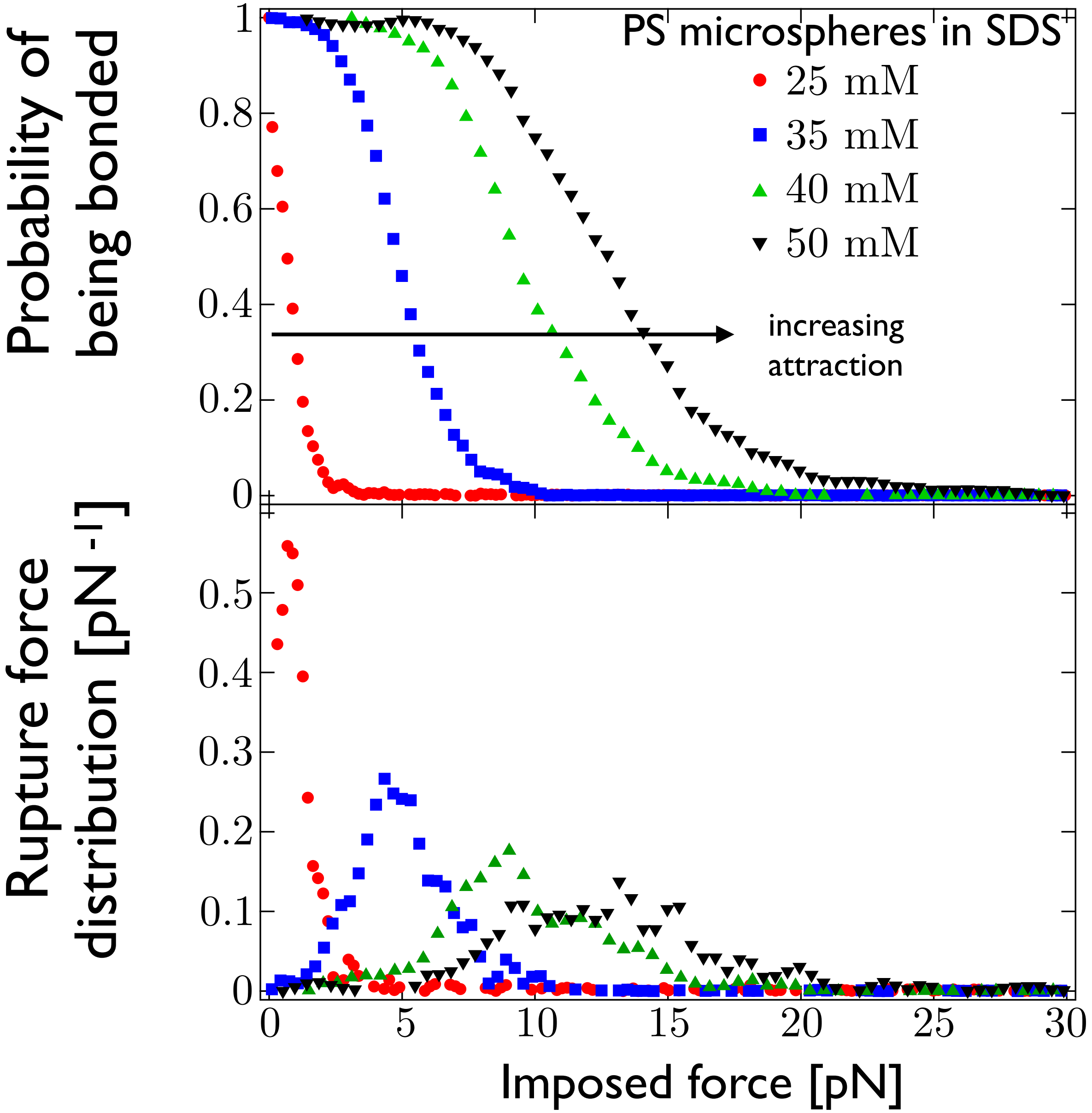

PMMA rupture distribution c/c* = 0.81

Hsiao, L. C.; Solomon, M. J.; Whitaker, K. A.; Furst, E. M., *J. Rheology* 2014, 58, 1485–1504.

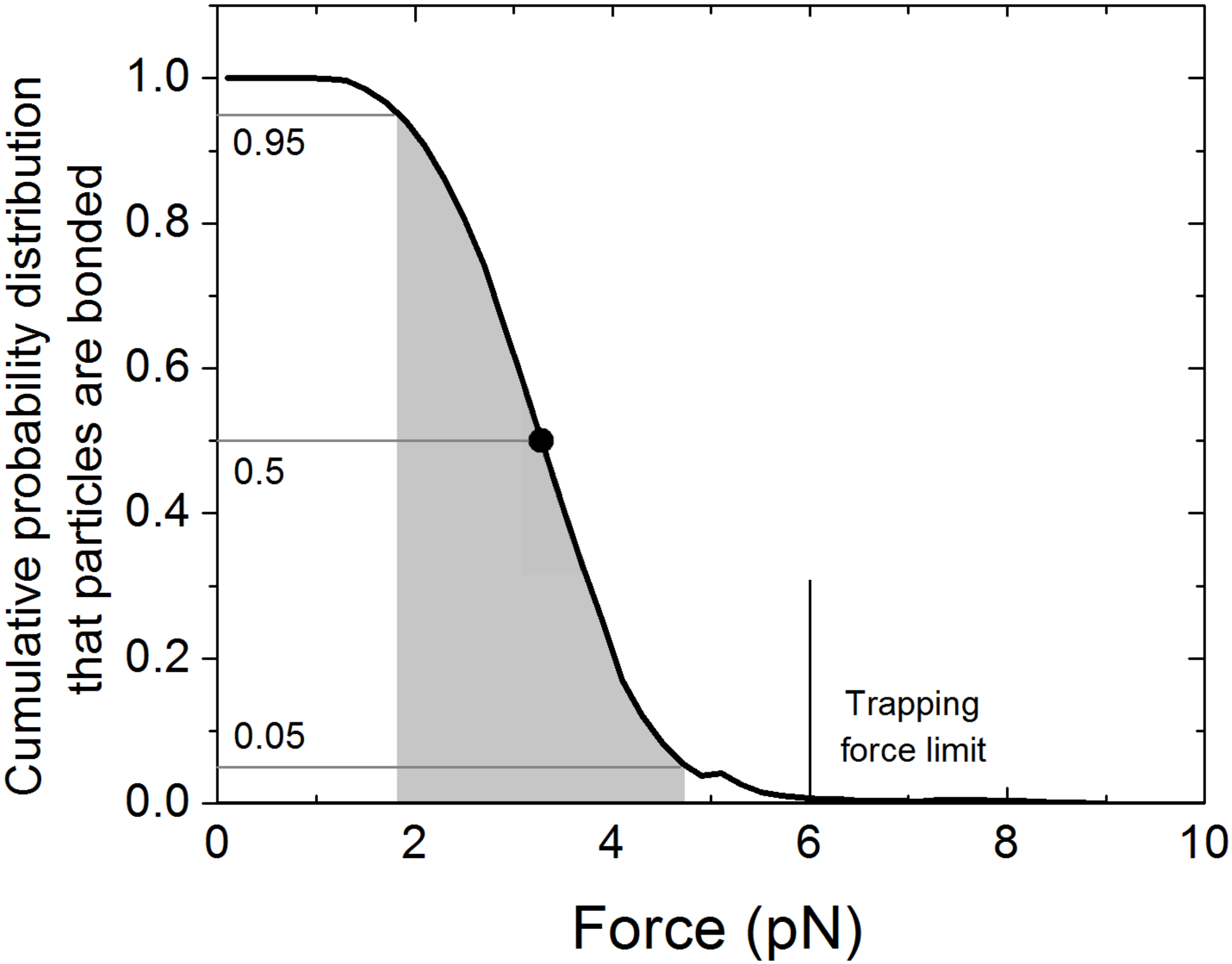

PHSA-PMMA in 75%/25% (v/v) cyclohexane/cyclohexyl bromide

Thermal model of bond rupture

Whitaker, K. A. & Furst, E. M. *J. Rheology* 60, 517–529 (2016).

H.A. Kramers. *Physica*, 7(4):284–304, 1940.
P. Hanggi, P. Talkner and M. Borkovec. *Reviews of Modern Physics*, 62(2):251–341, 1990.

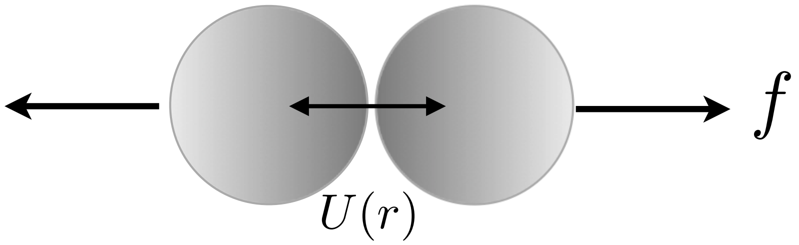

$$F = U(r) - fr$$

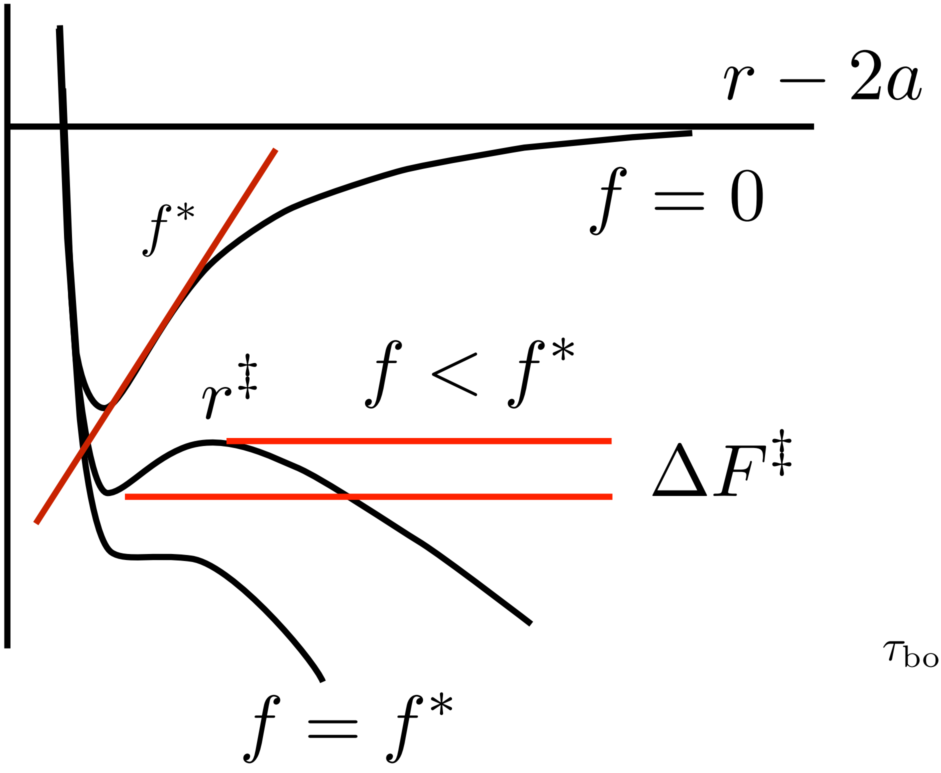

Mean first-passage time

$$\partial P/\partial t = -\mathbf{\nabla} \cdot \mathbf{D} \cdot [(\mathbf{f} - \mathbf{\nabla} U)P/kT - \mathbf{\nabla} P]$$

$$\frac{1}{\tau_{\mathrm{bond}}} = j_+ = D_r \left[\left(f - \frac{dU}{dr} \right) \frac{P}{kT} - \frac{dP}{dr} \right]$$

$$j_+ = -D_r \left[\frac{dP}{dr} + \frac{dF(r)}{dr} \frac{P}{kT} \right]$$

$$\tau_{\mathrm{bond}} = \frac{1}{j_+} = \int_{2a}^{r^\ddagger} e^{-F(r)/kT} \left[\int_{r}^{r^\ddagger} \frac{1}{D_r(y)} e^{F(y)/kT} dy \right] dr$$

$$D_r = \frac{2k_B T (r - 2a)}{3\pi a^2 \eta}$$

Thermal model of bond rupture

Whitaker, K. A. & Furst, E. M. *J. Rheology* 60, 517–529 (2016).

H.A. Kramers. *Physica*, 7(4):284–304, 1940.

P. Hanggi, P. Talkner and M. Borkovec. *Reviews of Modern Physics*, 62(2):251–341, 1990.

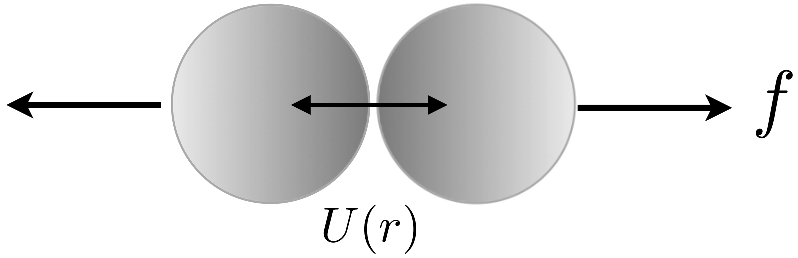

$$F = U(r) - fr$$

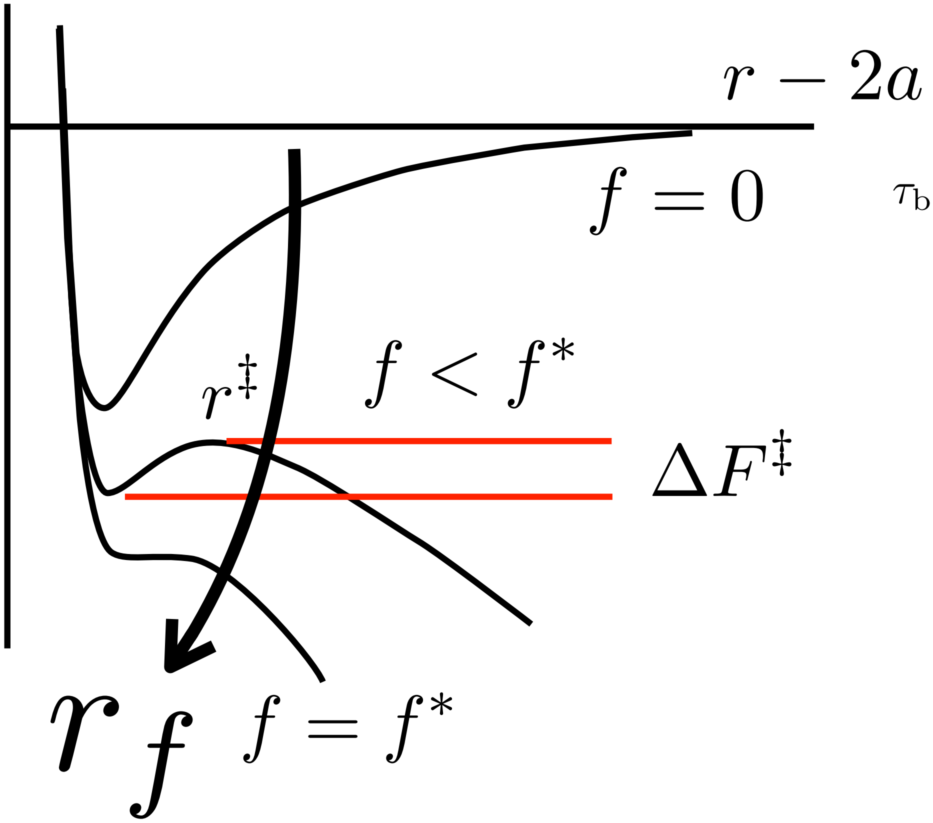

Bond lifetime

$$\tau_{\text{bond}} = \frac{1}{j_+} = \int_{2a}^{r^{\ddagger}} e^{-F(r)/kT} \left[\int_{r}^{r^{\ddagger}} \frac{1}{D_r(y)} e^{F(y)/kT} dy \right] dr$$

Rate of bond rupture | **Rate of loading**

$$\frac{dS_1}{dt} \approx -j_+ S_1 \longrightarrow r_f \frac{dS_1}{df} \approx -j_+ S_1$$

Cumulative bond probability distribution

$$S_1(f) = \exp\left(-\frac{1}{r_f} \int_0^f j_+(f) df \right)$$

DLVO+AO interaction potential

PHSA-PMMA 2a = 2.7 µm, R_g = 32 ± 2 nm, Steric brush length δ = 7 nm

R_g = 32 ± 2 nm

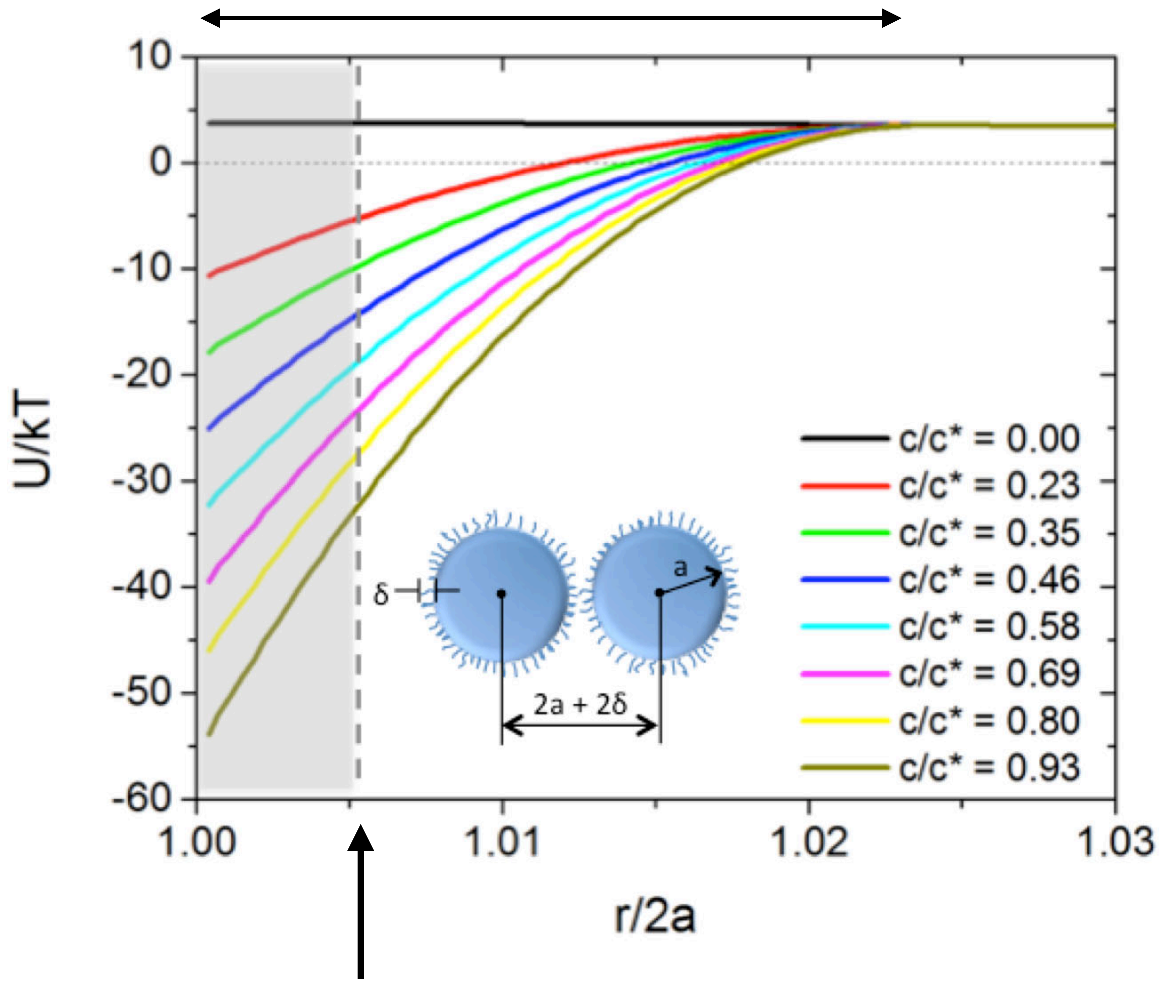

PHSA brush cutoff, 7nm

Rupture force distribution calculated from theoretical AO potential

Whitaker, K. A. & Furst, E. M. *J. Rheology* 60, 517–529 (2016).

PHSA-PMMA 2a = 2.7 µm, R_g = 32 ± 2 nm, Steric brush length δ = 7 nm

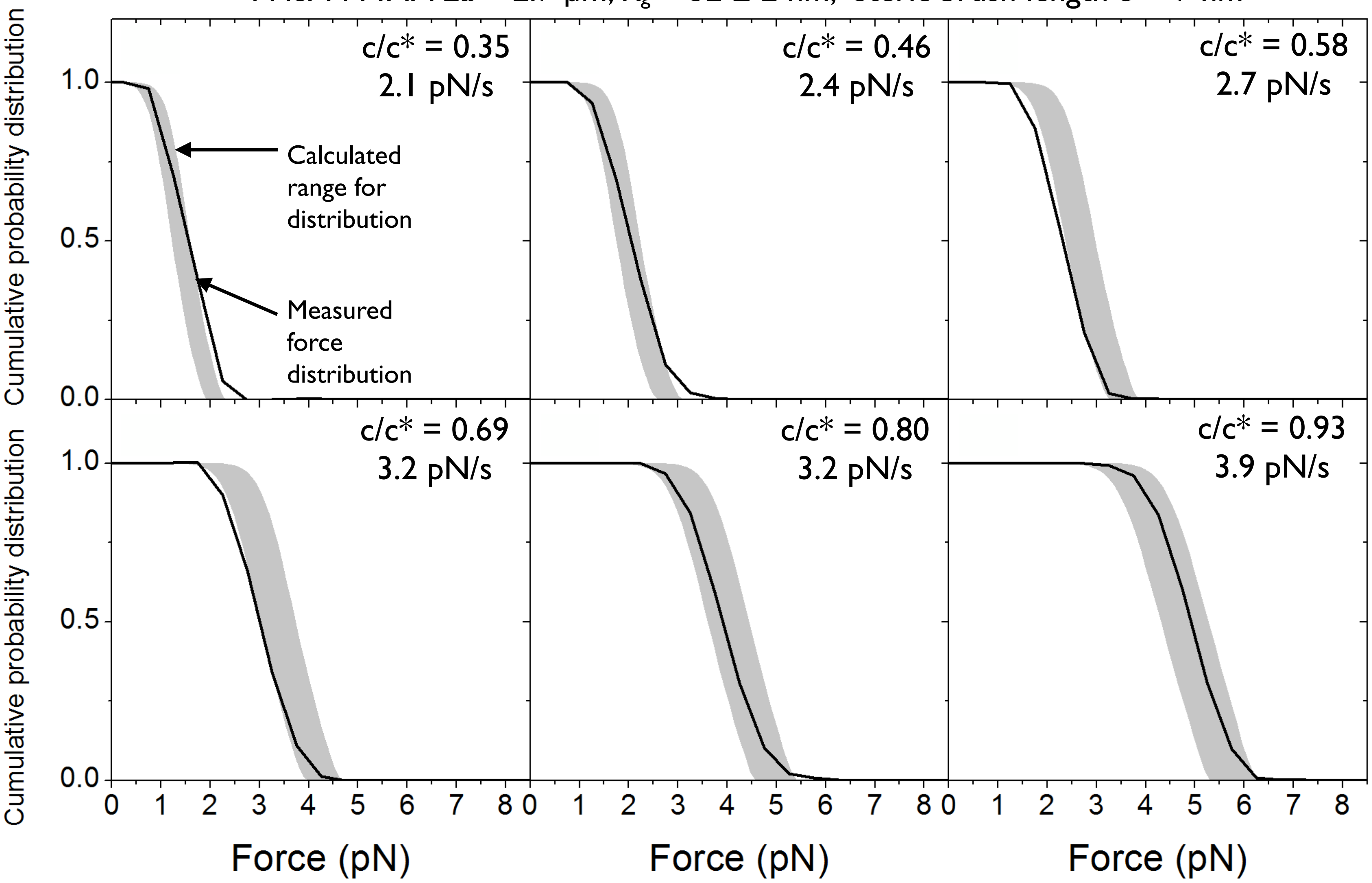

Rupture forces calculated from AO potential

Whitaker, K. A. & Furst, E. M. *J. Rheology* 60, 517–529 (2016).

PHSA-PMMA 2a = 2.7 μm, R_g = 32 ± 2 nm, Steric brush length δ = 7 nm

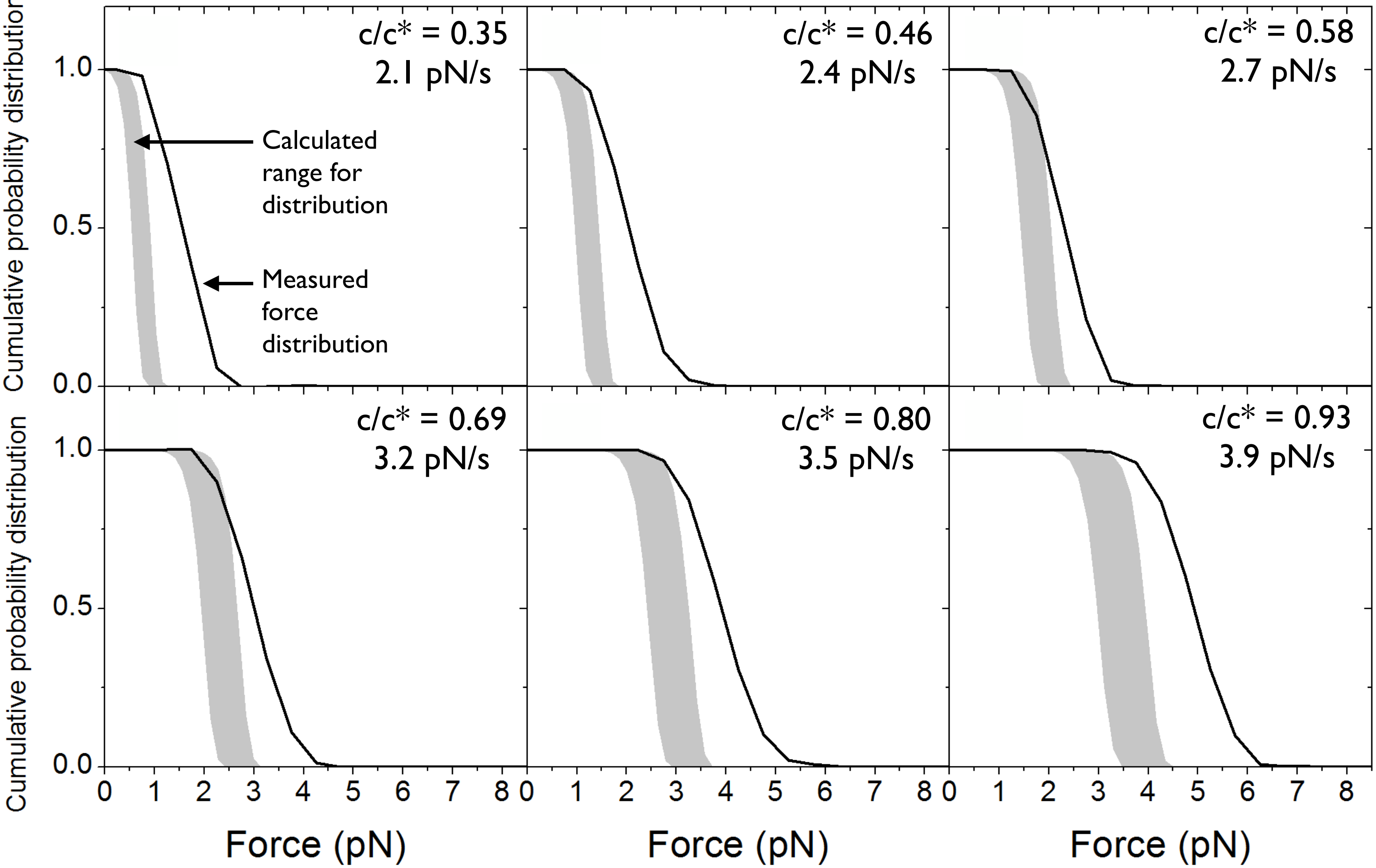

Directed assembly of aggregates

J. P. Pantina and E. M. Furst. Langmuir, 20:3940–3946, 2004.

Time shared and scanning optical traps

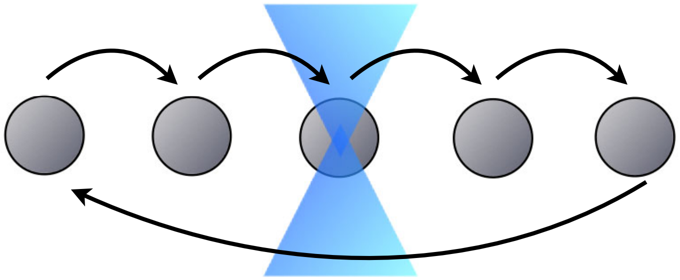

$$\nu = \frac{2k_B T[\mathrm{erf}^{-1}(\gamma)]^2}{3\pi a^3 b^2}$$

Mio and Marr, Langmuir. 15, 8565 (1999)
Faucheux et al., Phys. Rev. E. 51, 5239 (1995)
Crocker et al, Phys. Rev. Lett. 82, 4152 (1999)

High bandwidth positioning using AOD
Assembly in salt solutions

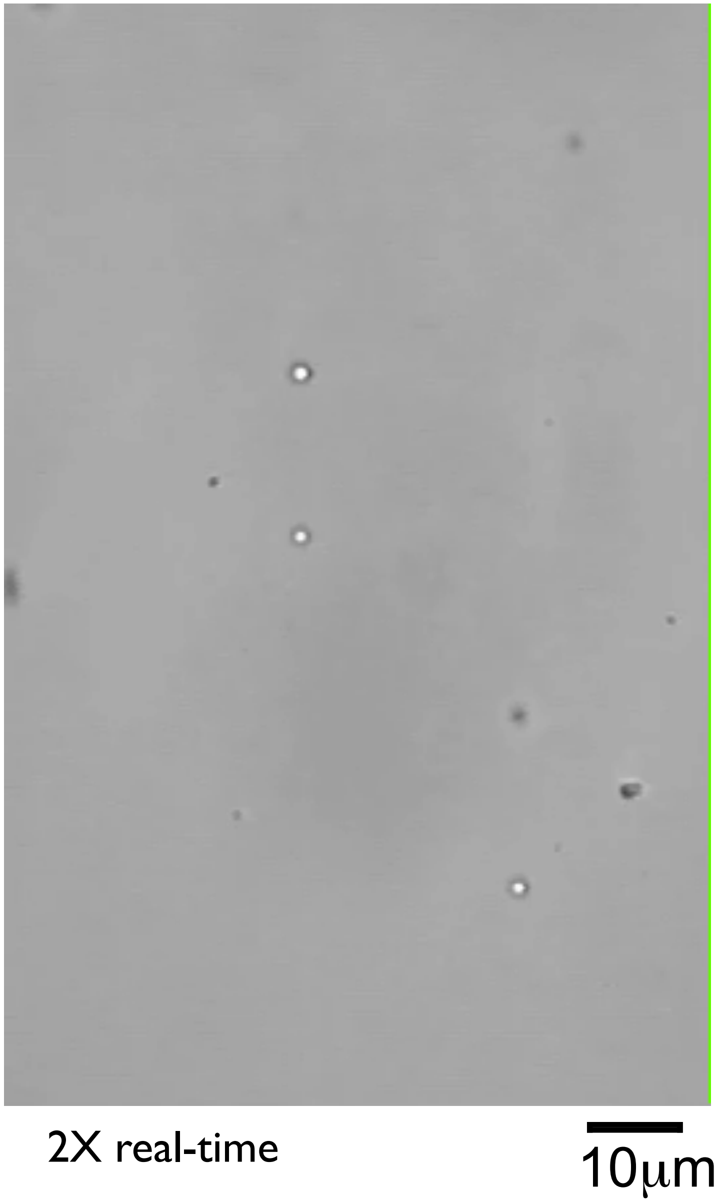

2X real-time

Linear elastic behavior of aggregates

Pantina and Furst, Phys. Rev. Lett. 94:138301, 2005.

1.47µm PMMA, 11 particles, 250mM $MgCl_2$

3-point bending geometry

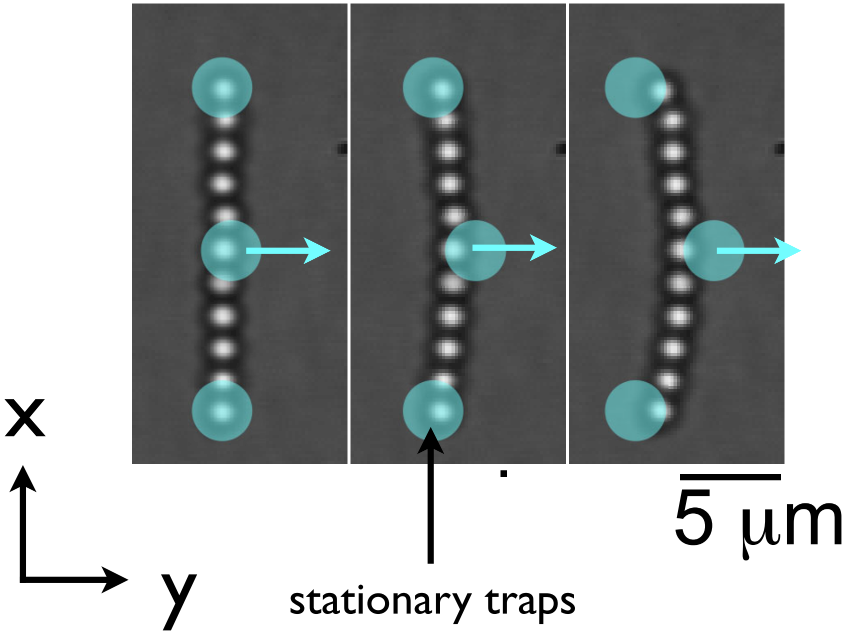

stationary traps

$$F = \kappa_T \Delta x$$

Note: aggregates > 100µm from interface

Comparison to beam equation

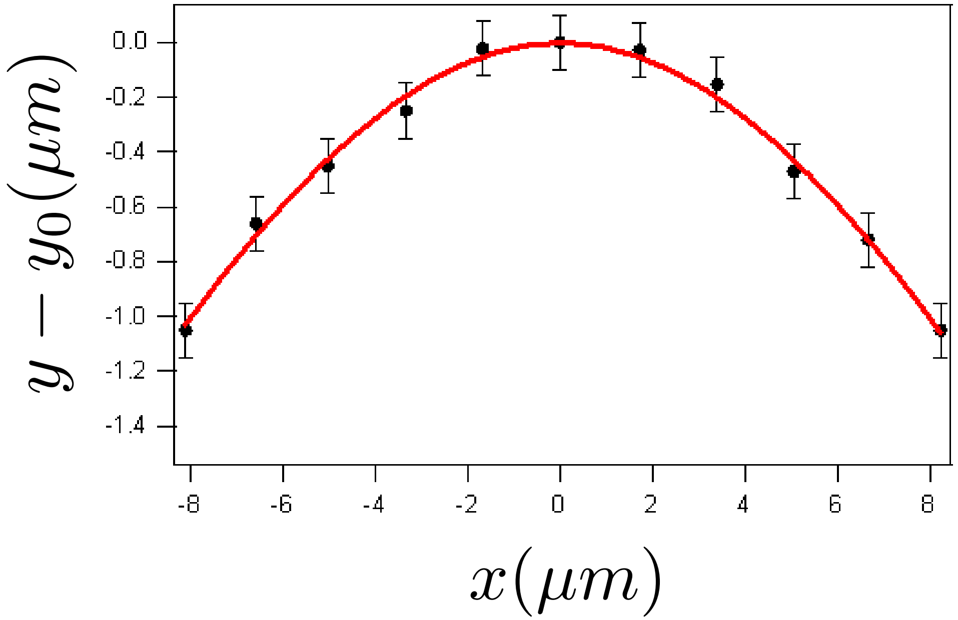

$$y_i(x_i) = -\frac{F}{EI}\left(\frac{Lx_i^2}{4} - \frac{|x_i^3|}{6}\right)$$

Linear bending mechanics in $MgCl_2$

Pantina and Furst, Phys. Rev. Lett. 94:138301, 2005.

Rigidity

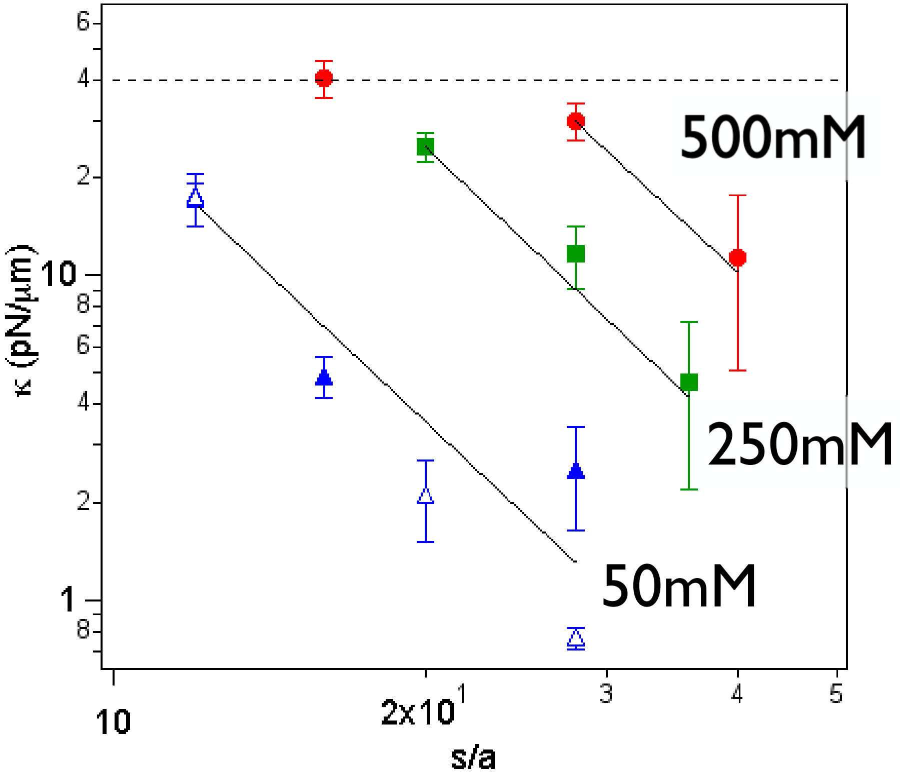

Scaling behavior

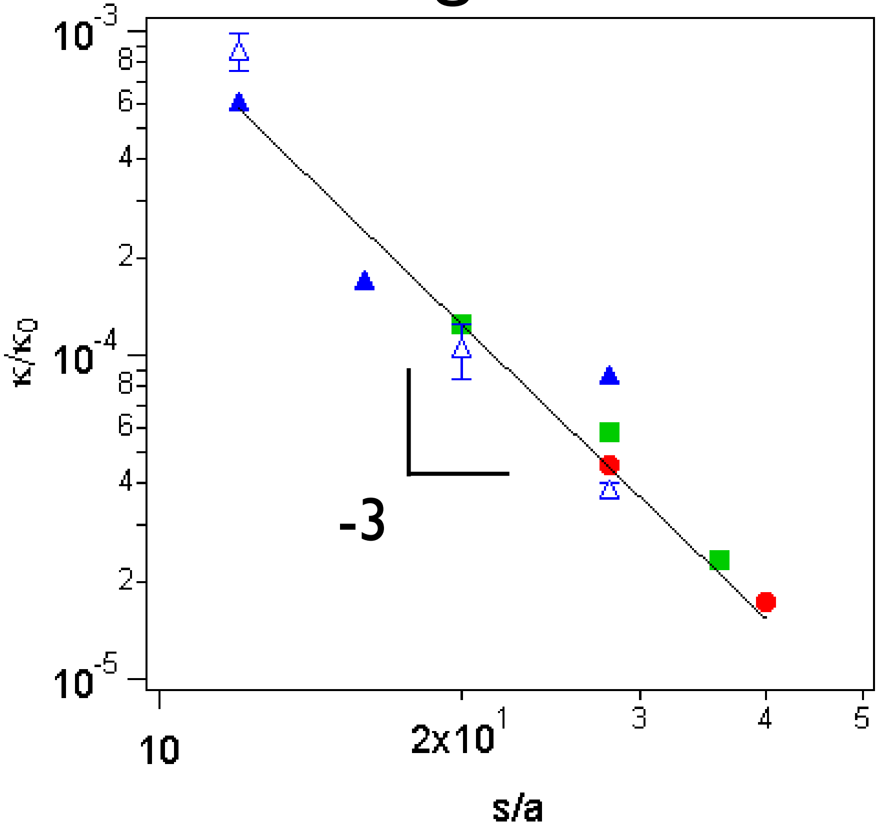

Open symbols: PS
Closed symbols: PMMA

Aggregate rigidity displays surprising dependence on salt concentration

Single bond bending rigidity

1.47μm PMMA

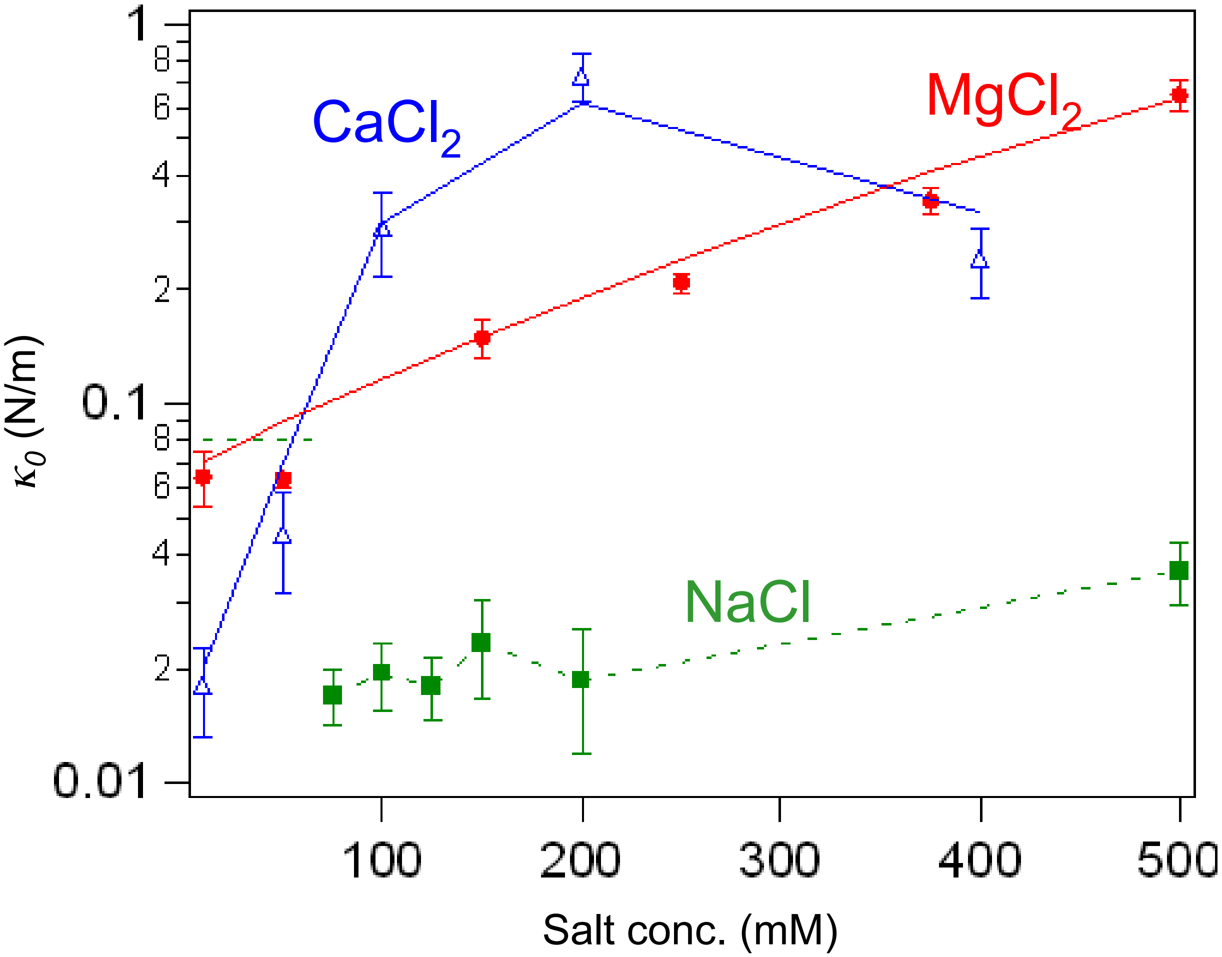

Typical colloidal interactions

DLVO-van der Waals + double layer

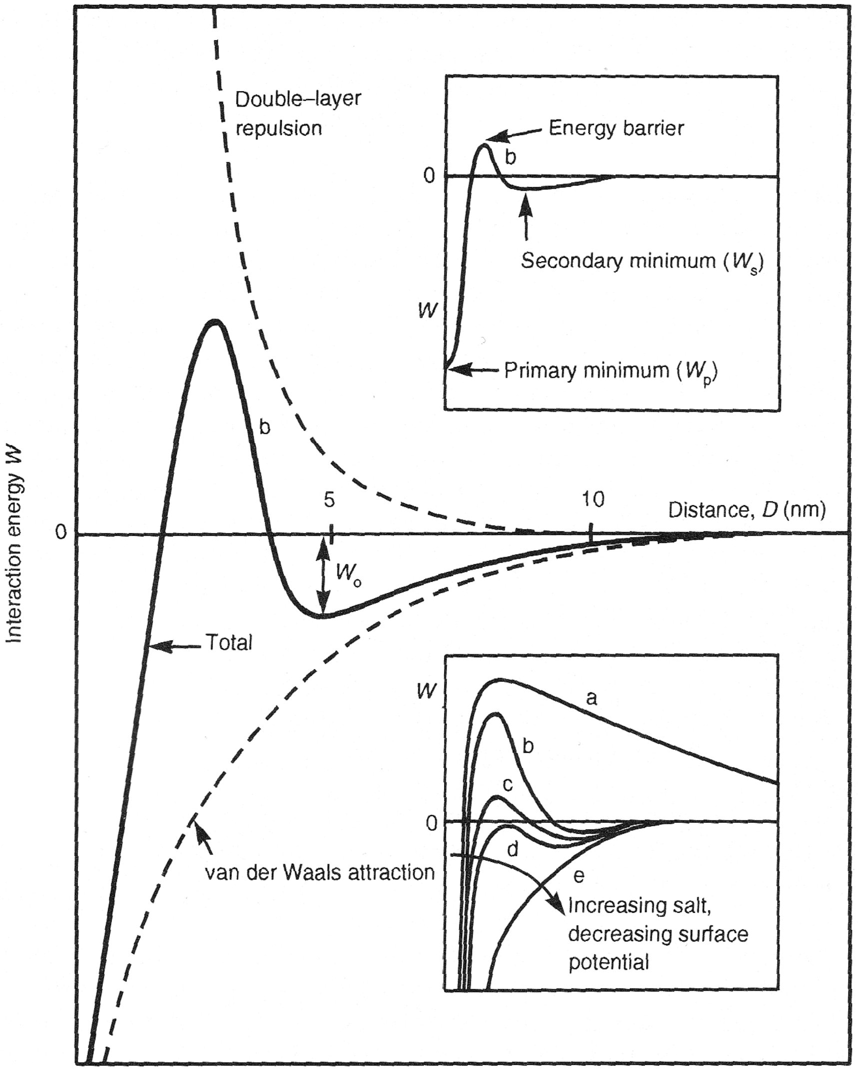

Israelachvili, Intermolecular and Surface Forces

DLVO cannot account for tangential forces or salt dependence

Bond rigidity

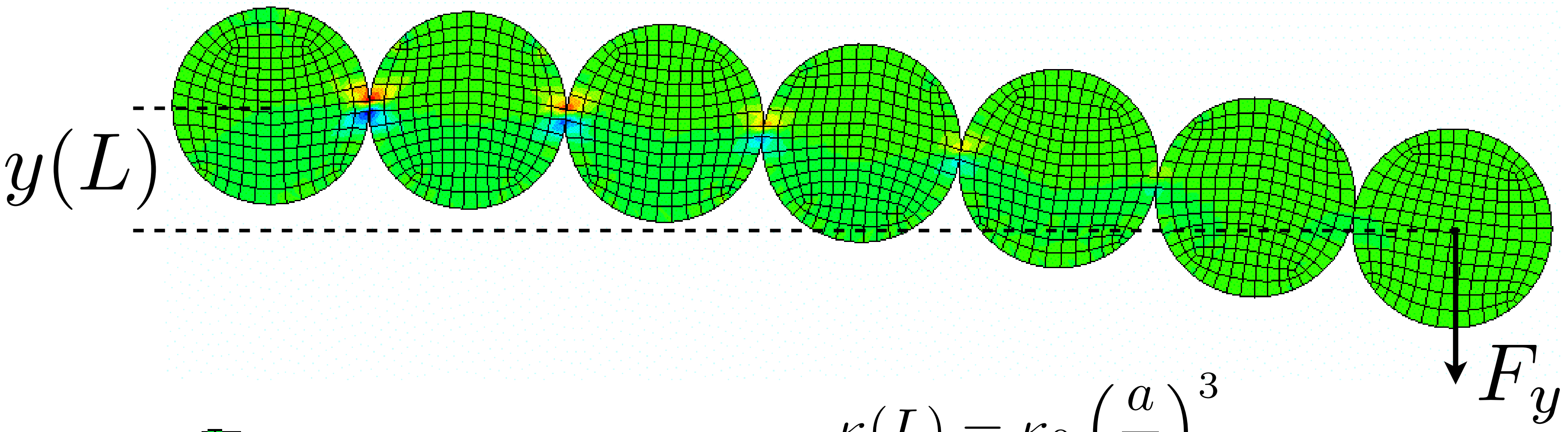

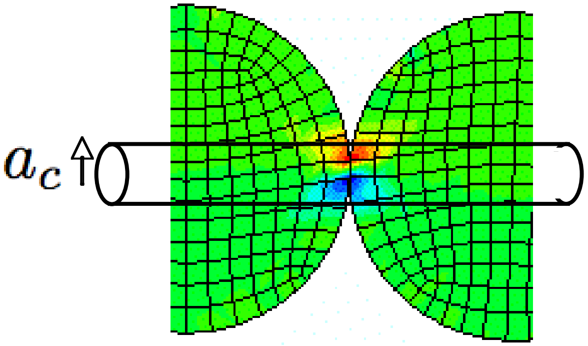

Area moment of inertia

$$I = \frac{\pi a_c^4}{4}$$

$$\kappa(L) = \kappa_0 \left(\frac{a}{L}\right)^3$$

$$= \frac{F_y}{y(L)} = \frac{3EI}{L^3}$$

$$\kappa_0 = \frac{3EI}{a^3} \quad \Longrightarrow \quad \kappa_0 = \frac{3\pi E a_c^4}{a^3}$$

Bending rigidity in terms of contact radius

JKR Theory

Johnson, Kendall and Roberts, Proc. R. Soc. London, Ser. A 324, 301 (1971).

$$P_0 = 0 \qquad a_c = \left[\frac{3\pi a^2 W_{SL}}{2K}\right]^{1/3}$$

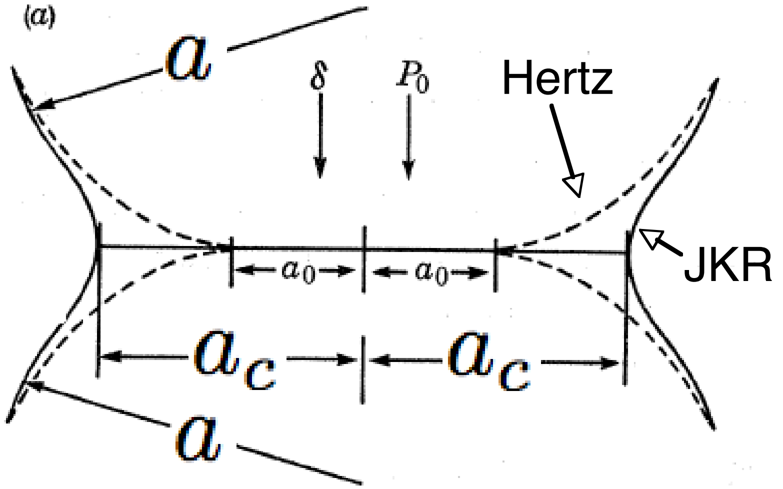

Surface adhesion energy:

$$W_{SL} = \gamma_S + \gamma_L - \gamma_{SL}$$

$$W_{SL} = \gamma_L(1 + \cos\theta_0) \approx 93 \mathrm{mJ/m^2}$$

where[1] $\theta_0 = 73.7 \pm 0.3^\circ$

$\gamma_L \approx 72 - 73 \mathrm{mN/m}$

Elastic modulus: $K = \dfrac{2E}{3(1-\nu^2)}$

$K \approx 2.5 \mathrm{GPa}$ [2]

Single-bond rigidity:

$$\kappa_0 = \frac{3\pi E a_c^3}{a^3} = \frac{3\pi E}{4a^3}\left(\frac{3\pi a^2 W_{SL}}{2K}\right)^{4/3}$$

Relates mechanics to adhesion energy (particle interfacial phenomena)

[1] Kwok et al. J. Colloid Interface Sci. 206, 44 (1998).

[2] Jarvis and Scheiman, J. Phys. Chem. 72, 74 (1968).

Calculated bending rigidity

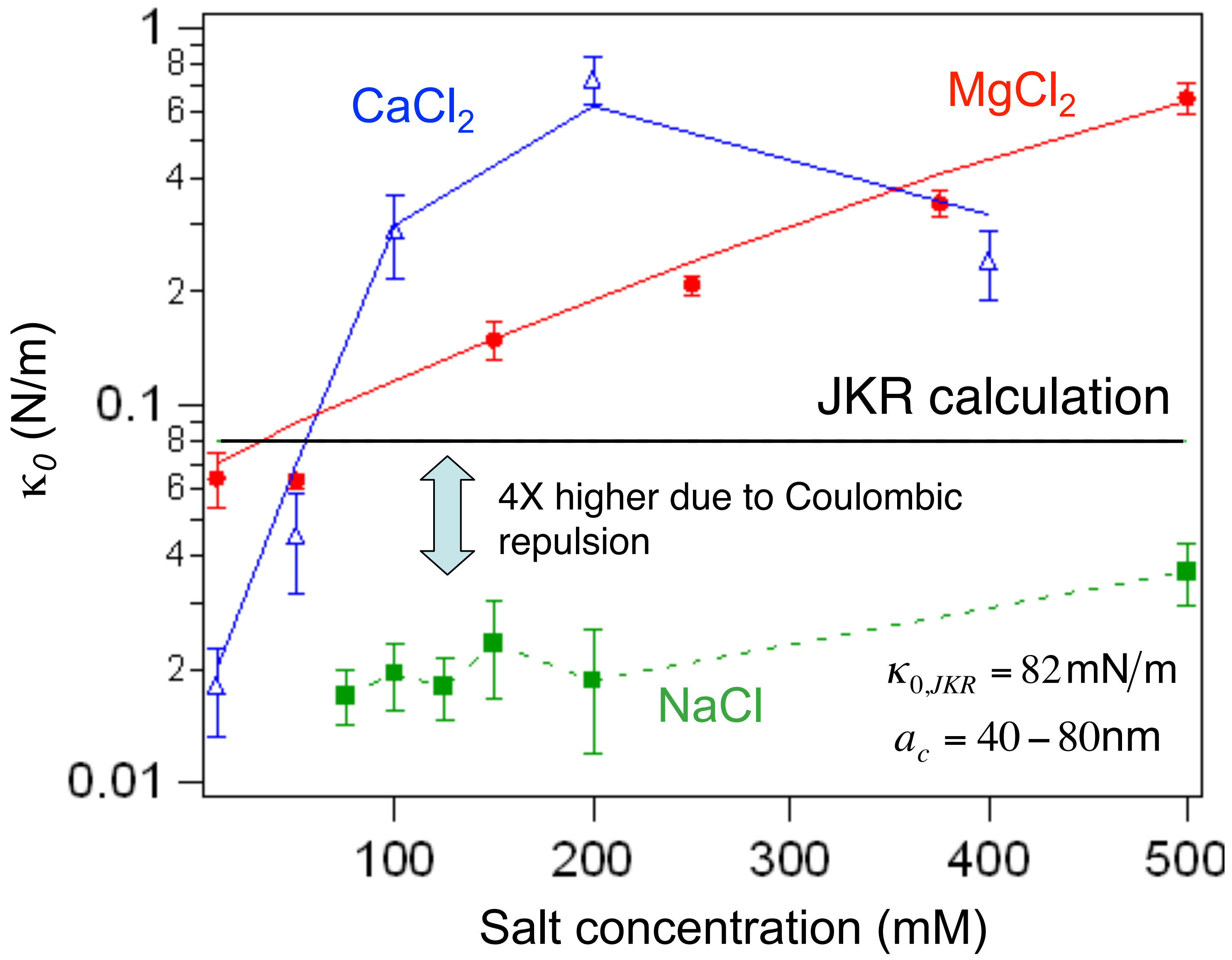

4X higher due to Coulombic repulsion

$$\kappa_{0,JKR} = 82\,\text{mN/m}$$

$$a_c = 40 - 80\text{nm}$$

Divalent ion adsorption to PMMA

Zeta-potential

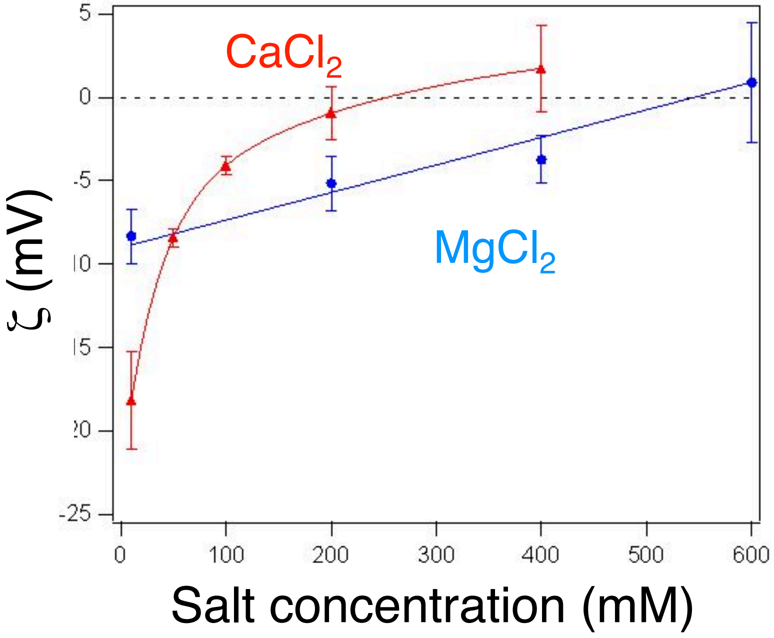

Bending rigidity

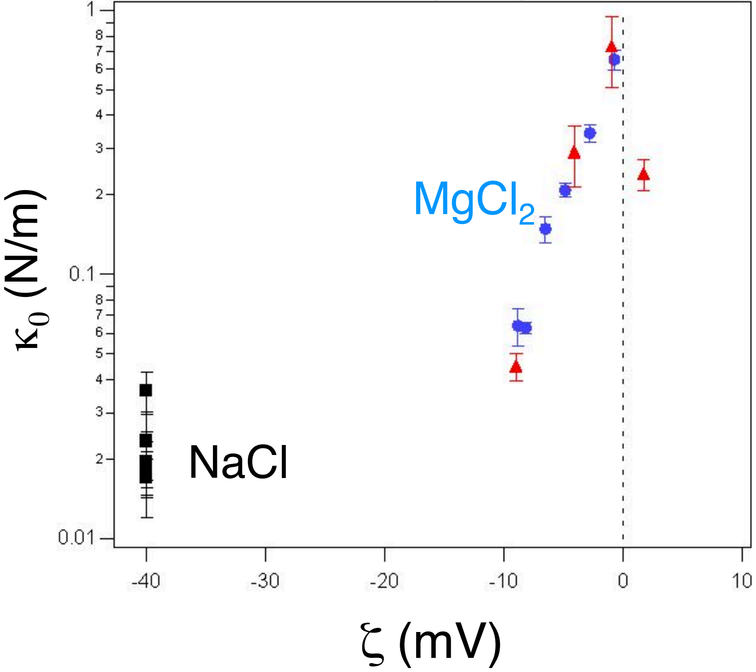

- Bond rigidity collapses with zeta potential
- Maximum at point of zero charge
- Calculate fractional coverage of divalent ion

$$\theta = \frac{[C^{++}S^{-1}]}{[S]^{Tot}}$$

Ion-bridge model

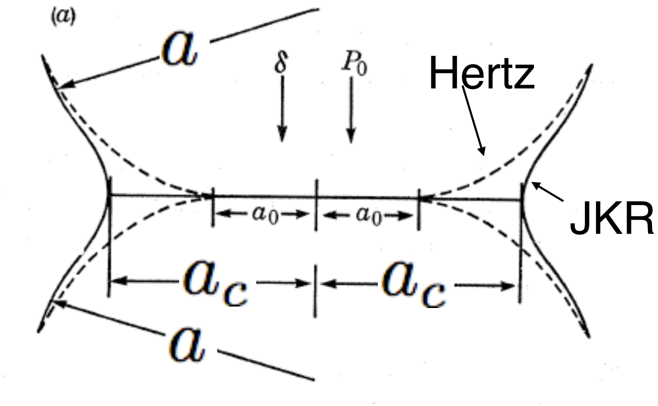

Total adhesion energy

$$W_{SL} = W_{SL}^{0} + W_{SL}^{ES} + W_{SL}^{div}$$

vdw

Coulomb

ion bridge

Divalent ions "bridge" charged adsorption sites

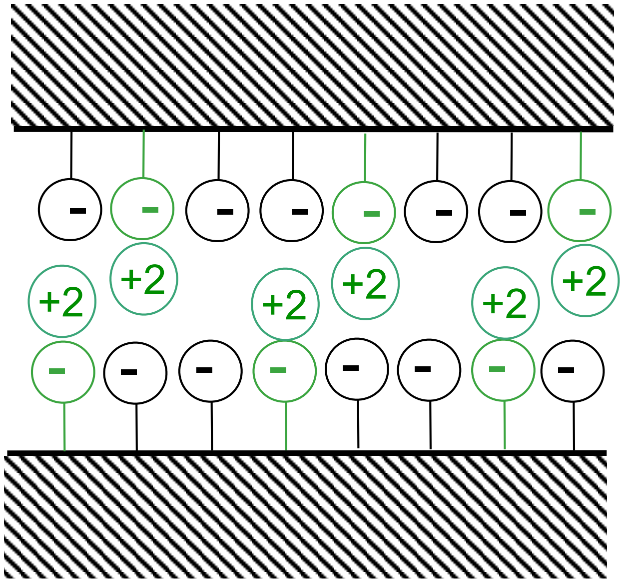

$$W_{SL}^{div} \sim \theta(1-\theta)$$

$$W_{SL}^{ES} \sim -(\sigma/e)^2 \pi a_c^2$$

$$\sim -(1-2\theta)^2 \pi a_c^2$$

$$\boxed{\kappa_0 = \frac{3\pi E a_c^3}{a^3} = \frac{3\pi E}{4a^3}\left(\frac{3\pi a^2 W_{SL}}{2K}\right)^{4/3}}$$

Ion bridge model

Pantina and Furst, Langmuir, 22:5282–5288, 2006.

$$W_{SL} = \underset{\text{vdw}}{W_{SL}^{0}} + \underset{\text{Coulomb}}{W_{SL}^{ES}} + \underset{\text{ion bridge}}{W_{SL}^{div}}$$

$$\kappa_0 = \frac{3\pi E}{4a^3}\left(\frac{3\pi a^2 W_{SL}}{2K}\right)^{4/3}$$

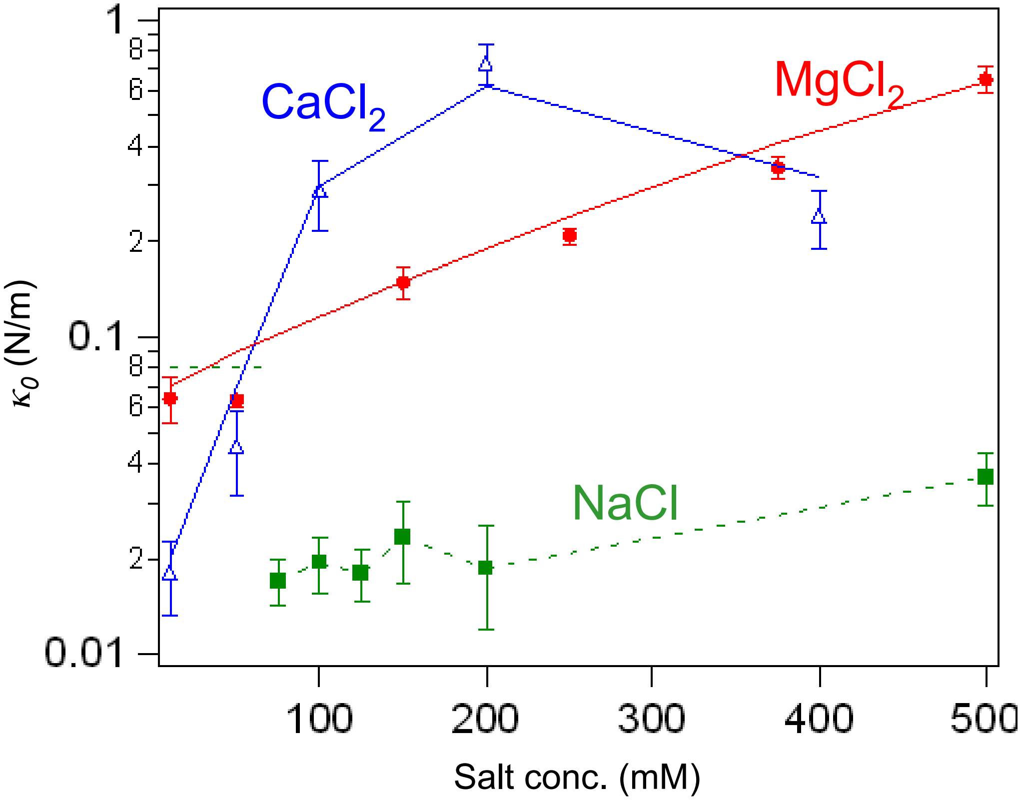

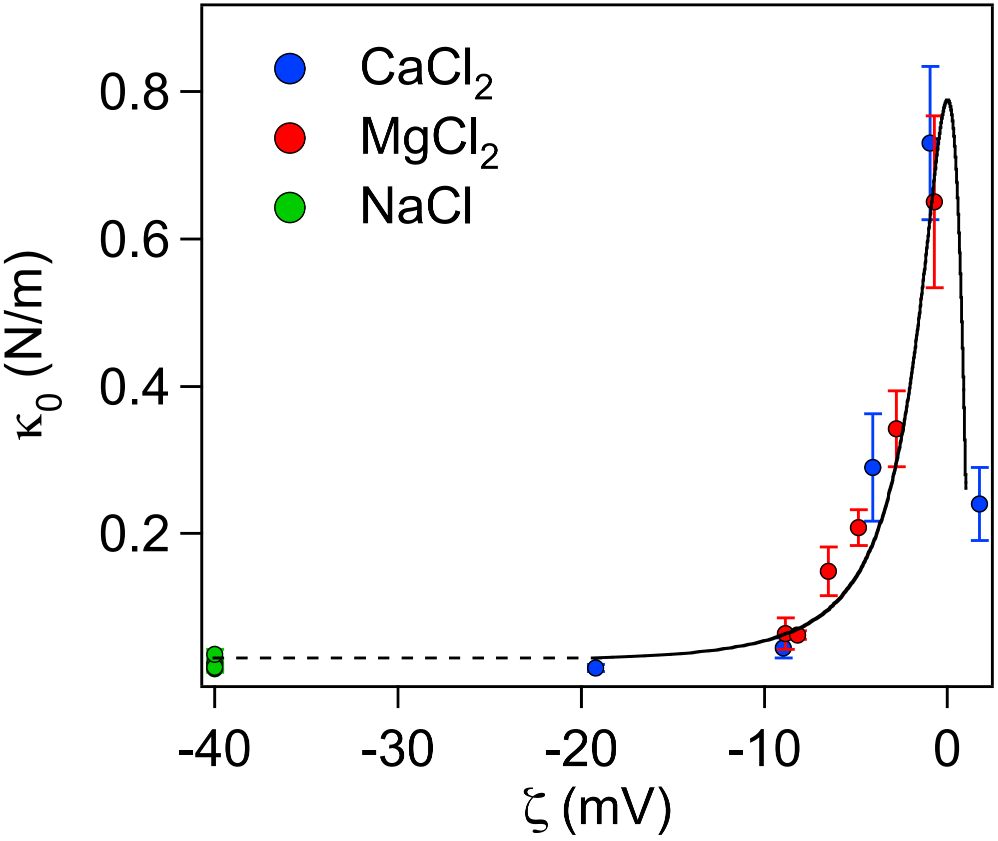

Non-linear mechanics

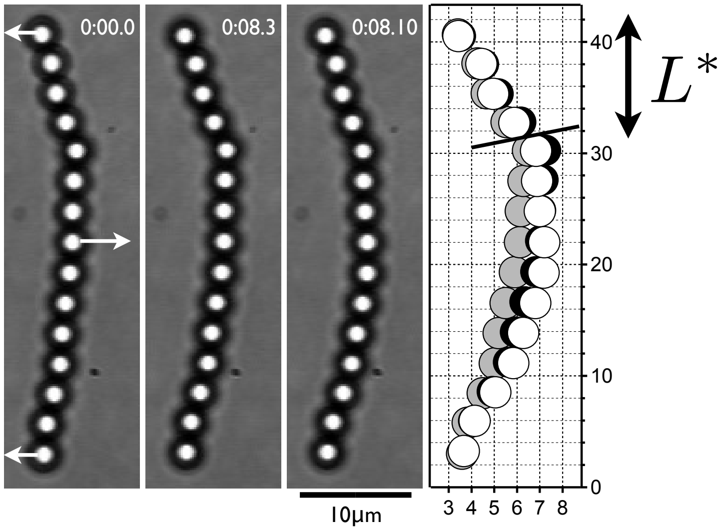

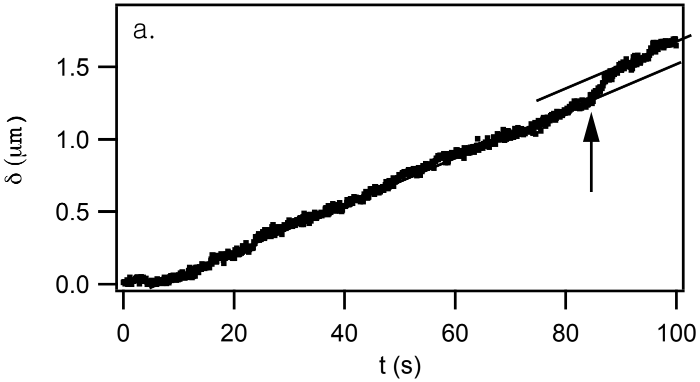

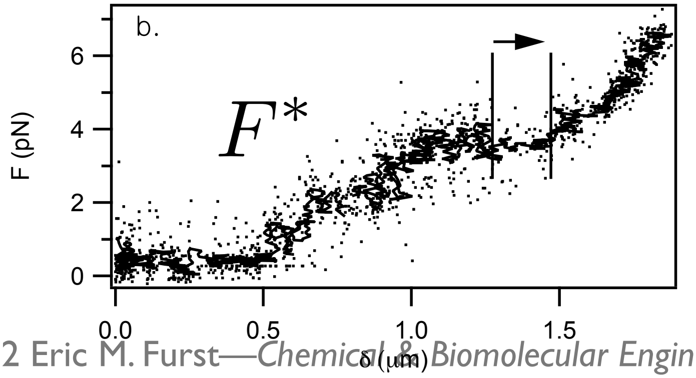

Critical bending moment

$$M_c = L^* F^*$$

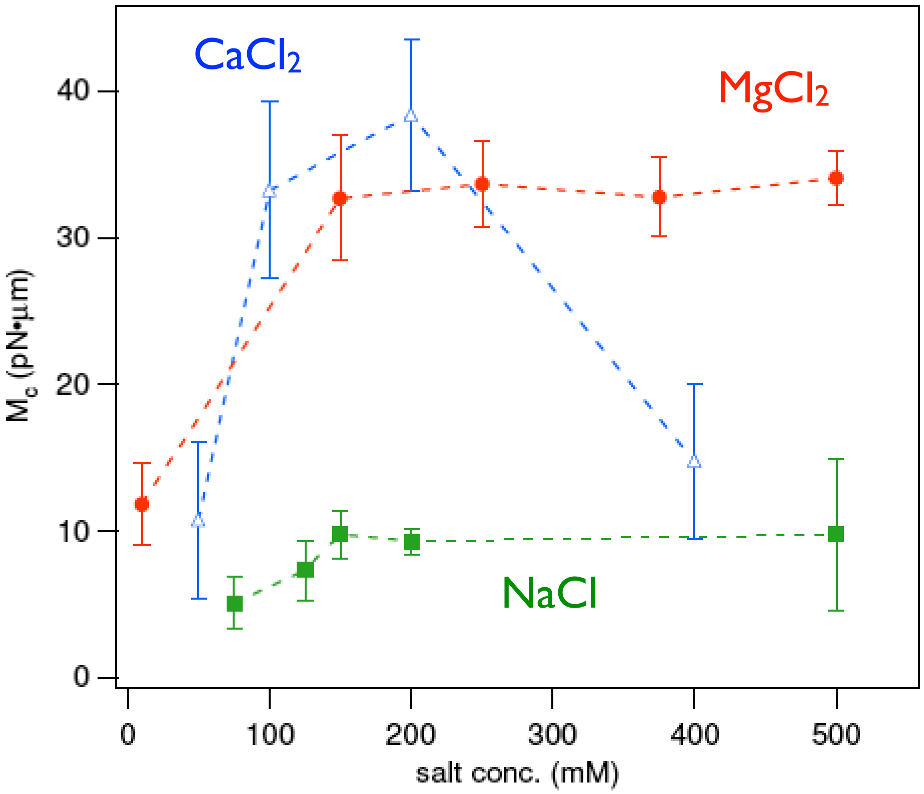

New microscopic yielding mechanism

Yield stress due to critical moment

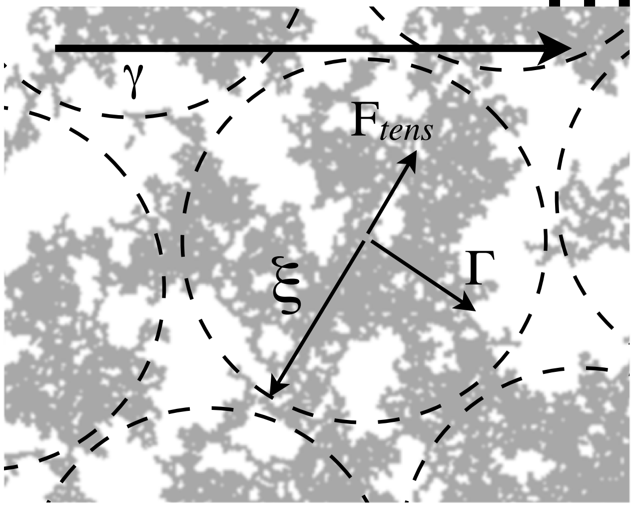

$$\xi \sim a(\phi/\phi_e)^{3/(d_f-3)}$$

Maximum tensile force

$$F_{tens} \sim \xi^2 \sigma_y$$

Maximum bending moment

$$\Gamma \sim \xi^3 \sigma_y$$

Predicted yield stress

$$\sigma_y^{bend} \sim M_c a^{-3} (\phi/\phi_e)^{3/(3-d_f)}$$

Predicted particle size dependence

$$M_c \sim a^{4/3}$$

$$\sigma_y^{bend} \sim a^{-5/3}$$

Critical moment versus contact radius

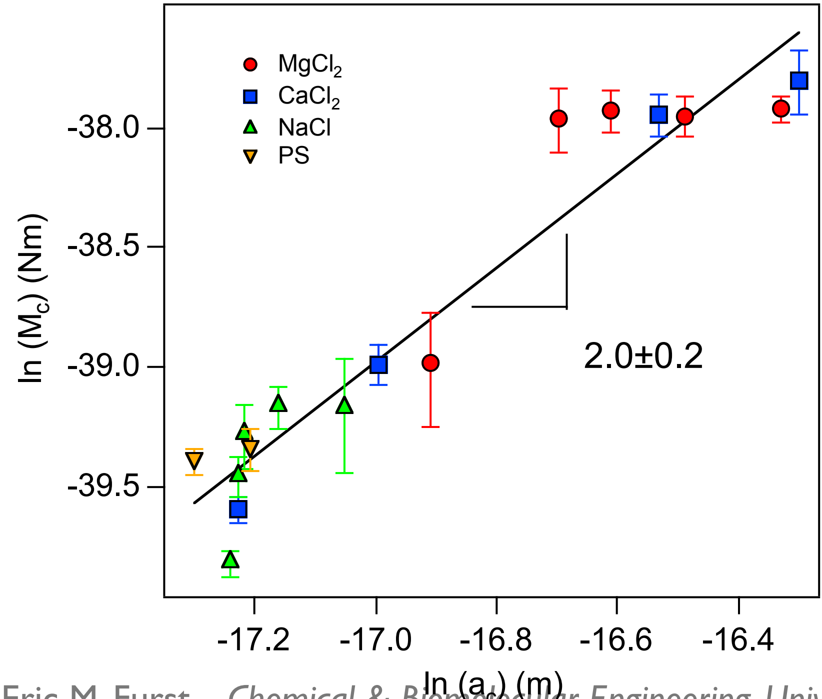

Comparison to bulk rheology

Bulk yield stress, PS latices

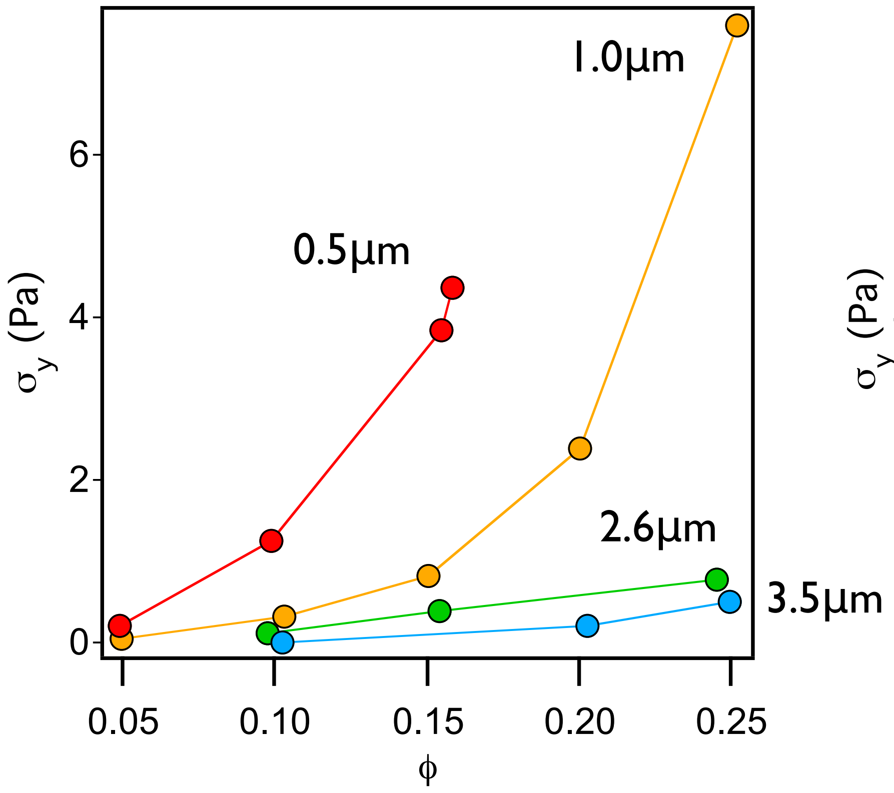

R. Buscall et al., J. Non-Newt. Fluid Mech., 24:183–202, 1987.

Expected from critical moment

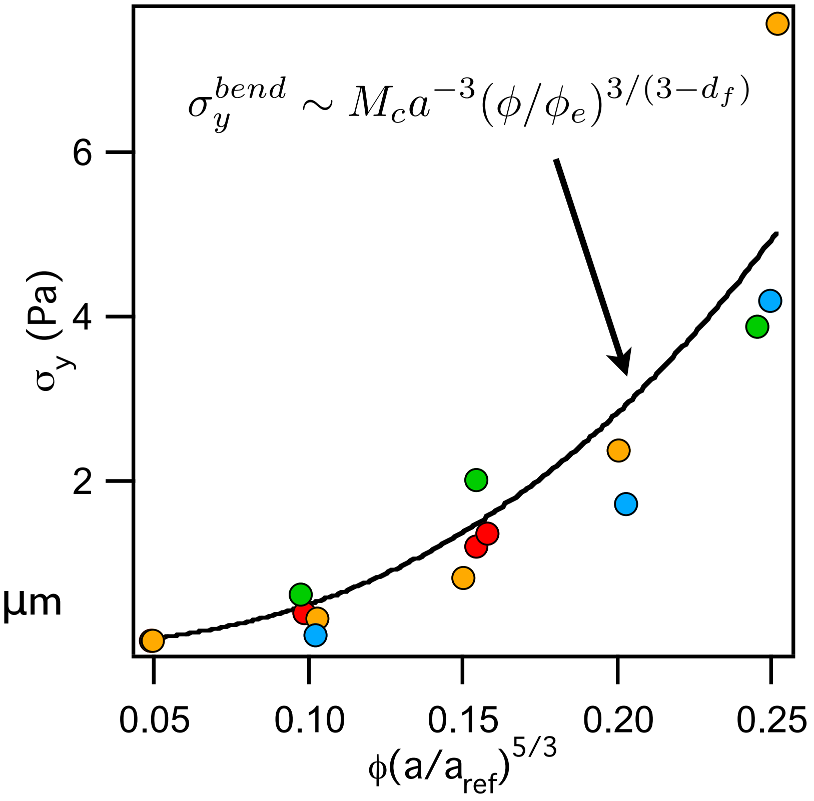

$$\sigma_y^{bend} \sim M_c a^{-3} (\phi/\phi_e)^{3/(3-d_f)}$$

$$\sigma_y^{bend} \sim a^{-5/3}$$

If yield due to maximum tensile force, $\sigma_y \sim F_{tens} \xi^{-2} \approx 1\text{kPa}$